Plume to global-scale atmospheric impacts of aviation emissions

by

Thibaud Matthieu Martin Fritz

S.M., Ecole Centrale Paris (2018)
S.M., Massachusetts Institute of Technology (2018)

Submitted to the Department of Aeronautics and Astronautics
in partial fulfillment of the requirements for the degree of
Doctor of Philosophy in Aeronautics and Astronautics
at the
MASSACHUSETTS INSTITUTE OF TECHNOLOGY
February 2022

Author . . . . . .
Department of Aeronautics and Astronautics
July 18, 2021

Certified by . . . . . .
Steven R.H. Barrett
Professor of Aeronautics and Astronautics
Thesis Supervisor

Certified by . . . . . .
Ronald G. Prinn
TEPCO Professor of Atmospheric Science

Certified by . . . . . .
Jaime Peraire
H.N. Slater Professor of Aeronautics and Astronautics

Certified by . . . . . .
Sebastian D. Eastham
Research Scientist, Aeronautics and Astronautics

Accepted by . . . . . .
Jonathan P. How
Chair, Graduate Program Committee

Plume to global-scale atmospheric impacts of aviation emissions

by

Thibaud Matthieu Martin Fritz

Submitted to the Department of Aeronautics and Astronautics
on July 18, 2021, in partial fulfillment of the
requirements for the degree of
Doctor of Philosophy in Aeronautics and Astronautics

Abstract

Commercial aircraft combustion emissions impact the atmospheric composition, alter the Earth's climate by accounting for ~4% of anthropogenic radiative forcing [72, 49] and affect surface air quality, causing an estimated ~16,000 premature mortalities per year [7, 28]. These environmental impacts are driven by chemical, microphysical and transport processes that span different magnitudes of temporal and spatial scales, from near-field in-plume chemistry that evolve over minutes and distances of ~100 m to global-scale phenomena taking place at the continental scale. To evaluate aviation's environmental impacts, all temporal and spatial scales need to be captured. In this thesis I develop and evaluate numerical models that span all modeling scales. First, I quantify the role of plume-scale processes in the atmospheric impact of aviation emissions. Previous literature has indicated that current global-scale modeling of aircraft emissions overestimates aviation-attributable ozone by instantly diluting emissions at a coarse resolution [86]. To estimate the magnitude of the ozone discrepancy, I use a recently-developed aircraft plume model to calculate the non-linear chemical conversions that occur in aircraft plumes. I then propagate the plume-scale results to the global atmospheric impact through the chemistry transport model (CTM) GEOS-Chem by embedding a plume-scale parameterization. After accounting for plume-scale processes, I find a ~5% downward correction in the simulated aviation-attributable ozone response.

High-altitude emissions from current subsonic aviation or from potentially future supersonic aircraft modify the total column ozone, thus leading to either increases in tropospheric ozone or a decrease in stratospheric ozone, with the latter causing larger UV flux at the ground. Both changes affect human health and, in this thesis, I identify a column ozone-neutral altitude for subsonic and supersonic aviation. Adjoint models of CTMs have been developed to quantify receptor-oriented sensitivities of environmental metrics (e.g. population-weighted ozone exposure) to emissions. Adjoint modeling overcomes the numerical cost of source-oriented sensitivity analysis, as performed by forward models. However, adjoint models of atmospheric chemistry have historically been limited to the troposphere. In this thesis, I build upon previous work and extend the GEOS-Chem Adjoint to further include stratospheric processes, and then validate the sensitivities with multi-year scenarios. I then present adjoint-derived sensitivities to identify column ozone-

neutral altitudes for subsonic and supersonic aviation, based on their respective emission characteristics. I find that the 12 - 15 km altitude band is approximately column ozone-neutral for aviation emissions. Neglecting the effects of plume-scale processes introduces a positive bias in the column ozone-neutral altitude that varies between 0.3 up to 1 km.

Finally, previous assessments of the environmental impact of aviation emissions using global climate models have found that coupled chemistry-climate feedback could have a magnifying effect on the response to commercial aircraft emissions. However, the aviation-induced environmental impact estimated with climate models have not been found to be consistent with CTMs [15]. To identify the cause of this discrepancy between climate models and CTMs and to evaluate the relevance of climate feedbacks in the assessment of the environmental response of aviation emissions, I develop a newly-coupled model for climate-chemistry simulations, CESM2-GC, coupling the climate model CESM2 to the model of atmospheric chemistry GEOS-Chem. I then validate CESM2-GC against atmospheric observations and results from the GEOS-Chem CTM and the "native" chemistry option in CESM2, CAM-Chem. Using CESM2-GC, I perform ensemble runs to evaluate the magnitude of the coupled chemistry-climate effects when evaluating aviation's ozone and particulate matter response. I find that the ensemble mean provides an aviation-attributable population-weighted ozone and particulate matter perturbations of 0.56 ppbv and 0.08 $\mu g/m^3$, consistent with previous estimates using the GEOS-Chem CTM. Besides an increase of ~70 mK in tropical and Northern mid latitudes tropospheric temperatures, I observe no statistically significant response in upper-tropospheric meteorology that could indicate that coupled chemistry-climate feedback magnifies the aviation-attributable environmental response.

Thesis Supervisor: Steven R.H. Barrett
Title: Professor of Aeronautics and Astronautics

Thesis Committee Member: Ronald G. Prinn
Title: TEPCO Professor of Atmospheric Science

Thesis Committee Member: Jaime Peraire
Title: H.N. Slater Professor of Aeronautics and Astronautics

Thesis Committee Member: Sebastian D. Eastham
Title: Research Scientist, Aeronautics and Astronautics

Acknowledgments

I would first like to thank my advisor, Prof. Steven Barrett, for his guidance, advice and support during my time at MIT. I am grateful that he gave me the opportunity to work on exciting and ground-breaking projects. I admire his ingenuity and understanding, which have been of tremendous value in his mentoring. I am also grateful to my PhD committee members, Prof. Ronald Prinn, Prof. Jaime Peraire, and Dr. Sebastian Eastham, who have provided their experienced guidance and feedback for this work. I also would like to thank Dr. Ray Speth and Prof. Ian Waitz whose feedback was valuable to improve the quality of this thesis.

I would like to thank both NASA and NCAR for funding me throughout various parts of my thesis. I have been extremely honored to work on innovative projects from both institutions. These projects have allowed me to meet and have fruitful discussions with researchers and engineers from both NASA and NCAR.

My time at LAE has been a truly wonderful experience. I would like to gratefully thank the LAE leadership for setting up an amazing work environment and making the lab a welcoming environment. I also would like to acknowledge the tremendous academic support provided by Seb all along my PhD journey. Thank you Seb for always living the dream, and for providing constructive criticism which pushed me towards high-quality work. In addition, your support has enabled me to learn, write, and think in Fortran. Ray has also been an incredible source of knowledge and my go-to person whenever I had a UNIX-related question. I also would like to thank Seb and Ray for letting me use 105 TB on d14 to only write checkpoints.

I would like to thank everyone outside of MIT that has helped me throughout my academic journey. I couldn't be more grateful towards the GEOS-Chem Support Team, Prof. Daniel Jacob and Haipeng Lin for their help on GEOS-Chem. I am also very thankful of the help provided by the NCAR researchers and software engineers. Special thanks to Dr. Louisa Emmons and Steve Goldhaber for providing their help on CESM2. Also in Boulder, I would like to thank Prof. Daven Henze and Yanko Davila for their guidance and help regarding the GEOS-Chem adjoint.

I would like to thank my colleagues at LAE, thanks to whom it has been such a pleasure working there. I would like to thank all the students who have been at LAE during my time there. Special thanks to a number of people. To Kingshuk "Shukky" Dasadhikari, thank you for having your own opinions and always being ready to engage in fruitful conversations. To Drew, thank you for being a great friend ever since we met. To Carla, thank you for always being joyful and putting a smile on people's faces. To Ines and Prashanth, thank you for having the coolest office and for the great "work-focused" conversations we've had. To Akshat, thank you for putting up with APCEMM and for always taking the time to answer my questions. To Irene, thank you for the GEOS-Chem adjoint. More seriously, thank you Irene for taking the time to teach me the basics of adjoint modeling. Thank you all for always being ready to have lunch or coffee breaks and enjoy great discussion. Thank you to all LAE members over the years. It has been an amazing and welcoming environment.

Last but not least, I would like to thank my parents for supporting from more than 3,000 miles away during this journey. They have been an amazing source of inspiration during these five years. I am grateful that they always found the time to talk to me despite the time difference. Your support throughout the years has meant a lot.

This PhD journey has been a wild ride. I still remember my first day in lab. I was not sure what my research was all about, but knew one thing: "Matlab is the way to go" and that I was into coding. Now, more than five years have past and Matlab is no where to be seen. Mission accomplished. I now peacefully stand in Fortran territory after having coded in C++ and writing Makefiles from scratch. I am however grateful for GNU Make. Compiling code does not only allow the user to typically run programs faster, it has also been a great boon to take coffee breaks. Sadly, I have learnt to write comments in my code. I used to stand by the following: "Real programmers do not comment their code. If it was hard to write, it should be hard to understand.".

Contents

1 Introduction **19**

1.1 Background and motivation 19

1.2 Thesis contribution 22

2 Impacts of plume-scale treatment of aviation emissions on atmospheric composition **25**

2.1 Introduction 25

2.2 Methods 26

2.2.1 Modeling of changes in chemical composition in individual aircraft plumes 27

2.2.2 Implementation of a plume-scale treatment of aviation emissions in a global chemistry transport model 30

2.2.3 Simulation setup 32

2.3 Results 33

2.3.1 External coupling 33

2.3.2 Embedded coupling 36

2.4 Discussion and limitations 42

3 Dependence of aviation's ozone impacts on altitude and exhaust composition **45**

3.1 Introduction 45

3.2 Methods and model validation 47

3.2.1 Adjoint modeling 47

3.2.2 Validation of full-model runs 48

3.2.3 Methods to estimate the column ozone-neutral altitude 54
3.3 Results 57
3.3.1 Decadal sensitivities 57
3.3.2 Identification of a column ozone-neutral altitude 60
3.3.3 Sensitivity to emission characteristics 62
3.4 Discussion and limitations 65

4 Coupled chemistry-climate feedback of commercial aviation emissions 69
4.1 Introduction 69
4.2 Coupling of CESM2 with GEOS-Chem (CESM2-GC) 72
4.3 Validation of CESM2-GC 73
4.3.1 Methods 73
4.3.2 Evaluation of CESM2-GC against atmospheric observations and other atmospheric models 74
4.4 Evaluation of the coupled chemistry-climate feedback of commercial aviation emissions 92
4.4.1 Methods 92
4.4.2 Results 94
4.5 Discussion and limitations 105

5 Conclusion 109
5.1 Key findings 109
5.2 Future work 111

A Appendix to Chapter 2 113
A.1 Plume-scale results 113
A.2 Aviation emissions 113

B Appendix to Chapter 3 117
B.1 Validation of the sensitivities of column ozone to stratospheric sulfur emissions 117
B.2 Sensitivity of aerosol optical depth to emissions 119

C Appendix to Chapter 4 **123**

C.1 Engineering of coupling GEOS-Chem with CESM2 123

C.2 Surface emission fluxes 125

C.3 Additional aircraft campaign observations and comparison to model evaluations 126

C.4 Aviation-induced feedback on atmospheric circulation, vertical stability, cloud fraction, and lightning NO_x emissions 127

List of Figures

2-1 Schematic of the discretized ring approach used in APCEMM 27

2-2 Perturbations in ozone (O_3), nitrogen oxides (NO_x) and the nitrogen reservoir species (NO_z) according to simulations using an instant-dilution approach and the APCEMM plume model 28

2-3 Zonally-averaged ozone perturbation from aircraft emissions after accounting for the non-linear processes in aircraft plumes 34

2-4 Zonally-averaged change in the aviation-attributable ozone from the inclusion of a plume-scale processing of aviation emissions 35

2-5 Zonally-averaged 24-hour NO_x remaining fractions owing to plume-scale processes in aircraft wakes as computed by GEOS-Chem 37

2-6 Zonally-averaged 24-hour ozone production owing to plume-scale processes in aircraft wakes as computed by GEOS-Chem 38

2-7 Absolute change in zonally-averaged ozone mixing ratios due to aviation emissions, due to plume-scale processes in aircraft wakes. The relative change in aviation-attributable ozone is also displayed 39

2-8 Seasonality dependence of the aviation-attributable ozone and relative change owing to plume-scale processes for North-Hemispheric winter and summer 40

2-9 Changes in surface ozone volumetric mixing ratio due to commercial aviation emissions, and owing to plume-scale effects occurring in aircraft wakes. The relative change in surface aviation-attributable ozone is also shown 41

2-10 Changes in surface $PM_{2.5}$ mass concentrations due to commercial aviation emissions, and owing to plume-scale effects occurring in aircraft wakes. The relative change in surface aviation-attributable $PM_{2.5}$ mass concentrations is also shown 43

3-1 Comparison of forward and adjoint sensitivities with respect to a scaling in aircraft NO_x emissions. 51

3-2 Response of total ozone column to a scaling in supersonic aircraft NO_x emissions according to GEOS-Chem and using atmospheric sensitivities from GEOS-Chem UCX Adjoint 52

3-3 Changes in the response of total ozone column to a scaling in supersonic aircraft sulfur emissions (released as SO_2 and H_2SO_4) according to GEOS-Chem and using atmospheric sensitivities from GEOS-Chem UCX Adjoint 53

3-4 Column ozone response to the injection of 32 Tg of water vapor from supersonic aviation. Zonally and yearly-averaged adjoint sensitivities of total ozone column mass with respect to water emissions 55

3-5 Temporal evolution of zonally-averaged sensitivities of total ozone column to NO_x emissions for different altitude bands, expressed in mDU/(Gg NO_2/year) 59

3-6 Sensitivities of total ozone column to changes in ice surface area density expressed in mDU/((mm^2/cm^3)/year) for the 8–12 km and 12–16 km altitude bands respectively 60

3-7 Adjoint sensitivity of mean ozone column to aviation fuel burn 63

3-8 Column ozone-neutral altitudes as a function of the NO_x emission index and fuel sulfur content 65

4-1 Dry deposition velocities of ozone as computed by CESM2-GC and the GEOS-Chem CTM, as well as their absolute and relative difference 77

4-2 Parity plot between the dry deposition velocities of ozone as computed by CESM2-GC and CAM-Chem. 78

4-3 Geographical distribution of the wet deposition flux of nitrogen at the surface for CESM2-GC, CAM-Chem and the GEOS-Chem CTM 79
4-4 Model evaluations of the dry deposition flux of nitrogen at the surface as evaluated by CESM2-GC, CAM-Chem, and the GEOS-Chem CTM 80
4-5 Wet deposition flux of non-sea salt sulfur as computed by CESM2-GC, CAM-Chem and the GEOS-Chem CTM 81
4-6 Annually-averaged surface ozone mixing ratios estimated by CESM2-GC and the GEOS-Chem CTM 82
4-7 Parity plots of surface ozone mixing ratios for January and July comparing CESM2-GC to the GEOS-Chem CTM 83
4-8 Surface NO_2 mass concentrations simulated by CESM2-GC, CAM-Chem and the GEOS-Chem CTM for 2016 for North America, Europe and South-East Asia alongside ground station measurements 84
4-9 Surface ozone mass concentrations simulated by CESM2-GC, CAM-Chem and the GEOS-Chem CTM for 2016 for North America, Europe and South-East Asia alongside ground station measurements 85
4-10 Parity plot of annually-averaged surface $PM_{2.5}$ mass concentrations for CESM2-GC and the GEOS-Chem CTM 87
4-11 Taylor diagrams of the comparison of CESM2-GC, CAM-Chem, and the GEOS-Chem CTM simulations to a present-day (1995-2010) ozonesonde climatology 88
4-12 Total ozone column as observed by OMI and MLS for the 2004-2010 time period compared to the simulation results from CESM2-GC, CAM-Chem and the GEOS-Chem CTM 89
4-13 Carbon monoxide column totals as observed by MOPITT and model results and biases for CESM2-GC, CAM-Chem and the GEOS-Chem CTM for April 2016 90
4-14 Airborne observations from aircraft campaigns and model results for CESM2-GC and CAM-Chem for CO, C_2H_6, C_3H_8, C_2H_2 in the 0 to 3 km altitude band 91

4-15 Airborne observations from aircraft campaigns and model results for CESM2-GC and CAM-Chem for CO, C_2H_6, C_3H_8, C_2H_2 in the 2 to 7 km altitude band 92

4-16 Ensemble average of the change in surface ozone mixing ratio owing to commercial aviation emissions 95

4-17 Standard deviation of the change in surface ozone mixing ratio owing to commercial aviation emissions 96

4-18 Change in zonally-averaged ozone mixing ratio from commercial aviation emissions 97

4-19 Temporal evolution of longitudinally-averaged surface ozone mixing ratios across all ensemble members 98

4-20 Change in zonally-averaged NO_x mixing ratio from commercial aviation emissions 99

4-21 Change in zonally-averaged temperature from commercial aviation emissions 100

4-22 Surface changes in surface ozone mixing ratios and surface $PM_{2.5}$ mass concentrations for the fully-coupled and nudged ensemble runs using CESM2-GC 102

4-23 Comparison of the change in zonally and annually-averaged surface ozone mixing ratios across all ensemble members in the fully-coupled and nudged simulations 102

4-24 Comparison of the change in zonally and annually-averaged surface $PM_{2.5}$ mass concentrations across all ensemble members in the fully-coupled and nudged simulations 103

4-25 Comparison of the ensemble means of the change in monthly-averaged surface ozone mixing ratio for the fully-coupled and nudged simulations . . 104

A-1 Two-dimensional histograms of in-plume remaining NO_x fractions as a function of flight-level temperature for a cruise pressure of 220 hPa and latitude of 60°N 114

A-2 Commercial aviation fuel burn density for the year 2015, as estimated by AEIC and its latitudinal and longitudinal dependence 115

B-1 Five-year forward model-derived response to supersonic sulfur emissions, assuming a fuel sulfur content of 600 ppm; zonally-averaged sensitivities of total ozone column to sulfur emissions when emitted as SO_2 and H_2SO_4; adjoint sensitivities weighted by sulfur conversion 118

B-2 Zonally-averaged adjoint sensitivities of total aerosol optical depth with respect to sulfur emissions 120

C-1 Surface CO emission flux for CESM2-GC and the GEOS-Chem CTM . . . 126

C-2 Surface NO emission flux for CESM2-GC and the GEOS-Chem CTM . . . 126

C-3 Surface NH3 emission flux for CESM2-GC and the GEOS-Chem CTM . . 126

C-4 Comparison of the results from CESM2-GC and CAM-Chem to aircraft observations in the 0 to 3 km altitude range 127

C-5 Estimated zonal wind in CESM2-GC and aviation-induced change in zonally-averaged zonal wind 128

C-6 Estimated meridional wind in CESM2-GC and aviation-induced change in zonally-averaged meridional wind 129

C-7 Estimated cloud fraction in CESM2-GC and aviation-induced change in zonally-averaged cloud fraction 130

C-8 Estimated vertical pressure velocity in CESM2-GC and aviation-induced change in zonally-averaged vertical pressure velocity 131

C-9 Estimated lightning NO_x emissions in CESM2-GC and aviation-induced change in zonally-averaged lightning NO_x emissions 132

List of Tables

2.1 Parameters used in the plume-scale look-up table 29

C.1 Emission totals for selected species in CESM2-GC 125

Chapter 1

Introduction

1.1 Background and motivation

Most commercial aircraft currently use combustion of Jet A or Jet A-1 as the energy source to provide thrust in gas turbine engines. As a result, commercial aircraft operations lead to the emissions of gases and particles, which are released throughout the troposphere up to the lower stratosphere for subsonic aviation. The combustion of conventional jet fuel releases carbon dioxide (CO_2) and water vapor (H_2O) into the atmosphere, increasing the Earth's greenhouse effect. Hydrocarbons and soot particles also get released from fuel combustion. In addition, conventional jet fuel contains sulfur, which gets released upon combustion, and can form sulfate aerosols. These aerosols induce atmospheric cooling by reflecting incoming solar radiation. The combustion process at high temperature also leads to the formation of nitrogen oxides (NO_x = NO + NO_2).

These emissions, mostly at high altitude, lead to changes in atmospheric composition and the Earth's climate. The ozone response to aviation emissions has been studied in prior studies and linked to human health [7, 28]. Ozone (O_3) is a gas that is found in the stratosphere, protecting life from ultraviolet (UV) radiation. However, near-surface ozone is detrimental to human life, crops and vegetation [6, 84, 24, 3, 5, 121, 12]. Particulate matter is also a harmful pollutant, which can be produced as a result of aviation emissions. Particles and liquid droplets of an aerodynamic diameter of 2.5 μm or smaller (referred to as $PM_{2.5}$) have been found to lead to health impacts under long-term exposure, such

as respiratory diseases, cardiovascular diseases [63, 121, 56, 22, 124]. Aviation-induced atmospheric perturbations have been found to lead to 16,000 premature mortalities for the year 2005 [136, 28, 7].

The impact of aircraft plume-scale processes on aviation-attributable ozone in global-scale models has been previously studied [86, 96, 17, 95, 42, 59]. These studies found that global-scale models overestimate the aviation-induced ozone perturbation by up to 20% at mid and high latitudes and nitrogen oxides perturbation by up to 35% in the North Atlantic Flight Corridor (NAFC) because aircraft emissions are instantaneously diluted into coarse grid cells (~100 km x 100 km) [69]. This prevents the model from resolving the small-scale non-linear processes in aircraft wakes that occur over the plume dimensions (~100 m up to ~50 km). Prior evaluation of the impact of plume-scale processes focused on upper-tropospheric ozone but the effects of aircraft plume-scale processes at the surface are unknown. Furthermore, no study quantifies the role of plume-scale processes on air quality and the Earth's climate. To accurately estimate and to prevent any overestimation of aviation's environmental response from instant dilution approximations, the role of aircraft plume-scale processes needs to be assessed. Previous assessments of aircraft plume-scale processes have used Gaussian plume models to represent subgrid-scale aircraft processes. Gaussian plume models represent a plume as an homogeneous cross-section evolving under idealized conditions [86, 96]. This approach fails at reproducing plumes or contrails with large spatial gradients that can arise either from non-linear chemistry or from microphysics of modal aerosols. In this thesis, I use a recently-developed aircraft plume model [42] to resolve plume-scale processes in aircraft wakes and calculate the discrepancies introduced with respect to the instant dilution approach. I then calculate the emission corrections to account for plume-scale processes for a large number of background and meteorological conditions, and aircraft and engine parameters. Finally, I develop an emission tool embedded in a chemistry transport model to process any aviation emission inventory to account for plume-scale processes and use this processing tool to estimate the impact of plume-scale processes on the environmental response of aviation emissions.

Next, recent renewed interest in supersonic aviation has raised concerns regarding stratospheric ozone damages from high-speed civil aircraft [8, 2]. Indeed, stratospheric

ozone is vital to human health as it dampens the surface UV flux, which can cause melanomas. Many studies have previously studied the impact of supersonic commercial aviation and the scientific literature on their atmospheric and climate impact is abundant [102, 48, 27, 111, 138]. However, the results from these studies use specific supersonic aviation scenarios and are subject to uncertainties in the fleet size, engine characteristics, and chosen commercial routes. In this thesis, I generate sensitivities of total ozone column, which allow for rapid evaluation of any aviation emission inventory. Furthermore, no previous studies consider pathways to minimize changes in total ozone column. Using these sensitivities, I derive a column ozone-neutral altitude, at which aviation emissions would lead to no net change in surface UV flux. This thesis is the first assessment of a globally-averaged column ozone-neutral altitude, alongside its sensitivity to fleet-wide emission characteristics and its dependency on plume-scale processes. The column ozone-neutral altitude is obtained from decadal adjoint sensitivities of a model of tropospheric-stratospheric chemistry, which I develop and validate in this thesis. Subsonic aircraft activities, which have been shown to lead to increased ozone column [28], could also be net ozone neutral by flying at this altitude.

Finally, chemistry transport models (CTMs) have been used extensively to evaluate the chemical response to aviation emissions [65, 7, 32, 64, 28, 15]. All CTMs from the previous studies find a surface ozone and particulate matter response owing to commercial aviation emissions, ranging from 0.17 to 0.52 parts per billion (ppbv) and 0.0034 to 0.0070 $\mu g/m^3$ respectively for the year 2006 [15]. However, CTMs are not able to capture the meteorological feedback associated with environmental response of aviation emissions. To capture both chemical and meteorological responses from aircraft activities, previous studies have used global climate models (GCMs) to investigate the coupled chemistry-climate feedback from aviation emissions [60, 15]. Using a GCM, a study found that there might be significant magnifying effects from atmospheric feedback [60]. According to this study, commercial aircraft emissions are found to increase in upper-tropospheric stability, and lead to surface ozone and dry particulate matter responses of 0.046 ppbv and 0.083 $\mu g/m^3$ [60]. However, a more recent study and larger model intercomparison suggested that the results from GCMs have too much variability to resolve any such atmospheric feedback

[15]. Other single-model studies have not found any coupled chemistry-climate feedback from aviation emissions based on single model evaluations. In this thesis, I resolve the discrepancy between GCMs and CTMs over the response from aviation emissions and I estimate if coupled chemistry-climate effects have an amplifying impact on aviation's response, as suspected by a previous study [60]. To study the climate feedback due to aviation emissions, I couple a CTM to a GCM. After validating the newly-developed model against atmospheric observations and other model results, I perform ensemble runs to evaluate to what extent are the climate feedbacks from aviation emissions significant in the evaluation of the environmental response to aviation emissions.

1.2 Thesis contribution

In this thesis, I address the three scientific literature shortcomings addressed previously: the role of plume-scale processes on the environmental impact of aviation emissions, the identification of a column ozone-neutral altitude, and the evaluation of the coupled chemistry-climate pathways affecting the aviation's atmospheric response. The main contributions of this thesis are:

- **Assessment of the role of plume-scale processes in the long-term environmental impact of aviation emissions**. Given the relatively coarse resolution used in global models, highly-concentrated sources of emissions, such as individual flights, cannot be resolved in the current generation of chemistry transport models [86, 96, 59, 17]. In Section 2, I develop an approach to account for aircraft plume-scale processes when evaluating aviation's environmental responses. This is achieved by (1) using an aircraft plume model to evaluate the in-plume chemical conversions of pollutants [42], (2) establishing a look-up table of in-plume ozone production, nitrogen and sulfur conversion factors, and (3) propagating these conversion rates to a global-scale chemistry transport model. This allows me to quantify the magnitude of the impact of aircraft plume-scale processes on tropospheric ozone and surface air quality.

- **Identification of a column ozone-neutral altitude for commercial subsonic and**

supersonic aviation. Previous reports on the impact of supersonic aviation on the ozone layer have concluded that aviation emissions in the lower stratosphere lead to the depletion of the ozone layer [102, 111, 48, 27]. In contrast, subsonic aviation has been shown to increase the oxidizing power of the troposphere, thus increasing tropospheric ozone levels [7, 28]. In this thesis, I quantify the column ozone-neutral altitude by (1) extending and validating an adjoint model of atmospheric chemistry to include stratospheric chemistry, (2) computing decadal sensitivities of globally-averaged column ozone to emissions, and (3) evaluating the sensitivity of the column ozone-neutral altitude to fleet-wide emission characteristics, emission location, and the inclusion of plume-scale processes.

- **Evaluation of the climate feedback of aviation emissions on the atmospheric composition**. Studies of the environmental impact of aviation emissions using global climate models have found different results. Using a global climate model, a study found that coupled chemistry-climate effects magnify the atmospheric response to aviation emissions [60]. Another study found that global climate models have too much inner variability to capture any coupled feedback between atmospheric chemistry and meteorology [15]. In this thesis, I evaluate the chemistry-climate interactions in response to aviation emissions by (1) coupling a chemistry transport model with a global climate model, (2) validating this coupled model against atmospheric observations and other global models, and (3) performing ensemble runs to evaluate the atmospheric response from aviation emissions and examine the relevance of climate feedback.

Overall, this thesis bridges the gap from aircraft plume-scale effects to the global-scale environmental impact of aviation emissions by developing and validating new approaches and models.

Chapter 2

Impacts of plume-scale treatment of aviation emissions on atmospheric composition

This chapter focuses on the role of plume-scale effects on the environmental impact of aviation emissions. Section 2.1 focuses on motivating this research area and presents the corresponding literature review. The methods are introduced in Section 2.2 and the results are presented in Section 2.3. Section 2.4 consists of a discussion about the results and limitations of this research topic.

2.1 Introduction

Commercial aviation emissions represent the only anthropogenic source of emissions in the upper troposphere / lower stratosphere (UTLS), and are thus characterized by a disproportionate environmental impact compared to surface emissions, on an emission mass basis. The release of atmospheric pollutants from such aircraft activities drives changes in both air quality and the Earth's climate.

Aviation emissions interact with the background atmosphere and induce upper-atmospheric localized chemical and microphysical perturbations persisting for hours up to several days [86]. Current generation CTMs fail to represent the small-scale, non-linear effects of

highly-concentrated aircraft plumes, given the relatively coarse spatial resolution. These global models simulate the release of aircraft emissions by instantly and homogeneously diluting highly-concentrated plumes into large grid cells, which are typically three or four orders of magnitude greater than the initial plume size [10, 85, 37, 16].

Previous studies have identified the modeling discrepancies and quantified the introduced bias between the instant dilution approach of emissions, as performed by CTMs, and a plume-scale treatment [86, 96, 70, 17, 16, 42]. These studies have found that the instant dilution approach of aircraft emissions leads to an inaccurate assessment of the plume's long-term environmental impact, as this assumption leads to enhanced modeled ozone and lower remaining fraction of in-plume NO_x.

Despite the number of studies on aircraft plume-scale processes, only a few have propagated the results of the plume-scale effects to a global model [69, 59]. These studies have found a decrease in the aviation-attributable ozone perturbation up to 15-18% at Northern mid and high latitudes [69]. Additionally, the perturbations of NO_x are reduced by 25 to 35% over the North Atlantic Flight Corridor [69]. The other study, even though using a different parameterization, has found similar changes in atmospheric composition due to the plume-scale correction applied in global CTMs [59].

2.2 Methods

In this section, I present the methods used to evaluate the environmental impact of aircraft plume-scale processes. I use an aircraft plume model to estimate plume-scale conversions and production of ozone, NO_x and sulfur. I then estimate the global-scale impact of aircraft plume-scale processes using a CTM with two different approaches. The first approach, whose results are presented in Section 2.3.1, uses an external processor to derive an aviation emission inventory accounting for plume-scale processes. For Section 2.3.2, I develop an embedded tool in a CTM that generates an aviation emission inventory accounting for plume-scale processes.

Previous studies have looked at the effect of modeling the aircraft plume compared to instantaneous dilution of emissions in large grid cells (~100 km), which is commonly

done in global or regional CTMs [16, 96, 17, 95]. The Gaussian plume approximation has been previously applied to power plant and ship plumes [41, 87, 4, 126] and then extended to aircraft plume models [70, 66, 96, 127]. In such models, the plume is discretized in a number N ($N < 15$) of concentric elliptic rings in which chemical concentrations are assumed to be constant. These rings can grow over time to model plume dispersion. This approach is computationally cheap as the time required by chemistry and transport are reduced. An intermediate approach is to adopt a fixed ring discretization, where plume growth and aerosol dynamics are performed on a finer grid, as described on Figure 2-1. The plume model used in this thesis, APCEMM, follows this approach, and has been used to study pollutant dispersion and contrail evolution over the course of the plume lifetime [42].

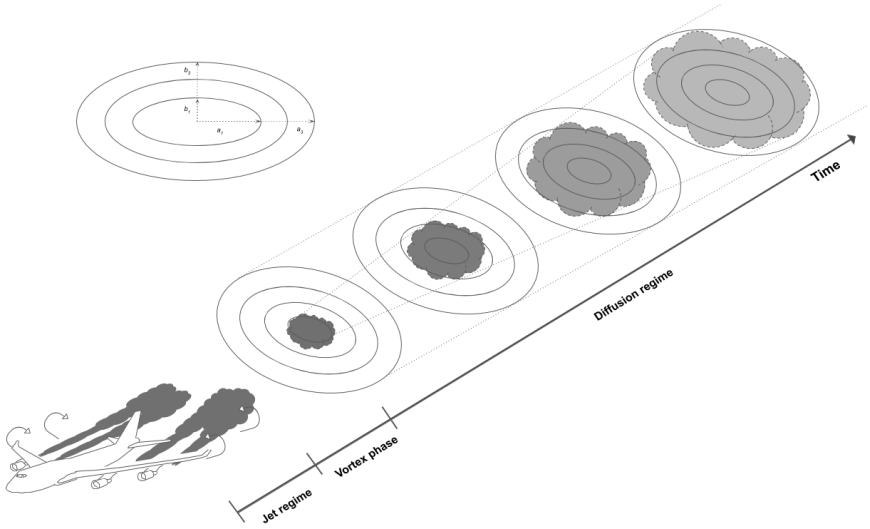

Figure 2-1: Schematic of the discretized ring approach used in APCEMM [42].

2.2.1 Modeling of changes in chemical composition in individual aircraft plumes

The aircraft plume model, APCEMM, models the plume growth, chemistry and microphysics at a fine scale (~100 m horizontally x 20 m vertically). The instant dilution approach instantly dilutes highly-concentrated sources of emissions into a large grid-box.

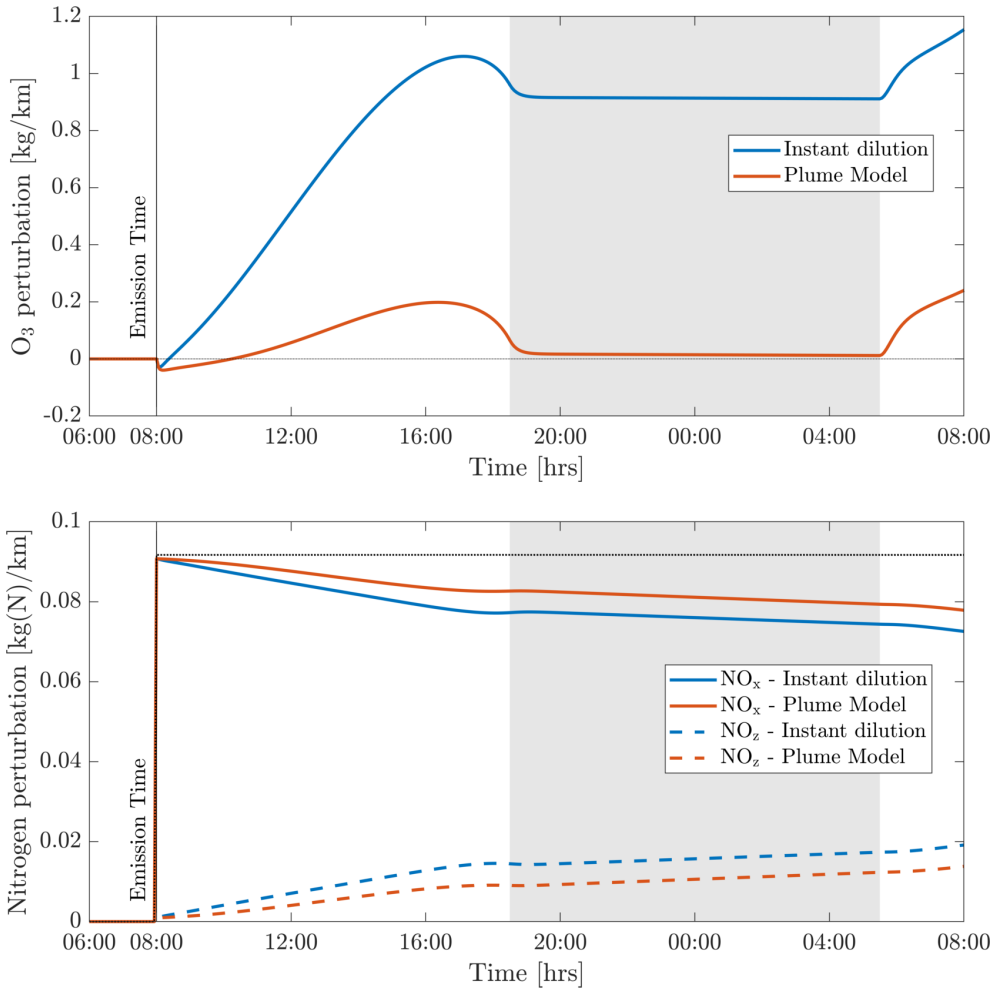

Figure 2-2: Perturbations in ozone (O_3), nitrogen oxides (NO_x) and the nitrogen reservoir species (NO_z) according to simulations using an instant-dilution approach and the APCEMM plume model [42]. Emissions are released at 08:00 local time in a polluted environment. The dotted black line represents all nitrogen species (NO_y), which is conserved. The shaded areas correspond to nighttime.

Figure 2-2 presents the ozone and nitrogen chemical responses of the instant dilution approach and the plume model simulation, over the first 24 hours after the initial release, assuming meteorological conditions at approximately 11 km, where subsonic aircraft cruise. The emission characteristics are chosen to represent a B747-8 equipped with General Electric next-generation (GEnx) engines. The instant dilution approach overestimates the amount of in-plume ozone production and the NO_x conversion rates, thus underestimating the remaining fraction of in-plume NO_x. The discrepancies between both approaches are due to the concentration of HO_x (HO_x = OH + HO_2) in the first few hours after emissions.

Parameters	Unit	Number of samples	Range	
			Minimum	Maximum
Temperature	K	10	210	250
Pressure	hPa	8	10 (30 km)	700 (3 km)
Latitude	°N	6	-90	90
Emission Day (cyclical)	-	6	1	365
Emission Time (cyclical)	hr	4	0	24
Total NO_x flow	g(NO_2)/m	11	0	2.36
Background NO_x	pptv	4	50	500
Background O_3	ppbv	5	50	1000

Table 2.1: Parameters used in look-up table. Cyclical here refers to the fact that the dimensions are treated as periodic (e.g. 24:00 and 00:00 are treated as identical).

In APCEMM, the plume becomes HO_x-limited, thus lowering the amount of produced ozone and NO_x conversion rates to reservoir species. A description of the different plume chemical regimes is provided in the literature [42, 110, 126].

Using APCEMM, a parameterization of plume-scale effects has been established for inclusion in global models. The chemical discrepancies between APCEMM and the instant dilution approach are found to be most influenced by the parameters listed in Table 2.1. I choose the parameters in Table 2.1 based on a sensitivity study varying each variable input in APCEMM. I find that latitude is a key variable that influences the in-plume ozone production and remaining NO_x fraction. The latitude of the flight affects how much sunlight an aircraft plume receives over a 24 hour time period. The noon-time photolysis rates and background mixing ratios also depend on the latitude of the flight. I exclude other parameters (such as longitude of the flight or background sulfur) because they modify the 24 hour ozone and NO_x plume concentrations by less than 2%. Parameters such as pressure, latitude, emission day, total NO_x flow, and background ozone and NO_x are not evenly sampled in the look-up table, while temperature and emission time have uniform increments. I then run APCEMM for ~2.5 million cases spanning the ranges of each parameter listed in Table 2.1, changing one parameter at each new case. The chemical output of ozone, NO_x, HNO_3, and HNO_4 are saved into a look-up table as a function of the input parameters. The look-up table consists of a netCDF file of 39 MB.

Table 2.1 lists out parameters that matter when evaluating the in-plume ozone pro-

duction and remaining NO_x fractions. Regarding in-plume sulfur, I carried out additional APCEMM simulations to compute the conversion rates of sulfur dioxide to sulfuric acid. This conversion process is found to be most dependent on the seasonality, and meteorological conditions, but is found to be independent of background concentrations.

2.2.2 Implementation of a plume-scale treatment of aviation emissions in a global chemistry transport model

This section describes the implementation detail of the correction to aviation emissions due to aircraft plume-scale effects in the global CTM GEOS-Chem version 13.0.0. Even though this chapter performs the atmospheric simulation using the GEOS-Chem model, the computation of corrected emission fluxes to account for plume-scale effects could be repeated in other CTMs, or even performed externally using archived meteorological data. GEOS-Chem uses the Unified Chemistry eXtension to explicitly model both the troposphere and stratosphere, thus allowing for chemical responses due to high-altitude emissions [29]. The Modern Era Retrospective analysis for Research and Applications version 2 (MERRA-2) is a satellite-era global reanalysis produced by NASA's Global Modeling and Assimilation Office (GMAO) spanning from 1980 to present. The intent of MERRA-2 is to assimilate space-based observations combined with the Goddard Earth Observing System (GEOS) atmospheric model and data assimilation system (DAS) [104]. The MERRA-2 reanalysis provides a record of the global atmosphere and land and ice surface representation [44, 104]. In this section, I use MERRA-2 to drive GEOS-Chem.

GEOS-Chem uses HEMCO to calculate emissions from different sources, regions and species (Keller et al. 2014). Previous emission extensions have been applied within HEMCO to deal with emission processing, such as lightning, biogenic or dust emissions [90, 50, 26]. A plume parameterization of ship emissions has been previously implemented in GEOS-Chem [126, 58]. I here implement the PaNiC emission extension as an extension of HEMCO to account for a plume-scale treatment of aircraft emissions. This extension interpolates emission corrections from the look-up table using meteorological conditions and chemical concentrations taken from GEOS-Chem and the grid-cell averaged NO_x emission

rate. This allows the substitution of the grid-cell emissions with the 24-hour plume concentrations, at which point the aircraft wake is sufficiently diluted to neglect any chemical non-linearities. This plume-scale treatment leads to emission corrections of NO_x, HNO_3, HNO_4, O_3, SO_2, and sulfuric acid. NO_x is partitioned into NO and NO_2 based on the background NO to NO_x ratio. I assume a constant fuel sulfur content of 600 parts per million on an elemental sulfur mass basis [105]. This plume-scale treatment of emissions is only applied between 500 and 10 hPa. Subsonic aircraft cruise pressures are in the range of 200 to 250 hPa (corresponding to an altitude range of 10 to 12 km). Outside of the 500 to 10 hPa range, a conversion fraction of SO_2 to sulfuric acid of 2% is applied, corresponding to the chemical production of H_2SO_4 in the aircraft engines and early-plume [55, 7]. The plume-scale extension conserves the emitted mass of nitrogen and sulfur (on an NO_2 and sulfur mass basis respectively). Seasonal variations of the remaining fractions of in-plume NO_x are presented in the Appendix A.1.

To apply corrections to aviation emissions, the first steps consist of acquiring the species concentrations and meteorological data required by the look-up table. The aviation emission inventories include the gridded emission fluxes for each emission species (NO_x, CO, hydrocarbons) expressed in kg/m^2/s. The next steps evaluate the gridcell-averaged NO_x mass per distance flown, in g/m, interpolates from the look-up table to estimate the correction, and then converts this value back to a corrected emission flux, in kg/m^2/s.

By averaging the NO_x mass per distance flown in each gridcell, I represent all the flights in a given gridcell as a single flight with the same averaged NO_x flow, which can be a limitation of the proposed method in gridcells with a large number of flights. Indeed, the look-up table provides the correction that needs to be applied for a single aircraft. An alternative would be to run the plume-scale processing step at the resolution of the aviation emission inventory, which is often finer than the model grid. This feature is currently being developed in GEOS-Chem [78].

The process described can either be used to compute a processed emission inventory externally by using archived meteorology and species concentrations, or embedded in a CTM, thus computing the corrections due to plume-scale processes during the model run. The embedded approach consists of implementing the flow process in HEMCO as an emis-

sion extension.

2.2.3 Simulation setup

The commercial aviation emission inventory is derived for the year 2015 from the Aviation Emissions Inventory Code (AEIC) [109, 112] and consists of ~220 Tg of fuel burn and 3.93 Tg NO_x (on a NO_2 mass basis). More details on the geographical distribution of commercial aviation emissions are provided in Appendix A.2.

To evaluate the long-term atmospheric response on upper-atmospheric composition and surface pollutant concentrations, I perform three five-year GEOS-Chem simulations, one without aviation emissions, one with aviation emissions and accounting for plume-scale processes, one with aviation emissions but without plume-scale treatment. The three simulations aim to quantify the role of plume-scale processes in the assessment of aviation emissions' impacts on atmospheric composition. The five-year integration time allows for the aviation-attributable ozone response to vary by less than 5% in simulation years 3 to 5. All GEOS-Chem simulations use a horizontal grid resolution of 4° x 5°. The vertical grid consists of 72 layers between the Earth's surface and 1 Pa (corresponding to ~80 km in pressure altitude). Chemistry is performed up to 1 hPa (~50 km) above which a simplified chemical representation is applied in the mesosphere. I also evaluate the change in aviation-induced radiative forcing from plume-scale processes by running GEOS-Chem with RRTMG (Rapid Radiative Transfer Model for General Circulation Models) for each first day of the month, to lower computational resources [52]. The simulations are summarized as following:

- Simulation 1: baseline, five-year run with default aviation emissions (non-processed)
- Simulation 2: same as Simulation 1, but without aviation emissions
- Simulation 3: same as Simulation 1, but with aviation emissions processed using the look-up table

2.3 Results

This section presents the changes in atmospheric composition due to plume-scale chemistry effects in aircraft wakes.

In Section 2.3.1, the correction in emission fluxes due to plume-scale effects are calculated externally using archived species concentrations and meteorology from MERRA-2 and fed into the GEOS-Chem model. In Section 2.3.2, the process flow is implemented in HEMCO as an emission extension module, thus enabling the calculation of emission corrections during the model run.

The two approaches presented in this section assume that the aircraft emission inventory is available at a fine resolution. A gridcell-averaged NO_x flow is computed from the total NO_x emissions and distance flown, thus replacing all flights with a single flight with the same NO_x flow as the gridcell average.

2.3.1 External coupling

In this section, I apply the process flow using archived monthly-averaged species concentration as well as meteorology from MERRA-2. I process the default aviation inventory to generate an emission inventory that accounts for plume-scale processes. This updated inventory is used in Simulation 3 only. Simulation 1 uses the default aviation emission inventory.

The zonally-averaged ozone volumetric mixing ratio changes due to aviation emissions, while accounting for plume scale processes, are shown in Figure 2-3. The average is performed over the last four years of the simulation to allow for sufficient spin-up time. An increase in ozone concentrations can be seen through the troposphere, with a maximum of ~16 ppbv reached around subsonic cruise altitudes between 30°N and 90°N. The relative increase is greater at lower altitudes, reaching a maximum in the descending branch of the Hadley cell, in agreement with previous studies [7].

Subsonic aviation emissions lead to a different response in the stratosphere. In the lowest part of the stratosphere, below 25 km, there is a positive ozone response, while, at higher altitudes in the tropics, ozone is depleted through catalytic chemical cycles. I

find a small increase in stratospheric ozone in extra-tropical regions of ~1 ppbv. This ozone depletion occurs more than 15 km higher than the altitude at which subsonic aviation emissions are released. This shows that aviation emissions are transported and that their effects are not localized.

The tropospheric response displays a strong hemispheric asymmetry, while the stratospheric response displays a more symmetric pattern around the Equator. In the troposphere, the ozone response is largest where most aviation fuel is burnt, at mid and high northern latitudes and at ~11 km. I observe a 2 ppbv perturbation in the Southern Hemisphere, while it reaches 15 ppbv in the Northern Hemisphere, in the 10 to 12 km altitude band. In the stratosphere, the aviation-induced ozone perturbation reaches -5 ppbv in tropical regions, while I find that extra-tropical regions are characterized with an increase of ~1 ppbv. I find that the ozone perturbation in the stratosphere is better distributed across both hemispheres than in the troposphere. A possible explanation is that aviation emissions enter the stratosphere through the Brewer-Dobson circulation and are thus distributed more evenly between the North and South Hemisphere.

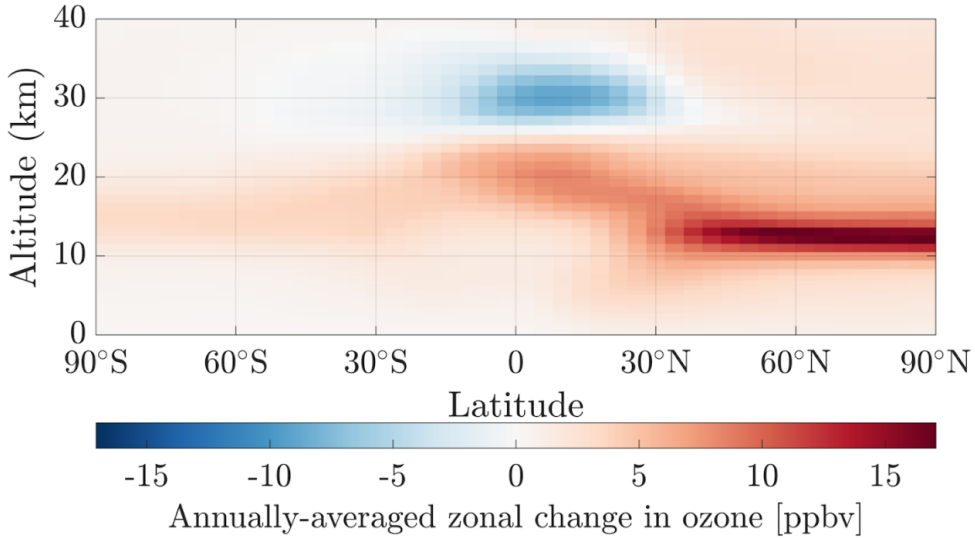

Figure 2-3: Zonally-averaged ozone perturbation from aircraft emissions after accounting for the non-linear processes in aircraft plumes. The averaging is performed over the last four years of a five year run, allowing for one year of spin up.

Figure 2-4 shows the change in the aviation-attributable ozone response due to the inclusion of plume-scale processes. The reduction is change is computed as following:

$$\frac{[O_3]^{(3)} - [O_3]^{(2)}}{[O_3]^{(1)} - [O_3]^{(2)}}, \tag{2.1}$$

where $[O_3](i)$ represents the ozone concentration as evaluated by GEOS-Chem in Simulation i (i between 1 and 3).

The aviation-attributable ozone response is decreased throughout the troposphere by ~8% due to the inclusion of plume-scale processes. The reduction is stronger in the Northern Hemisphere, especially at the subsonic cruise altitudes, where it reaches a reduction of 10%. At the surface, the change is smaller with a reduction of ~5%. Previous studies have found a reduction in the ozone response due to aircraft emissions by up to 18% at subsonic altitudes and northern middle and high latitudes [69]. From the simulations carried out, a ~5% reduction in surface $PM_{2.5}$ is observed.

In the stratosphere, a reduction of 20% in aviation-attributable ozone can be observed in the tropical region. An increase in the aviation-induced ozone response can be observed in the 45°N-90°N latitude band at 20 km. However, the magnitude of the positive ozone response does not exceed 10%.

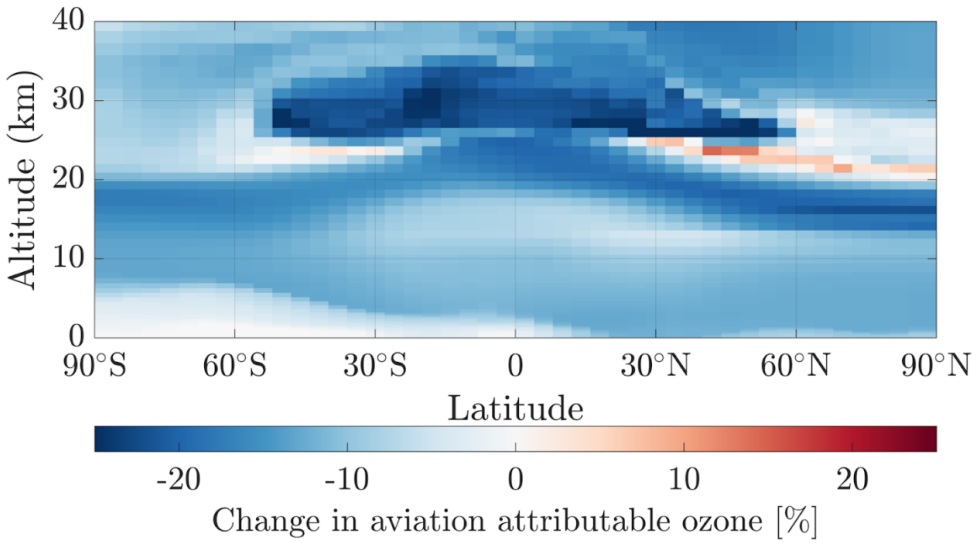

Figure 2-4: Zonally-averaged change in the aviation-attributable ozone from the inclusion of a plume-scale processing of aviation emissions. The averaging is performed over the last four years of a five year run, allowing for one year of spin up.

2.3.2 Embedded coupling

In this section, I embed the methods described in Section 2.2.2 within the emission routines of GEOS-Chem. This allows the use of species concentrations as computed by the model and the use of high-frequency and spatially-refined meteorology.

Emission diagnostics

This section presents the changes in aviation emissions, as calculated by GEOS-Chem, due to the introduction of a plume-scale processing routine. For this section, I implemented an emission extension in HEMCO that processes aviation emissions to include for plume-scale processes, as described in Section 2.2.2. The results in this section are obtained by saving out emission diagnostics from the embedded processing tool in HEMCO and by taking the difference between three GEOS-Chem runs, as described in Section 2.2.3.

Figures 2-5 and 2-6 present the emission diagnostics archived by the GEOS-Chem simulation with the plume-scale processing of aviation emissions (Simulation 3). Figure 2-5 displays zonally-averaged NO_x remaining fractions as estimated by the model meteorology and calculated concentrations. The results are broken down by season. I find that the 24-hour NO_x remaining fraction is correlated with background temperatures in agreement with previous studies [42, 127]. I also show that this fraction reaches a minimum at lower altitudes in the tropical region due to the warmer air, promoting the conversion of NO_x to nitrogen reservoir species. This agrees with the past literature, which found a reduced lifetime of NO_x (against conversion to HNO_3) at lower altitudes of ~3 days at 8 km, compared to ~10 days at 12 km [61].

Because of the coarse computational representation, modern-day CTMs fail to accurately capture the in-plume ozone changes in aircraft wakes. In-plume ozone is the sum of a NO titration effect (depleting ozone on a short time-scale) and long-term day-time ozone production. Figure 2-6 shows the zonally-averaged ozone changes introduced into GEOS-Chem due to plume-scale processes. I first observe that the ozone production scales with incoming sunlight, leading to greater ozone production in tropical areas. The peak ozone production occurs South of the Equator during the North-Hemispheric winter sea-

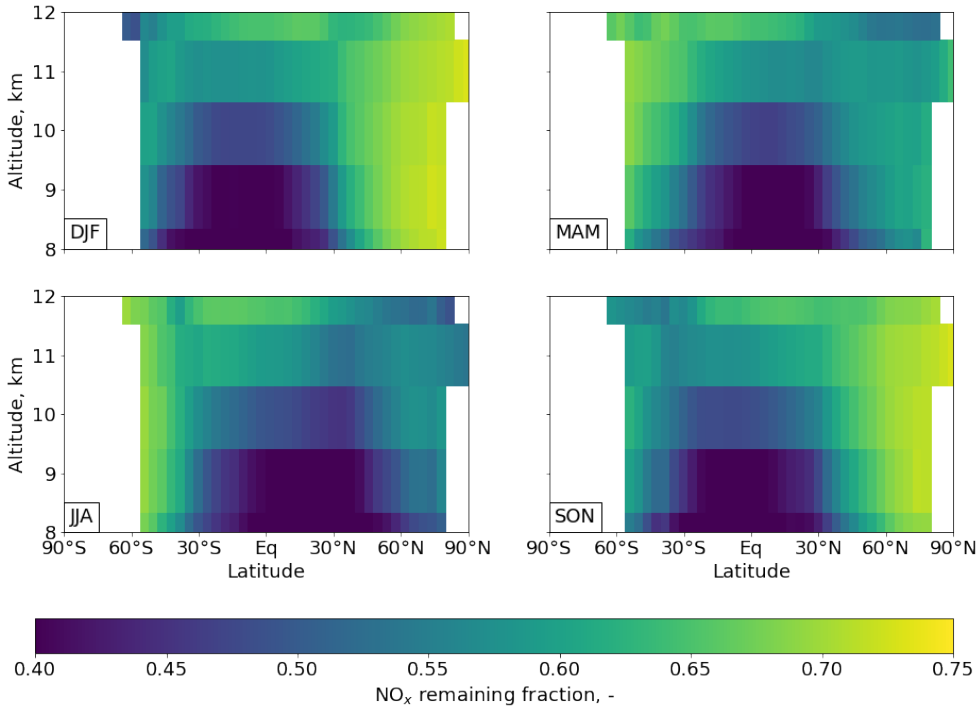

Figure 2-5: Zonally-averaged 24-hour NO_x remaining fractions owing to plume-scale processes in aircraft wakes as computed by GEOS-Chem. The average is only performed in regions where aviation fuel burn is non-zero.

son (DJF) and slightly North of the Equator during North-Hemispheric summer (JJA). I also find that day-time ozone production increases with lower altitudes [42]. I show that flights at high latitudes (60°N-90°N) during the North-Hemispheric winter are characterized with net negative ozone change, as the ozone loss due to the titration effect overcomes the day-time ozone production, due to the scarcity or absence of sunlight.

The inclusion of plume-scale processes for aviation emissions leads to the conversion of 0.77 Tg of NO_x to nitrogen reservoir species (on a NO_2 mass basis), emitted as either HNO_3 or HNO_4. Additionally, plume-scale effects lead to the production of ~7 Tg of ozone, corresponding to an average ~1.8 g(O_3) per emitted grams of NO_x (on a NO_2 mass basis).

Changes in upper-tropospheric composition

This section presents changes in upper-atmospheric composition owing to aviation plume-scale processes. The left panel of Figure 2-7 shows the environmental response of ozone

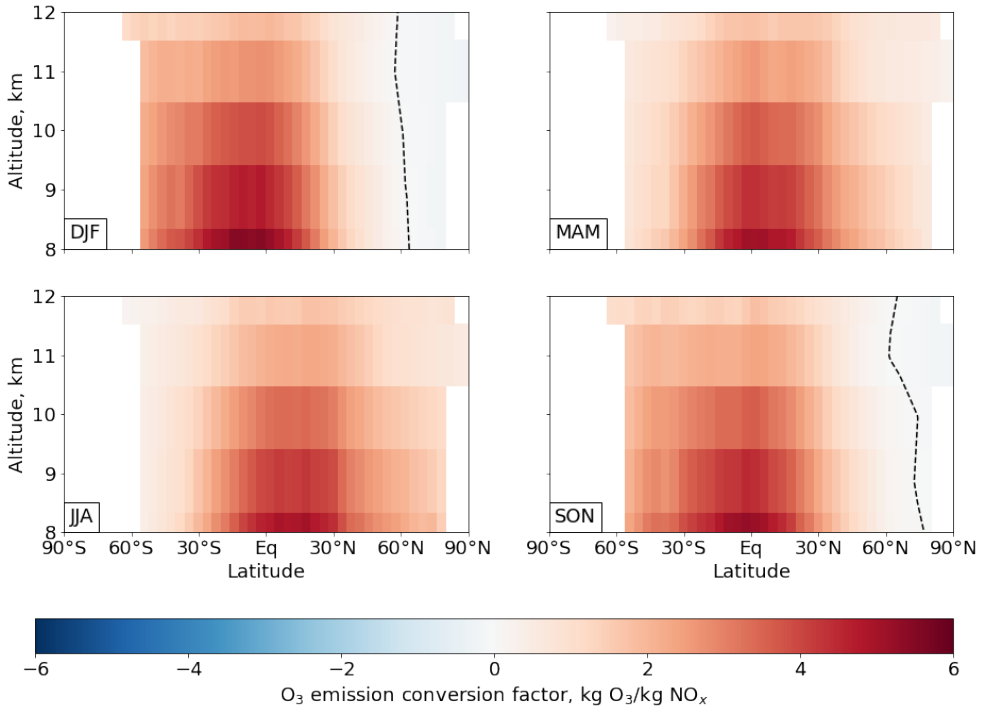

Figure 2-6: Zonally-averaged 24-hour ozone production owing to plume-scale processes in aircraft wakes as computed by GEOS-Chem. The average is only performed in regions where aviation fuel burn is non-zero. The dashed line represents the isoline of net zero ozone production.

volumetric mixing ratios to aviation emissions. Subsonic aircraft emissions lead to an increase in tropospheric ozone concentrations, in agreement with previous studies [28, 31, 64, 7]. The greatest increase in ozone mixing ratio can be found in the 10 to 12 km altitude band (near cruise altitudes) and at latitudes between 30°N and 90°N. At lower altitudes, the aviation-induced changes in ozone mixing ratios are smaller in absolute terms, but still reach ~2-3 parts per billion in the descending branch of the Hadley cell [7]. The contribution of plume-scale processes to the aviation-induced ozone response are shown in the middle panel of Figure 7. This environmental feedback is the compound response due to reduced aircraft NO_x emissions (due to the in-plume chemical conversions), reservoir nitrogen and ozone emissions, as well as a repartitioning of emitted sulfur into SO_2 and sulfate aerosols. The ozone response owing to plume-scale processes is negative at all altitudes, corresponding to ~2% of the local change due to aviation emissions at cruise altitudes. Plume-scale processes lead to the depletion of tropospheric ozone but seasonal

patterns vary. The annually-averaged relative change in aviation-attributable ozone due to plume-scale processes is displayed in the right panel of Figure 2-7. I find that this relative change lies within ±5% of the total aviation-induced ozone, but seasonality influences the magnitude of the ozone response.

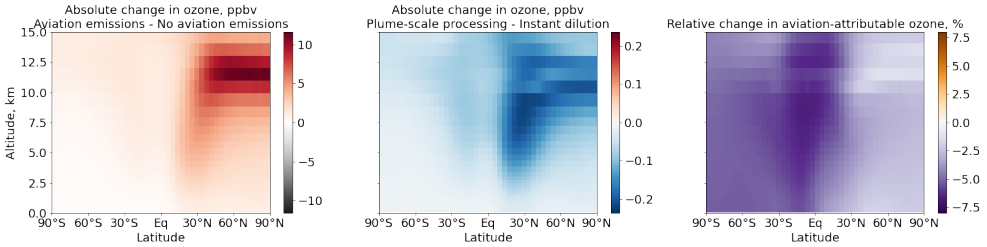

Figure 2-7: Absolute change in zonally-averaged ozone mixing ratios due to aviation emissions (left), due to plume-scale processes in aircraft wakes (middle). The relative change in aviation-attributable ozone is displayed in the right panel. All figures are plotted with different color scales. The averaging is performed over the last four years of a five year run, allowing for one year of spin up.

The seasonal dependence of the role of plume-scale processes is shown in Figure 2-8, in which the North-Hemispheric relative change in aviation-attributable ozone is compared for boreal winter (DJF) and summer (JJA). Previous studies have found that wintertime aircraft emissions lead to greater tropospheric and surface perturbations [75, 28, 114]. During winter, the ozone tropospheric lifetime is at its maximum, leading to enhanced aviation-attributable ozone at the ground [131]. Figure 2-8 shows that plume-scale processes lead to a negative ozone response at all latitudes in the Northern Hemisphere, extending from cruise altitudes to the surface. However, during summertime, the relative change is greater, reaching ~5-8%, compared to ~1-4% in the winter. I also find that the inclusion of plume-scale effects reduces the atmospheric NO_x concentrations at cruise altitudes, where aviation emissions can locally account up to 90% of the NO_x budget during boreal winter. This fraction goes down to ~80% after accounting for plume-scale processes. This reduction in NO_x concentrations is balanced by the release of by-products of in-plume chemistry, HNO_3 and HNO_4.

Finally, I find that the North-Hemispheric ozone column increases by 2.3 DU due to aviation emissions, however, the inclusion of plume-scale processes reduces the total ozone column by less than 50 mDU. The instantaneous top-of-the-atmosphere aviation-induced

longwave radiative forcing is reduced by 4%.

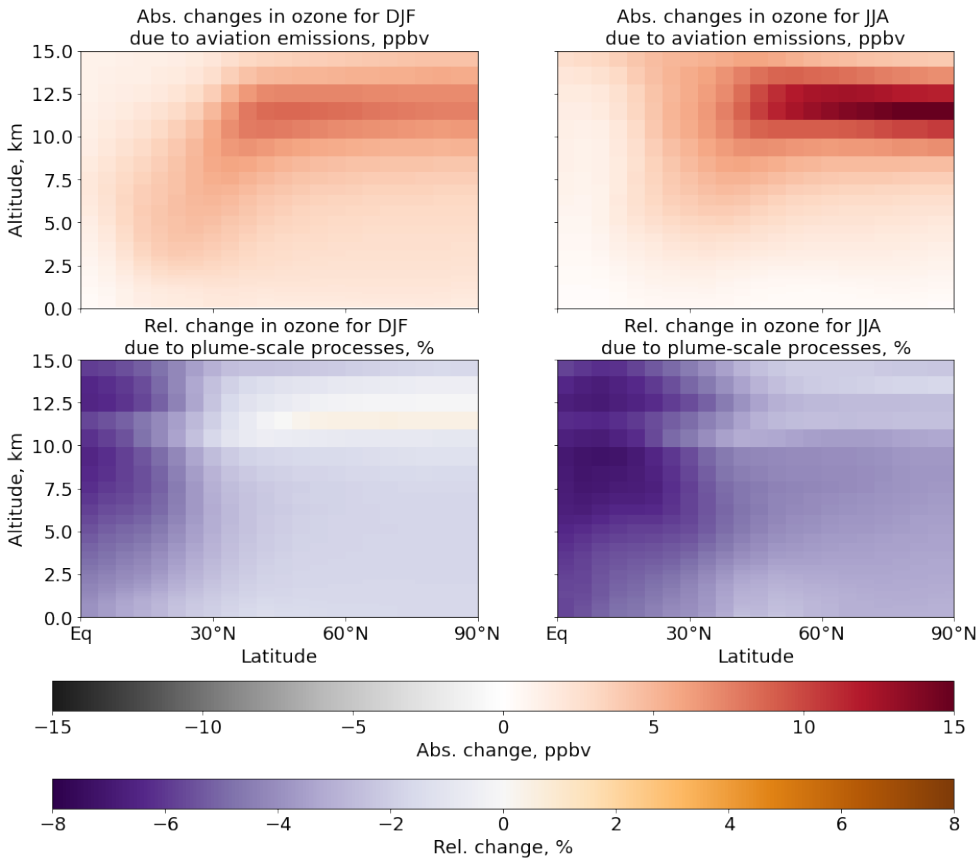

Figure 2-8: Seasonality dependence of the aviation-attributable ozone (top) and relative change owing to plume-scale processes (bottom) for North-Hemispheric winter (left) and summer (right). The averaging is performed over the last four years of a five year run, allowing for one year of spin up.

Changes in surface air quality

This section focuses on surface changes induced by aviation emissions and the contribution of plume-scale processes to ozone and particulate matter with a radius smaller or equal to 2.5 µm ($PM_{2.5}$), both of which are known to negatively contribute to human health [38, 11, 136]. Figure 2-9 displays surface changes in ozone volumetric mixing ratio due to commercial aviation emissions (top panel). I find that commercial aviation emissions lead to a population-weighted surface ozone perturbation of 0.73 ppbv, in agreement with previous studies [28]. The inclusion of plume-scale processes reduces the annually-averaged surface ozone perturbation by ~10-50 pptv (middle panel of Figure 2-9), with important

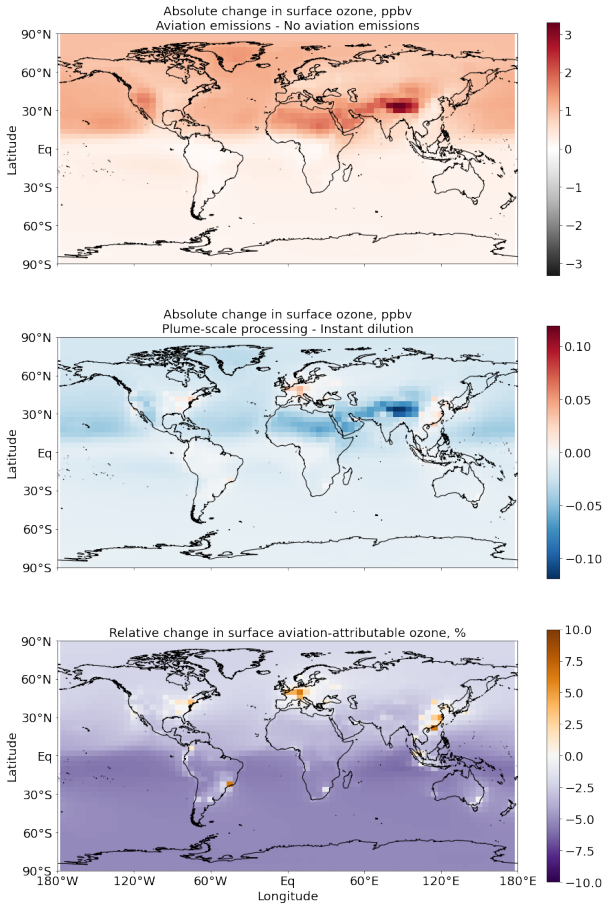

Figure 2-9: Changes in surface ozone volumetric mixing ratio due to commercial aviation emissions (top), due to plume-scale effects occurring in aircraft wakes (middle). The relative change in surface aviation-attributable ozone is shown in the bottom panel. Each plot uses a different color scale. The averaging is performed over the last four years of a five year run, allowing for one year of spin up.

spatial variations. Regions with large background NO_x concentrations and high-population density, such as Western Europe, South-East Asia or the New England area are characterized with increased ozone exposure after accounting for plume-scale effects from aviation. These regions of increased surface ozone are characterized by annually-averaged background NO_x mixing ratios greater than 8 ppbv. However, Northern India, which also has high background NO_x, does not experience an increase in aviation-attributable ozone from aircraft plume-scale processes. In regions with large NO_x and volatile organic compounds (VOCs) concentrations, a decrease in NO_x concentrations leads to enhanced ozone mixing ratios, as observed in previous studies linking decreases in NO_x emissions and aggravated

ozone air pollution [130].

The perturbations in surface $PM_{2.5}$ concentrations due to aviation emissions, and plume-scale effects are shown in Figure 2-10. I find that commercial aviation emissions lead to an annually-averaged, population-weighted increase of 0.095 μg/m^3 in the $PM_{2.5}$ exposure. The spatial variations are more heterogeneous compared to the aviation-attributable ozone response, as the $PM_{2.5}$ exposure is more concentrated in South-East Asia, India and Western Europe [28, 7]. Globally, the inclusion of plume-scale processes leads to no change in the population-weighted $PM_{2.5}$, however, this is due to both positive and negative contributions. The change in $PM_{2.5}$ exposure due to plume-scale effects corresponds to changes in surface concentrations of nitrates (NO_3^-). In regions of increased ozone, formation of $PM_{2.5}$ is enhanced, thus explaining the large $PM_{2.5}$ contributions over Europe and more moderately in East Asia.

2.4 Discussion and limitations

The change in the environmental response from aviation emissions due to plume-scale effects is evaluated by two different approaches. A look-up table containing the emission corrections is constructed using the APCEMM aircraft plume model, which enables the processing of the aircraft emission inventory to account for plume-scale effects.

I find that our plume-scale processing of aircraft emissions, whether processed externally or embedded in GEOS-Chem, leads to the conversion of ~40% of emitted NO_x to nitrogen reservoir species after 24 hours. To account for these plume-scale conversions, ~7 Tg of ozone are emitted, corresponding to 1.8 g(O_3) per emitted gram of NO_x. I also find that the season and location of emissions affect the NO_x conversion rates and in-plume ozone.

When processed externally, the aircraft emission inventory used in GEOS-Chem showed a ~8% decrease in the aviation-attributable ozone atmospheric burden. At subsonic cruise altitudes, the reduction in the ozone response reaches up to ~10%. This is in agreement with previous studies on the plume-scale impacts of commercial aviation emissions [69]. At the surface, aviation-attributable $PM_{2.5}$ and ozone exposure are reduced by ~5% with

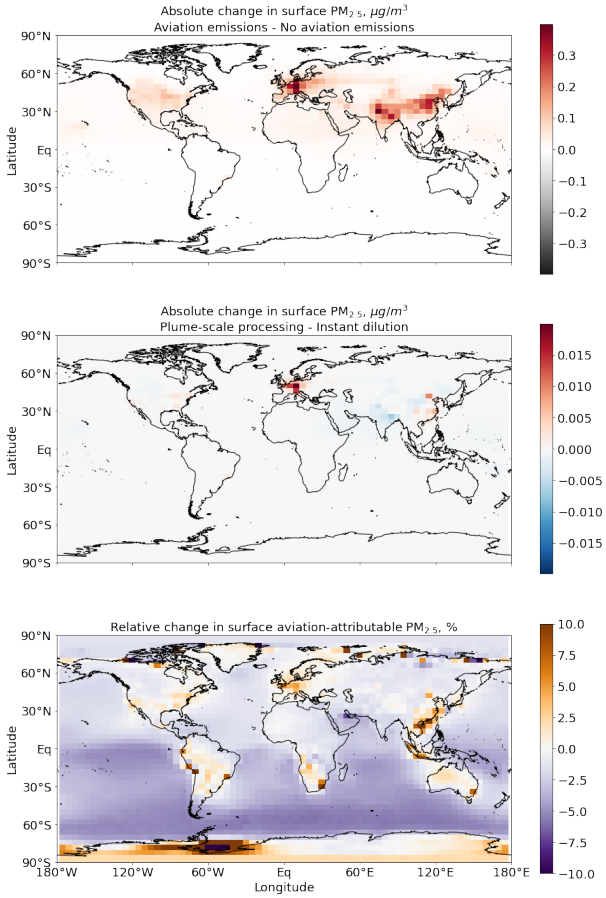

Figure 2-10: Changes in surface $PM_{2.5}$ mass concentrations due to commercial aviation emissions (top), due to plume-scale effects occurring in aircraft wakes (middle). The relative change in surface aviation-attributable $PM_{2.5}$ mass concentrations is shown in the bottom panel. Each plot uses a different color scale. The averaging is performed over the last four years of a five year run, allowing for one year of spin up.

spatial and seasonal heterogeneities.

By computing emission corrections during the model run, the embedded approach produces results that are in agreement with the external processing. With the embedded approach, I find that accounting for plume-scale processes leads to a reduction in the globally-averaged aviation-attributable ozone mass perturbation by ~5%, with non-negligible seasonal and spatial variations. I show that the plume-scale conversions of NO_x to HNO_3 and HNO_4 lower the aviation-attributable contribution to cruise altitude NO_x from 90% to 80% during Northern-Hemispheric winter. Additionally, I find that commercial aviation emissions lead to an increase in population-weighted ozone and $PM_{2.5}$ exposure by 0.73 ppbv

and 0.095 μg/m^3 respectively. Plume-scale effects contribute to reducing this ozone exposure by 10 to 50 pptv globally, while the change in population-weighted $PM_{2.5}$ exposure is negligible from plume-scale effects. I also show that this surface ozone and $PM_{2.5}$ change from plume-scale effects is spatially heterogeneous, with regions with high background NO_x experiencing increases in surface ozone and $PM_{2.5}$, while remote locations such as marine conditions are characterized by decreases in $PM_{2.5}$.

Chapter 3

Dependence of aviation's ozone impacts on altitude and exhaust composition

This chapter focuses on the different pathways influencing the ozone response to aviation emissions and introduces the notion of column ozone-neutral altitude, at which emissions would lead to a net zero change in column ozone. Section 3.1 presents the motivation for this research area, while Section 3.2 describes the validation of the adjoint model as well as the methods to estimate the column ozone-neutral altitude. In Section 3.3, I calculate a column ozone-neutral altitude and estimate its variations as a function of time, location of flight as well as emission characteristics. Additionally, in Section 3.3, I estimate the global ozone impact from individual contrails as well as its dependence on contrail location. Forward model estimates of the impact of aircraft induced cloudiness on atmospheric composition are limited given the lack of publicly-available contrail ice inventories. I also tie Section 2 to the present chapter by evaluating the impact of plume-scale processes on the column ozone-neutral altitude. In Section 3.4, I present some future steps for this research area and I discuss current limitations.

3.1 Introduction

The recent renewed interest in supersonic civil aviation from several private companies revives the environmental concerns related to high-altitude emissions from supersonic air-

craft [2, 8]. Previous commercial supersonic projects, such as the Concorde, were undermined by the growing fear of large-scale environmental damage from emissions at a cruise altitude of 18 km. Prior studies have quantified the magnitude of ozone depletion due to high-altitude emissions of supersonic aircraft with specified fleet size [21, 116, 102, 48]. A fleet of 500 aircraft for the year 2015 is for instance estimated to modify between -2.5% and +0.5% of the North Hemispheric ozone column [102]. These studies link emissions of NO_x to catalytic depletion of stratospheric ozone and mention a non-negligible contribution from emitted water vapor. A contribution from sulfur on total column ozone is also observed in previous reports [102], which finds that the inclusion of sulfur emissions doubles the ozone response for a supersonic fleet owing to NO_x and water vapor only. Recent work on the environmental impact of a new fleet of supersonic aircraft found that sulfur is responsible for ~50% of the ozone depletion for a cruise altitude of 17.5 km [111].

In contrast, a number of studies of subsonic commercial aviation, with cruise altitudes in the 10 to 12 km range, have found that subsonic emissions lead to a positive global column ozone contribution [28, 31, 64, 94, 15]. All the studies have found that nitrogen oxides are the dominant contributor to the global ozone response to subsonic aviation emissions. Additionally, the contribution of water vapor is found to be negligible, while sulfur is only responsible for a non-significant fraction of the total column ozone perturbation.

This variation in the behavior of aviation emissions leads to the hypothesis that there must exist an altitude at which aviation emissions lead to a net zero contribution to the global ozone column. This net zero change in column ozone would be explained by a balance between tropospheric ozone production and stratospheric ozone depletion. Both effects would be detrimental to public health, by either increasing the surface level of ozone and $PM_{2.5}$ or enhancing the amount of UV-radiation reaching the ground, and thus, heightening the incidence rate of skin cancer.

In this section, I build upon previous work on the GEOS-Chem Adjoint to implement stratospheric chemistry and further validate stratospheric chemistry. Prior work had produced an adjoint model which could only operate over short integration periods, but the model was unstable when the integration time was longer than two months [23]. Prior validations have only focused on comparing sensitivities from individual modules [23] but

no full-model validations of the GEOS-Chem Adjoint with stratospheric chemistry had been generated prior to this thesis. I further develop the GEOS-Chem Adjoint to allow for decadal simulations. In this chapter, I present the validation of full-model runs by comparing adjoint-derived to forward sensitivities. I then compute adjoint sensitivities of column ozone with respect to aviation emissions over a full decade, as required due to the longer lifetimes in the stratosphere. Additionally to direct aircraft emissions, I also examine the magnitude of the sensitivities to contrail ice surface area, despite the lack of global publicly-available contrail ice inventories. The derived adjoint sensitivities allow me to calculate a column ozone-neutral altitude for subsonic and supersonic aviation emissions. Finally, I evaluate the dependency of the column ozone-neutral altitude on emission composition and location, while also accounting for plume-scale processes.

3.2 Methods and model validation

The future market for the supersonic aviation industry is subject to significant uncertainties, whether related to the fleet size or the emission characteristics. Uncertainty quantification thus appears as a crucial cornerstone for this study. The evaluation of the environmental response of various emission datasets, each representing a different scenario for the aviation industry, through a CTM is computationally expensive as the number of key design variables is increased. Another approach is to estimate the sensitivity of the change in the simulated atmospheric composition to emissions using adjoint modeling. The adjoint of a CTM allows for the rapid environmental assessments of various aircraft designs, regulatory scenarios and market adoption while maintaining fidelity, and using emission datasets as input.

3.2.1 Adjoint modeling

Three-dimensional atmospheric CTMs can be used to quantify the natural and anthropogenic influences on the environment. Given the complexity of current CTMs and spatial and temporal variations in emission sources, estimating forward-based sensitivities is computationally expensive. Over the past two decades, adjoint-based models of 3-D regional

and global CTMs have been developed [88, 89, 107, 51, 53], used to constrain emission sources from measurements [19, 68, 140] and to assess atmospheric sensitivities to ozone and particulate matter exposure [108, 54, 46, 67, 6].

However, most of the recent work on adjoint-based CTMs has been focused towards estimating surface population exposure or constraining ground emission sources and no previous studies quantified sensitivities to stratospheric-oriented objective functions. Objective function here refers to the quantity that I want to estimate sensitivities to (e.g. sensitivity of column ozone to emissions). The introduction of the Unified Chemistry eXtension (UCX) in GEOS-Chem offers the potential to capture long-term stratospheric responses and to more accurately represent tropospheric-stratospheric exchanges [29]. The GEOS-Chem Adjoint had been lacking stratospheric capabilities and I present, in this chapter, the validation of the GEOS-Chem UCX Adjoint by comparing forward to adjoint-derived sensitivities. This validation step is necessary to make sure that the stratospheric ozone response is accurately captured, as supersonic aviation is known to lead to damages to the ozone layer [21, 102, 133].

3.2.2 Validation of full-model runs

The GEOS-Chem Adjoint consists of a forward and a differentiated model. The latter evaluates sensitivities around the "base" state of the atmosphere as computed by the forward component of the adjoint model. Validation of the GEOS-Chem Adjoint capabilities has been previously performed, but focuses on sensitivities of near-surface processes [53]. The introduction of the UCX into GEOS-Chem Adjoint, thus unifying tropospheric and stratospheric chemistry, requires the validation of the forward model and the differentiated model. No previous full-model validations of the GEOS-Chem UCX Adjoint existed prior to this work, as only partial validations of adjoint modules have previously been validated [23]. Prior to this thesis, the GEOS-Chem UCX Adjoint was lacking adjoint modules and suffered from instabilities in the stratosphere that would prevent any simulation for more than multiple months. To resolve these instabilities, I develop and validate additional adjoint modules that were not previously incorporated in the GEOS-Chem UCX Adjoint.

This new development allows for the inclusion of heterogeneous chemistry when evaluating sensitivities. For instance, in this thesis, I present sensitivities of total column ozone to contrail ice surface area. Additionally, I remove lumped tracers from GEOS-Chem, which were previously causing instabilities in the stratosphere and I update the emission inventories to more recent versions (especially for aviation emissions), which allows for a more accurate estimate of the atmospheric composition.

The validation of the differentiated model requires the evaluation of upper-tropospheric and stratospheric-oriented objective functions (e.g. total ozone column). Forward sensitivities for a given control parameter are obtained by taking the difference between two GEOS-Chem runs. Given the complexity of GEOS-Chem as a state-of-the-science CTM, it is computationally expensive to calculate and validate component-wise adjoint-derived gradients with respect to each control parameter. However, I present the validation of the GEOS-Chem UCX Adjoint by comparing aggregated adjoint and forward sensitivities of full-model multi-year runs. While the location of the impact cannot be deciphered from adjoint modeling, the sensitivities offer the possibility to identify the emission sources that contribute the most to the objective function. Atmospheric sensitivities express how a change in concentration in a given species (e.g. NO) and at a given time and location affect the aggregated objective function.

Given the differences between tropospheric and stratospheric chemical behaviors, I validate the adjoint-derived sensitivities by using an emission scaling of the aviation inventory, with emission scaling varying between $\pm 100\%$ of baseline values. The emission inventories are obtained from market analysis.

Figure 3-1 displays the forward and adjoint-derived changes in averaged ozone column, expressed in Dobson Units (DU), to a scaling in subsonic aircraft NO_x emissions. The estimated yearly adjoint sensitivities reproduce the results from GEOS-Chem with a maximum error of 50 mDU, corresponding to a relative difference of 8%. Using a spline fit for the forward results, I obtain a root mean square error of 18 mDU for the emission range analyzed, spanning up to 7.5 Tg of emitted NO_x (on an NO_2 mass basis). The right axis of Figure 3-1 displays the normalized ozone response with respect to a 1% scaling in aviation NO_x. Since the adjoint sensitivities are based on first-order gradients, discrepan-

cies between the adjoint-derived and forward-derived results are in part an indicator of the presence of chemical non-linearities.

Both forward and adjoint approaches estimate that aviation emissions lead to an increase of ~208 mDU per Tg of emitted NO_x (on an NO_2 mass basis) around the baseline scenario. The forward model response is slightly concave with respect to the annual aviation NO_x emissions, meaning that the gradient is greater at reduced emissions compared to the adjoint-derived sensitivity.

Figure 3-1 allows us to quantify the impact of aviation nitrogen oxides emissions on total ozone column. I find that including aircraft NO_x emissions results in an increase of approximately 600 mDU (compared to a simulation with no aircraft emissions), corresponding to a globally-average increase of 0.21% in total ozone column mass, consistent with prior estimates [28]. These results are obtained using a single-year adjoint simulation (for 2007), during which I expect the response to aviation to not yet be in steady state. This explains the smaller increase in column ozone than is calculated for the longer-term simulations shown earlier. Long-term feedbacks on upper-tropospheric and stratospheric ozone are captured in longer, five-year simulations.

Next, I evaluate the accuracy of computed lower and mid-stratospheric sensitivities through a scaling in supersonic aviation emissions. I here focus on the role of nitrogen oxides and sulfur emissions. The stratospheric behavior of these species is expected to significantly differ from that in the troposphere. Five year adjoint simulations are performed to capture long-term stratospheric responses to supersonic aviation emissions. The following three model tests are conducted to evaluate simulation accuracy: scaling of supersonic NO_x emissions, scaling of supersonic sulfur emissions, and scaling of supersonic water vapor emissions.

Figure 3-2 compares the five-year adjoint and forward responses to a scaling in NO_x emissions from supersonic aviation. The adjoint model is able to reproduce the results of the forward model, however with a larger gradient. High altitude NO_x emissions have a greater potential for stratospheric depletion compared to subsonic emissions. The adjoint-derived sensitivities indicate that this supersonic emissions scenario, with a cruise ceiling at 20 km, leads to 2.8 DU of depleted ozone per Tg of emitted NO_x on an NO_2 mass basis

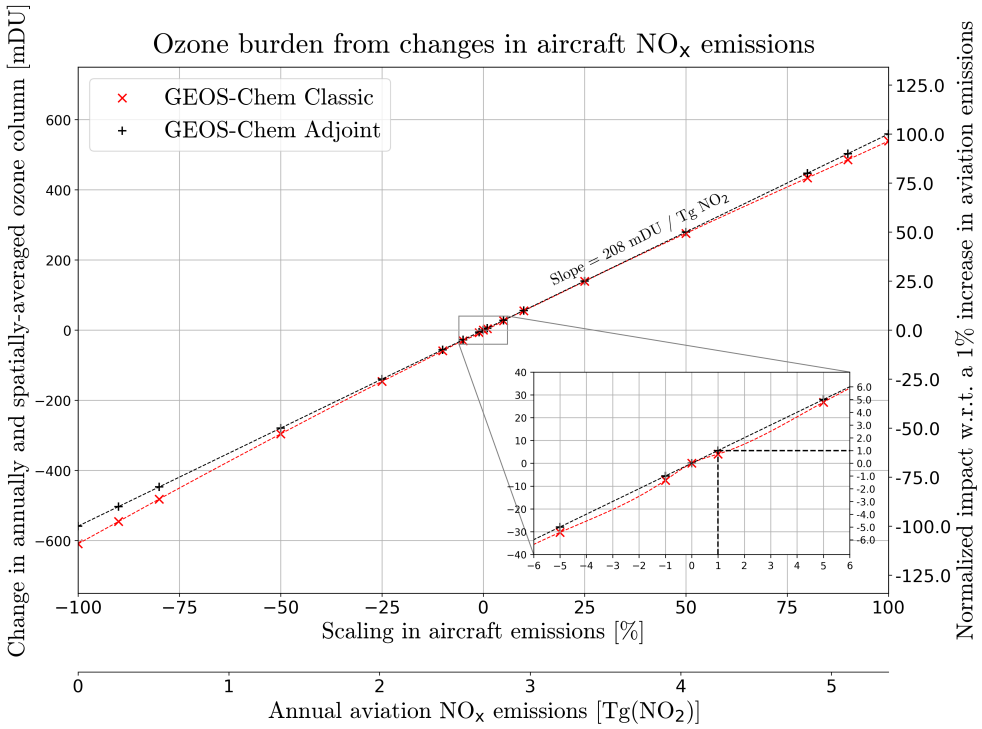

Figure 3-1: Comparison of forward and adjoint sensitivities with respect to a scaling in aircraft NO_x emissions.

(approximately corresponding to 28 mDU / (Tg fuel burn/year)).

The gradient of the ozone response from aviation NO_x emissions shows a strong dependence on the cruise ceiling. Sensitivities of ozone column to NO_x emissions reverse at ~15 km at northern mid-latitudes, going from positive to negative. The altitude of this reversal also depends on season, varying from 13.5 km in July to 16 km in January.

Figure 3-3 displays the five-year mean ozone response to a scaling in supersonic sulfur emissions, simulated as a change in the fuel sulfur content with a fixed 2% conversion factor. The forward and adjoint models agree with a root mean square error of 29 mDU.

Both models estimate the ozone response to scale linearly with the amount of emitted sulfur, with a slope of -19.5 DU per Tg of elemental sulfur per year, for emissions at 20 km. In the 15-20 km band, sensitivities to SO_2 and H_2SO_4 emissions are approximately 10 times larger than sensitivities to NO_x emissions.

Altitude and latitude play a key role in determining the role of sulfur on ozone column. Figure 3-3 displays zonally-averaged adjoint sensitivities of ozone column to sulfur

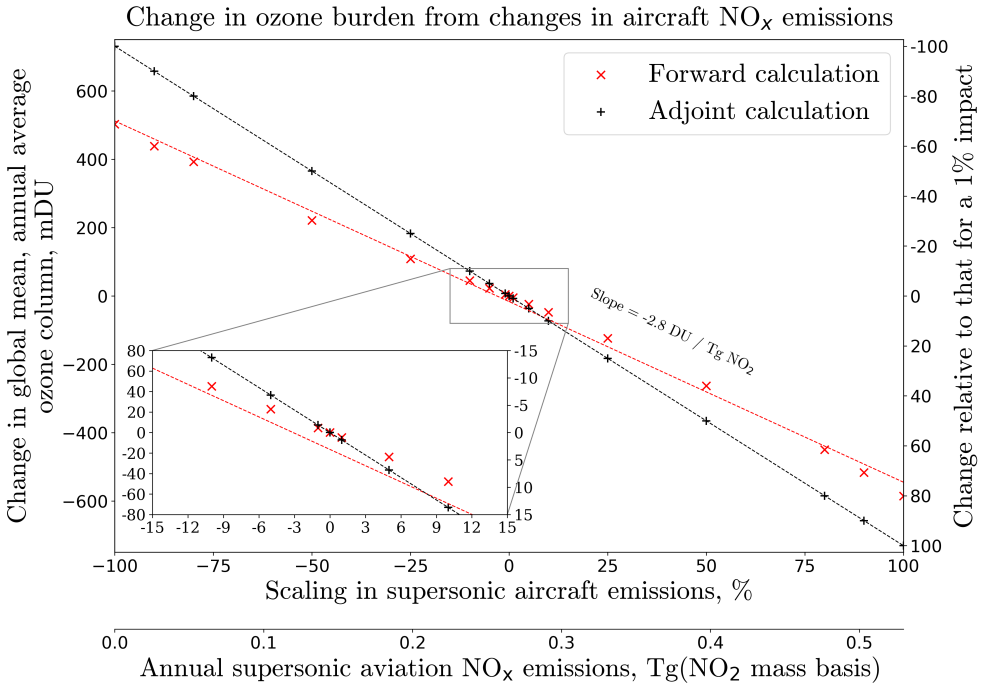

Figure 3-2: Response of total ozone column to a scaling in supersonic aircraft NO_x emissions according to GEOS-Chem (red) and using atmospheric sensitivities from GEOS-Chem UCX Adjoint (black). Red data points show the results of a series of forward model simulations, in which the supersonic aviation emissions are scaled, from an annual baseline of 0.26 Tg (on an NO_2 mass basis). The right axis displays the normalized impact with respect to a 1% scaling in aircraft NO_x emissions.

emissions. Sulfur has a limited impact in the troposphere. In the stratosphere, sulfur emissions lead to ozone depletion due to the heterogeneous reactions taking place on the aerosol surface, converting reservoir chlorine (e.g. $ClONO_2$) to active chlorine, which catalytically depletes ozone. The amount of ozone depletion from sulfur emissions is expected to reduce with decreased stratospheric chlorine loading.

The magnitude of sulfur-induced ozone depletion varies with altitude and latitude, peaking at -15 mDU per Gg SO_2 per year in the extra-tropics. Figure 3-3 shows that the equatorial region is characterized by lower sensitivities to sulfur emissions. Additional validation experiments regarding the role of stratospheric sulfur are presented in Appendix B.1.

Given the complexity of the tropospheric hydrological cycle, the UCX chemistry mechanism treats water vapor as a passive tracer throughout the troposphere [28, 29]. GEOS-5

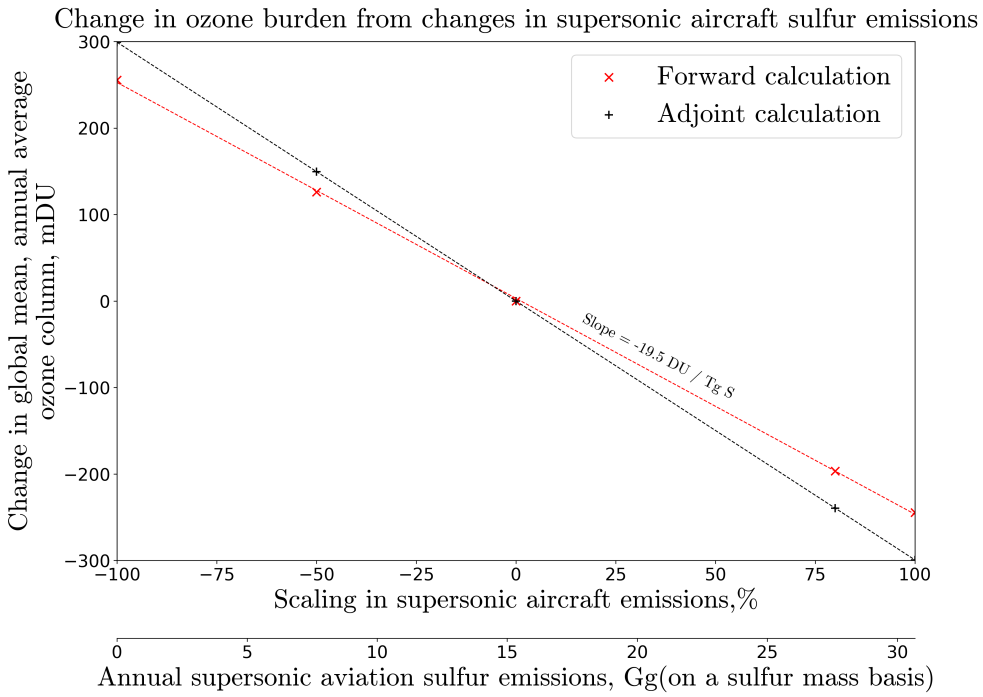

Figure 3-3: Changes in the response of total ozone column to a scaling in supersonic aircraft sulfur emissions (released as SO_2 and H_2SO_4) according to GEOS-Chem (red) and using atmospheric sensitivities from GEOS-Chem UCX Adjoint (black). Red data points show the results of a series of forward model simulations, in which the supersonic aviation emissions are scaled, from an annual baseline of approximately 15 Gg of sulfur.

humidity fields are used to derive tropospheric water mixing ratios. At the tropopause, the low temperatures lead to an effective freezing out of water vapor, driving a low water mass flux to the stratosphere that explains the arid conditions in the upper atmosphere [43]. This allows us to treat H_2O as a chemically-active and advected tracer in the stratosphere and to capture events such as dehydration through sedimentation of ice polar stratospheric clouds (PSCs). This translates to sensitivities with respect to water emissions identically equal to zero in the troposphere.

Figure 3-4 displays the column ozone response to water vapor emissions from the supersonic aviation scenario, which consists of 32 Tg of water vapor emitted between ground and cruise altitude. Additionally, Figure 3-4 also shows zonally and temporally-averaged adjoint sensitivities of total ozone column to water vapor emissions, expressed in mDU / (Tg H_2O/year) for a five year adjoint simulation. Out of the 32 Tg of water vapor, approximately 65% are released above the 20 km threshold, and thus have a significant impact on

the ozone column response.

Water vapor is the primary source of HO_x (H, OH, HO_2) which catalytically destroys ozone, thus explaining the negative sensitivities in the stratosphere. Additional OH also converts the abundant and stable chlorine species, HCl, into active chlorine (Cl, ClO) which further depletes ozone through rapid ClO_x-cycling and further enhances the sensitivities to water vapor [36].

For the supersonic emission, 17 Tg of fuel burn are released above 20 km, corresponding to approximately 21 Tg of water vapor emitted per year. At the cruise ceiling, the averaged sensitivity of total ozone column to H_2O emissions is -5 mDU / (Tg H_2O/year). According to the adjoint-sensitivities, the water vapor emissions leads to a reduction of approximately 105 mDU for this scenario, while the time-averaged forward response is -95 mDU. As displayed in Figure 3-4, the role of water vapor emissions on column ozone depends strongly on the altitude of emissions and becomes negligible at altitudes lower than 16 km.

3.2.3 Methods to estimate the column ozone-neutral altitude

In this section, I describe the methods used to derive the column ozone-neutral cruise altitude, and to quantify its sensitivity to emission characteristics. Using the GEOS-Chem Adjoint with stratospheric chemistry, I generate decadal sensitivities of globally-averaged column ozone to aviation emissions. The long integration time is required given the longer lifetimes in the stratosphere, compared to tropospheric lifetimes. Indeed, the troposphere is characterized by removal processes (wet and dry deposition) that do not occur in the stratosphere. In the stratosphere, previous literature indicates that the age of air in the stratosphere varies from two to six years [18].

The obtained adjoint sensitivities express the change in global column ozone to a change in emissions as a function of location, time and species. For instance, a sensitivity of 2 mDU/(Gg NO_2/year) in a given grid cell indicates that releasing 1,000 tonnes of NO_x (on a NO_2 basis) per year would lead to a globally-averaged ozone perturbation of 2 mDU.

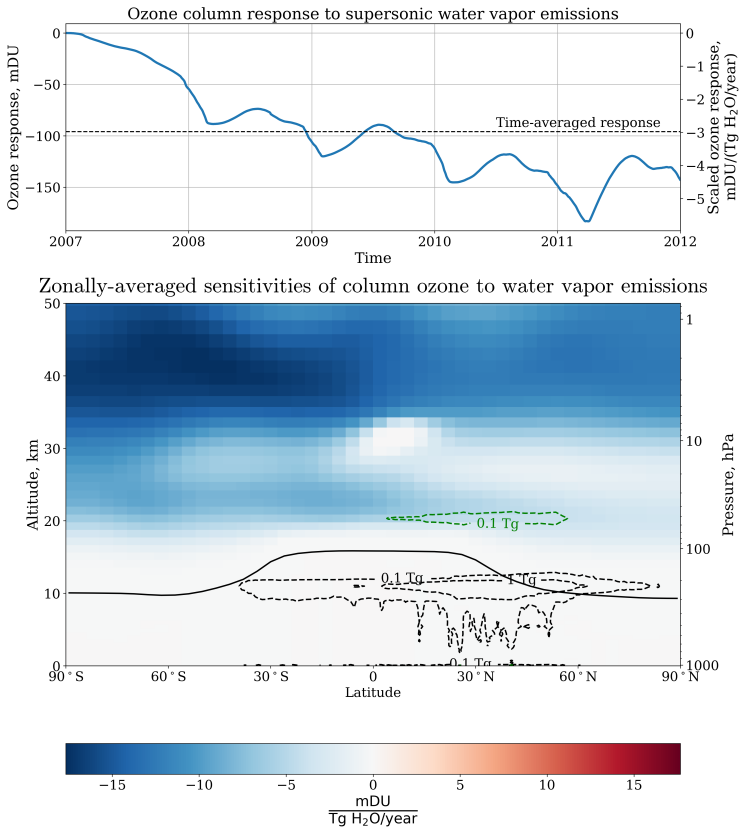

Figure 3-4: Column ozone response to the injection of 32 Tg of water vapor from supersonic aviation (top). The right axis displays the ozone response normalized by the total water emissions. Approximately 65% of the water vapor emissions are released above 20 km. Zonally and yearly-averaged adjoint sensitivities of total ozone column mass with respect to water emissions (bottom). Water vapor is a chemically-inert species in the troposphere and sensitivities are identically zero below the tropopause. Contours of subsonic (black) and supersonic fuel burn (green), with a cruise ceiling of 66,000 ft, are displayed, depicting typical cruise altitudes. The annual-mean tropopause height is plotted as a continuous black line.

To evaluate sensitivities to aviation fuel burn, I scale the sensitivities with uniform emission indices, representation of the aviation industry. I use a constant CO emission index of 2 g/kg$_{\text{fuel}}$, representative of cruise conditions. Similarly, I keep the black carbon and organic carbon emission indices fixed to 20 mg/kg$_{\text{fuel}}$. I assume a water vapor emissions index of 1.26 kg/kg$_{\text{fuel}}$. Aviation fuel currently contains sulfur and, for this project, I use, unless otherwise specified, a baseline fuel sulfur content of 600 parts per million on an elemental sulfur mass basis. However, fuel sulfur is subject to large uncertainties in the mean, with standard jet fuel having a mean fuel sulfur content between 300 and 800 ppm [105].

Using the global aviation inventory from the Federal Aviation Administration (FAA) Aviation Environmental Design Tool (AEDT) for 2015, subsonic aviation used 240 Tg of fuel, with a fleet-wide NO_x emission index of 15 g/kg_{fuel}, on an NO_2 mass basis. Unless otherwise specified, I thus keep the nitrogen emission index at 15 g(NO_2)/kg_{fuel}, representative of subsonic aviation operations.

The component-wise share of each emission component is computed as:

$$100 \times \frac{\mid \frac{\partial J}{\partial c_i} \mid \times E_i}{\sum_i \mid \frac{\partial J}{\partial c_i} \mid \times E_i}, \tag{3.1}$$

where $\frac{\partial J}{\partial c_i}$ represents the sensitivities of column ozone to a change in concentration in species c_i and EI_i represents the emission index of species i in g/kg_{fuel}. For instance, this means that an overall net zero contribution, consisting of e.g. -10 mDU from sulfur and +10 mDU from NO_x, would yield a 50% relative contribution from both species.

For fuel sulfur, I estimate the share of sulfur as:

$$100 \times \frac{\mid \frac{\partial J}{\partial c_{SO_2}} \mid \times E_{SO_2} + \mid \frac{\partial J}{\partial c_{H_2SO_4}} \mid \times E_{H_2SO_4}}{\sum_i \mid \frac{\partial J}{\partial c_i} \mid \times E_i}. \tag{3.2}$$

As described in Chapter 2, plume-scale effects can have a non-negligible impact on aviation-induced ozone. I here introduce a parameterization to account for the non-linear small-scale conversions occurring in individual aircraft plumes. The plume-scale conversions are derived using a recently-developed aircraft plume model [42]. For each pair of NO_x and sulfur emission indices, I compute the remaining fraction of NO_x after 24 hours, as well as the amount of produced nitrogen reservoir species. The conversion between SO_2 and sulfate aerosols is also estimated from the same simulations. All of the plume model simulations use identical meteorological conditions.

I then estimate the column ozone-neutral altitude in a similar fashion, but this time, accounting for plume-scale changes in NO_x, HNO_2, HNO_3, HNO_4, N_2O_5 and peroxyacetyl nitrate (PAN), and SO_2 and H_2SO_4.

3.3 Results

The focus of this section is to use adjoint sensitivities to quantify the sensitivity of the aviation-induced ozone response to emission characteristics and to identify regions of net zero column ozone change. I describe the methods used here in Section 3.2.3. I set the adjoint objective function to the globally-averaged ozone column. Given that the objective function depends heavily on stratospheric chemistry, multi-year runs are necessary to obtain quasi-steady sensitivities. This is due to the long timescales associated with stratospheric chemical processes and the typical age of air that ranges between two and six years above 100 hPa [18].

In this section, I present decadal adjoint-derived sensitivities of globally-averaged column ozone to aviation emissions and also examine the magnitude of the sensitivities to contrail ice. The sensitivities are obtained from full-model decadal runs of the GEOS-Chem UCX Adjoint, each requiring significant disk space. The adjoint simulation requires the generation of continuous checkpoints, and a 10-year adjoint simulation requires approximately 40 TB of storage space for a horizontal resolution of 4° x 5°.

In addition to the sensitivities of global ozone column to gaseous emissions, sensitivities of ozone column to aerosol surface area are also presented in this section. These sensitivities are used to estimate the adjoint-derived impact of aviation on total column ozone from aircraft-induced cloudiness. Sensitivities of total area-weighted aerosol optical depth (AOD) are presented in Appendix B.2.

3.3.1 Decadal sensitivities

Figure 3-5 displays the time evolution of zonally-averaged adjoint sensitivities to NO_x emissions, expressed in mDU / (Gg NO_2/year), used for this analysis. The sensitivities cover different altitude bands, representing subsonic and supersonic cruise altitudes (approximately 11 km and above 14 km respectively). Sensitivities to NO_x emissions vary by two orders of magnitude between the near-surface and 25 km. Two color scales are hence used in Figure 3-5 to distinguish between low altitude (below 16 km) and higher altitude behaviors.

In the troposphere, an asymmetry can be observed in the sensitivities between hemispheres. Sensitivities are greater in the less polluted Southern Hemisphere; a greater ozone response is expected in a cleaner environment for the same amount of NO_x emissions. The polar nights are characterized by sensitivities close to zero in the troposphere. No significant interannual variability is observed in the lowest altitude band, despite the variations in meteorological conditions. Indeed, I find that, in the 2005-2012 simulation period, the sensitivities of total ozone column vary by approximately 11% of the mean at an altitude of 11 km, corresponding to less than 0.1 mDU/(Gg NO_2/year). This signifies that tropospheric sensitivities have reached a steady-state in this time range. Above 12 km, the hemispheric asymmetry disappears, seasonal patterns, such as the Antarctic winter and spring seasons, appear and the interannual variability becomes significant. In the 2005-2009 time period, the fluctuations in sensitivities vary by 25 to 35% of the mean above 15 km, corresponding to ±0.7 mDU/(Gg NO_2/year).

In the lower-stratosphere (16-20 km band in Figure 3-5), sensitivities to nitrogen oxides reach a quasi-steady state after an initial time of three years (adjoint integration time is backwards). After the first few years of adjoint integration, the ozone-depleting NO_x cycles lead to a negative sensitivity in the tropics and the sunlit poles of approximately -15 mDU/(Gg NO_2/year). As a reference point, this value compares to an average of approximately +0.5 mDU/(Gg NO_2/year) in the 8 to 12 km band.

Figure 3-6 displays the sensitivity of total ozone column to changes in ice aerosol surface area density expressed in mDU/((mm^2/cm^3)/year). The two panels show the averaged sensitivity for the 8 to 12 km and 12 to 16 km altitude bands respectively. The column ozone sensitivity to changes in ice aerosol surface area is negative. Any positive change in ice surface area (e.g. from contrails) leads to a net ozone depletion.

I find an average sensitivity of -0.64 and -16 mDU/((mm^2/cm^3)/year) for the 8-12 km and 12-16 km altitude bands. However, seasonal patterns are significant for each Hemisphere and are tied to local winter events, with sensitivities reaching up to -1.1 and -1400 mDU/((mm^2/cm^3)/year) for each altitude band. Additional aerosol surface area during polar nights leads to enhanced conversion of reservoir species to active chlorine and bromine, which catalytically deplete ozone once polar night ends. Outside of the polar nights, the

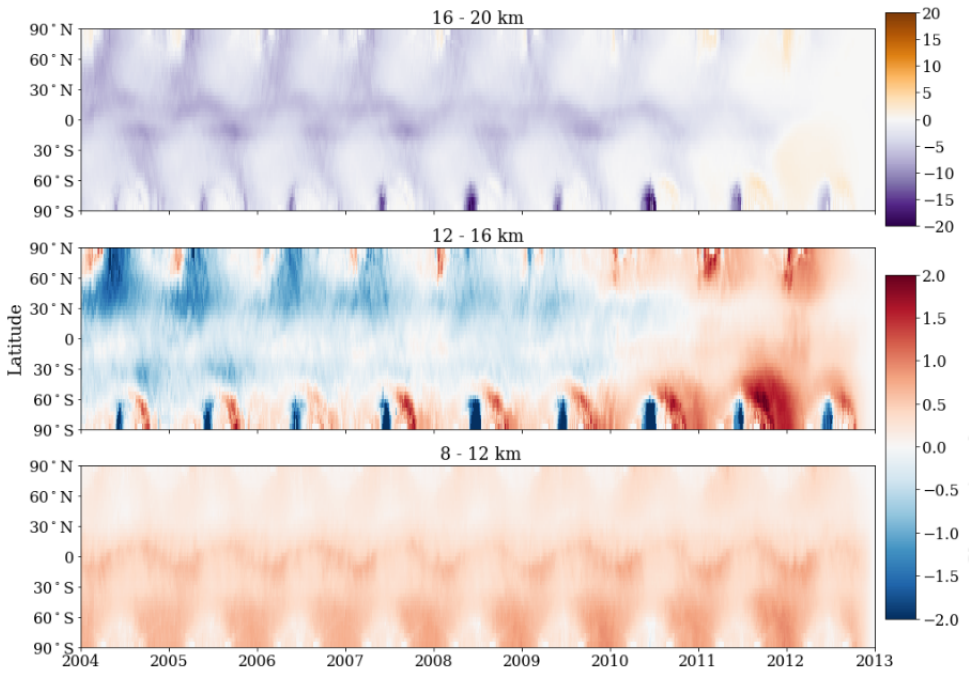

Figure 3-5: Temporal evolution of zonally-averaged sensitivities of total ozone column to NO_x emissions for different altitude bands, expressed in mDU/(Gg NO_2/year). Different color scales are used to differentiate between the low altitude (below 16 km) and higher altitude behaviors. Commercial subsonic aviation typically cruises between 10 and 12 km, while Concorde flew at 18 km.

sensitivities reach background values of -0.1 and -1 mDU/((mm^2/cm^3)/year) for 8-12 and 12-16 km bands.

The latitudinal variations of the sensitivities to ice aerosol surface area are significant as well. The extra-tropical region is characterized with the largest sensitivities, while sensitivities are negligible around the equator.

I now estimate the impact on total ozone column from a single contrail. Using an aircraft plume mode, I find that the total contrail aerosol surface area typically ranges between 10^3 and 5×10^3 m^2 per meter of flight path [42]. The total contrail length is estimated from the literature. Using infrared channels from the Advanced Very High Resolution Radiometer, a prior study finds an average contrail length of 20 km, with contrail streaks varying from 2.4 to 600 km [83]. Releasing a single contrail in an extra-tropical grid box leads to a total surface area density of approximately 8×10^{-7} mm^2/cm^3. Using adjoint sensitivities, I estimate the decadal column ozone impact of a single contrail to be -6×10^{-7} mDU for the

8-12 km band. For the 12-16 km band, I find that the impact ranges up to -6×10^{-4} mDU during polar night, with a mean value -1×10^{-5} mDU. However, more work is needed to establish a spatial and temporal contrail ice inventory.

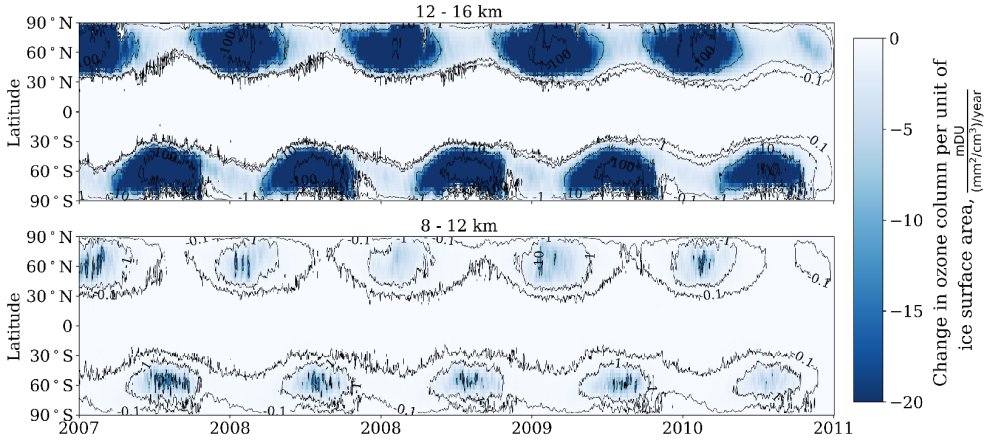

Figure 3-6: Sensitivities of total ozone column to changes in ice surface area density expressed in mDU/((mm^2/cm^3)/year) for the 8–12 km (bottom) and 12–16 km (top) altitude bands respectively. Contour lines display the magnitude and range from -0.1 to -100, varying by a factor of 10 between each level.

3.3.2 Identification of a column ozone-neutral altitude

In this section, we use the decadal sensitivities presented in Section 3.4.1 to derive a column ozone-neutral cruise altitude.

I find that, averaging globally and assuming modern-day fuel sulfur content and fleet average NO_x emissions indices, aircraft emissions are column ozone-neutral in the 12 to 15 km altitude range (Figure 3-7). Below this altitude, aviation emissions lead to a net increase in column ozone, with higher sensitivities in the less polluted Southern Hemisphere of up to 10 mDU / (Tg_{fuel}/year). At higher altitudes, aircraft engine emissions instead lead to increasing ozone depletion, reaching -100 mDU / (Tg_{fuel}/year) at 20 km.

I find that there are seasonal variations in the sensitivities of total ozone column to aviation emissions. Figure 3-7A shows the sensitivity of global mean column ozone to aircraft emissions occurring between 30 and 60°N, a latitude band which includes 67% of year-2005 aircraft emissions [109]. I find that the 30°N-60°N averaged sensitivities peak in October in the troposphere reaching 4 mDU / (Tg_{fuel}/year) at an altitude of 8 km, con-

sistent with previous studies [46]. In this latitude band, the ozone-neutral altitude varies between 12 and 13.6 km, for July and November, respectively. For comparison, typical subsonic aircraft cruise at altitudes of 10-12 km [109]. At 11 km, the seasonal variations in the sensitivity of column ozone exhibit two maxima in April and October, and two minima, during boreal winter and July. In the stratosphere, I find a seasonal trend where local sensitivities are minimal in April and maximal in October and November. The magnitude of the seasonal trend increases with altitude. For instance, an aircraft cruising in the Northern Hemisphere above 14 km in April would lead to double the ozone depletion when aggregated over the following decade, compared to a similar flight in October.

The response of global mean ozone to emissions also varies outside of this latitude band. Figure 3-7B shows zonally-integrated adjoint sensitivities for the same period. Aircraft emissions in the less polluted Southern Hemisphere between 8 and 12 km altitude lead to twice the amount of ozone produced than the same emissions in the Northern hemisphere. Above 15 km, this asymmetry disappears, but a new disparity appears between emissions in the tropics (30°S - 30°N) and the higher latitudes. The net ozone depletion per unit of fuel burn at 16 km varies between -25 and -15 mDU / (Tg_{fuel}/year), but at 22 km altitude, the net ozone depletion per unit fuel burn in the tropics is -250 mDU / (Tg_{fuel}/year) compared to an average of -150 mDU / (Tg_{fuel}/year) at higher latitudes. This suggests that high Mach number supersonic aviation, which cruises at higher altitude, would cause greater ozone depletion if flights take place in the tropics, but that the opposite may be true for subsonic or low Mach number supersonic flights.

Accordingly, I find that the ozone-neutral cruise altitude varies with latitude. At Northern latitudes, the neutral altitude is approximately constant at 13 km. This behavior differs from the intertropical region where the ozone-neutral altitude varies between 13 km and 14.3 km, at approximately 30°N and 10°S, respectively. In the Southern Hemisphere, the neutral altitude averages to 14 km, with a global maximum at the South Pole at 14.6 km. I find that the South Pole maximum and the upward shift of the neutral altitude are linked to positive time-averaged sensitivities of column ozone to NO_x emissions in the 12-16 km band, over Antarctica. NO_x emissions over the South Pole binds active chlorine into chlorine reservoir species, thus lowering the potential stratospheric ozone depletion during

austral spring.

From Panels A and B of Figure 3-7, I find that sensitivities display variations with respect to the cruise altitude between -2 and +6 mDU / (Tg_{fuel}/year) between 8 and 14 km, compared to -2 and -300 mDU / (Tg_{fuel}/year) in the 14 to 25 km altitude band. The larger magnitude at higher altitudes is due to the greater role played by chemical catalytic cycles in the stratosphere. In the 14 to 20 km altitude range, the aggregated sensitivities double every 2 km, going from -15 to -125 mDU / (Tg_{fuel}/year). Between 20 and 25 km, the magnitude increases linearly, with a change in magnitude of 35 mDU / (Tg_{fuel}/year) for every additional km.

Figure 3-7C shows the sensitivity of global column ozone to each component of aviation emissions. This is re-interpreted in Figure 3-7D as the percentage share contributed by each emission component to the total aviation-induced response, respectively. The percentage share is here defined in absolute terms, such that two individual contributions of -10 and 10 mDU respectively, would each contribute 50% of the aggregated response. I find that NO_x emissions below 15 km produce a net increase in ozone, but produce a net decrease in ozone above this point. They are also responsible for 80% of all ozone changes for cruise altitudes below 12 km or above 20 km. At all altitudes, sulfur emissions lead to a net depletion of ozone, but this depletion is greater at altitudes above 12 km. Assuming an aviation fuel sulfur content of 600 parts per million (ppm) by mass, I find that sulfur is the emission component with the largest net ozone impact when emitted in the 13 to 16 km altitude band. Above 16 km, NO_x emissions again become the largest contributor to net ozone change. HO_x-driven ozone depletion through water vapor emissions also becomes significant in this region, with its contribution to ozone changes reaching 10% at 20 km.

3.3.3 Sensitivity to emission characteristics

Figure 3-8 shows how the globally-averaged ozone-neutral cruise altitude varies as a function of both NO_x emission index and fuel sulfur content. Panels A and B of Figure 3-8 display the average ozone-neutral cruise altitude globally and in the 30°N-60°N latitude band respectively. The dashed lines represent the effect owing to the inclusion of plume-

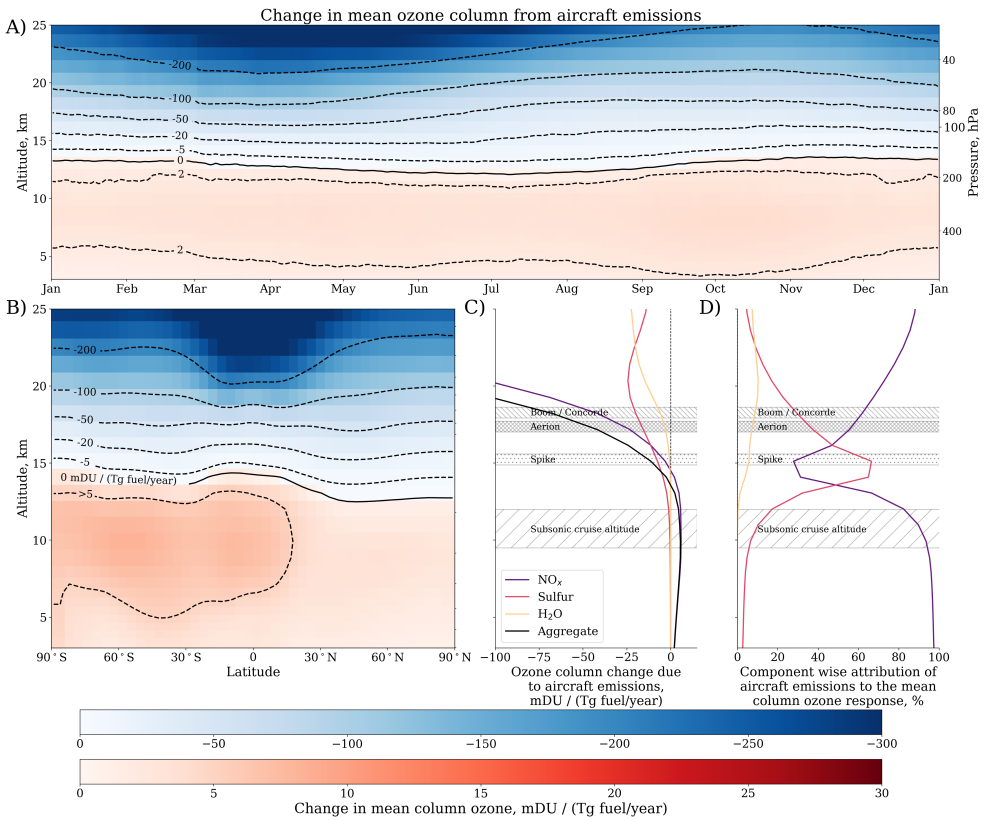

Figure 3-7: Adjoint sensitivity of mean ozone column to aviation fuel burn. The displayed sensitivities are averaged over the last five years of a nine-year run, allowing for four years of spin-up. Panel A: Annually-averaged adjoint sensitivity weighted by aircraft emission indices in the 30°N-60°N latitude band. Panel B: Zonally-averaged sensitivity weighted by aircraft emission indices. Panel C: Contribution of each emission component to the total emission-weighted sensitivity of mean column ozone. Different cruising altitudes of subsonic and supersonic aircraft designs are displayed. Panel D: Component wise attribution of aircraft emissions expressed as a percentage.

scale processes. As a reference point, I assume a current fleet-wide subsonic NO_x emission index of 15 g/kg$_{\text{fuel}}$, on an NO_2 mass basis, as measured at the engine exit plane while I use a fuel sulfur content of 600 ppm by mass. Assuming these emission characteristics and including plume-scale conversions, I find that flights between 13.4 and 13.6 km altitude are column ozone-neutral. This is equivalent to a relative change in column ozone of less than 1.7×10^{-4}% / (Tg$_{\text{fuel}}$/year). In comparison, previous estimates have found that subsonic aviation increases column ozone by 3.5×10^{-3}% / (Tg$_{\text{fuel}}$/year) [28]. I also find that, in the 30°N-60°N latitude band, the neutral altitude is approximately 1 km lower than the global average. Using an aircraft plume model, I compute the plume-scale chemical conversions

of nitrogen oxides and sulfur as a function of the NO_x emission index and fuel sulfur content [42]. I use the results of the aircraft plume model to compute the role of plume-scale processes on the column ozone-neutral altitude. Neglecting the effects of plume scale processes introduces a significant positive bias in the estimation of the ozone neutral cruise altitude. I find that this would result in the ozone neutral cruise altitude being overestimated by between 0.3 and 1.0 km, at NO_x emission indices of 15 and 5 $g(NO_2)/kg_{fuel}$ respectively. This bias in the neutral altitude is similar in magnitude for both the global average and the 30°N-60°N average, as shown in Figure 3-8.

I find that cruise emissions at altitudes of up to 14.5 km are ozone-neutral for desulfurized fuel. At such altitudes, the column ozone-neutral altitude is sensitive to the fuel sulfur content but nearly independent of the NO_x emission index. However, above 14.5 km, NO_x, sulfur, and H_2O emissions all independently cause net ozone depletion.

On a mass basis, sensitivities of column ozone to NO_x emissions are smaller than the sensitivities to sulfur. However, NO_x emissions, on a NO_2 mass basis, are typically one order of magnitude greater than sulfur emissions, on a SO_2 mass basis. Assuming a fuel sulfur content of 600 ppm, the ratio between sulfur and NO_x aircraft emissions makes both emission components account for a similar fraction of the aviation-attributable ozone response in the altitude range. This study does not however account for uncertainty and variability in fuel sulfur content.

Figure 3-8 shows that, at lower NO_x emissions, fuel desulfurization has a greater effect on the cruise neutral altitude. The contribution of sulfur emissions on the column ozone response is increased at reduced NO_x emissions. At a fleet-wide NO_x emission index of 15 $g(NO_2)/kg_{fuel}$, fuel desulfurization would increase the ozone-neutral altitude by 1 km. However, the same reduction in sulfur emissions at a NO_x emission index of 6 $g(NO_2)/kg_{fuel}$ would lead to an increase of 1.5 km, from 13 km to 14.5 km. Water vapor emissions do not significantly affect the column ozone-neutral altitude, as its contribution only exceeds 5% of the aggregated response above 15 km.

Finally, current fuel sulfur content is subject to significant variability and uncertainty. Assuming that the mean fuel sulfur content is uniformly distributed between 300 and 800 ppm [105], I estimate the globally-averaged neutral altitude range under uncertainty to be

13.3 and 14.1 km at a NO_x emission index of 15 $g(NO_2)/kg_{fuel}$. In the 30°N-60°N latitude band, this uncertainty range becomes 12.4-13.2 km, with a mean value of 12.8 km.

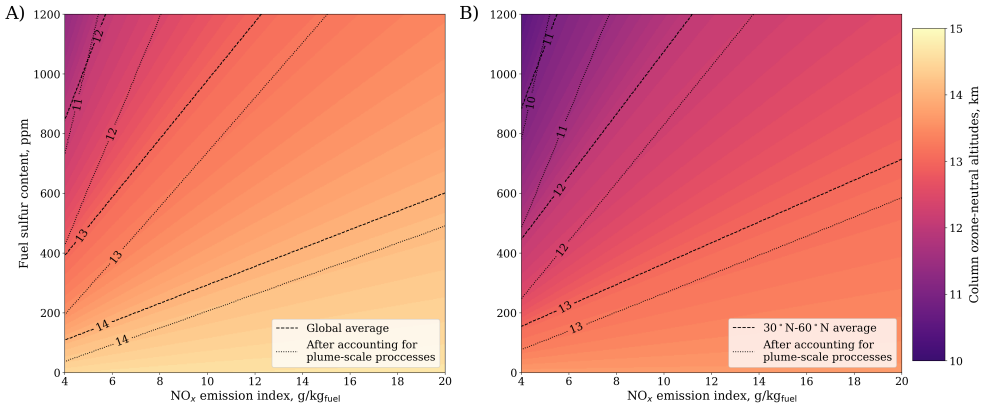

Figure 3-8: Column ozone-neutral altitudes as a function of the NO_x emission index and fuel sulfur content. The black dashed lines in Panel A represent contour levels of the globally-averaged column ozone-neutral altitude, while, for Panel B, the averaging is performed in the 30°N-60°N, where most of aviation's fuel is burned. For both panels, the dotted lines represent the same isolines after accounting for plume-scale processes.

3.4 Discussion and limitations

In this chapter, I extend the GEOS-Chem Adjoint to include stratospheric chemistry. I present validation experiments that focus on a scaling of aircraft emissions at different cruise altitudes, and the results indicate that adjoint-derived sensitivities in the stratosphere are in good agreement with forward model runs. I also include additional validation experiments in Appendix B.1.

Using the GEOS-Chem Adjoint, I generate decadal sensitivities of total column ozone to emissions as well as to changes in aerosol surface area (e.g. through aircraft-induced cloudiness). When considering adjoint sensitivities of ozone column to emissions, I find that seasonal variations in the troposphere are characterized by smaller variations compared to the stratosphere. The standard deviation of the sensitivities to ozone column are 11% of the mean for a cruise altitude of 11 km, with a global maximum in October. This value compares to 25% to 35% above 15 km. Below 12 km, NO_x emissions are the major contributor to the aviation-attributable ozone response, accounting for more than 80%. In

the 12 to 18 km altitude band, sulfur emissions increase in importance, reaching the same order as NO_x emissions. Above 18 km, NO_x emissions are again the major contributor with contributions from both sulfur and water vapor.

I find that the sensitivities with respect to changes in aerosol surface area are negative in the 8 to 16 km band, peak at mid and high latitudes and are tied to polar nights. Using results from contrail modeling experiments, I find that a single contrail at 60°N leads to a change of -6×10^{-7} mDU in the 8 to 12 km range and up to -6×10^{-4} mDU at 16 km. Given that no publicly-available global inventories of contrail ice currently exist, more work is needed to establish the global impact of contrail ice on ozone.

This thesis provides the first estimate of global column ozone-neutral altitude for aircraft emissions as well as its sensitivity to emission characteristics while accounting for the role of plume-scale processes. I find that, based on current engine emission indices and fuel characteristics, the 12 to 15 km altitude band is column ozone neutral, with deviations in the altitude explained by seasonal and latitudinal variations in the adjoint sensitivities. Emissions in the Northern Hemisphere lead to a lower response compared to similar emissions in the Southern Hemisphere, such that the Northern Hemispheric ozone-neutral altitude lies between 12 and 13.6 km. In the tropics and in the Southern Hemisphere, this altitude is 14 to 15 km.

I find that reduction in the NO_x emission index could reduce the neutral altitude to current subsonic altitudes (approximately 10 to 12 km). For instance, after accounting for plume-scale effects, a globally-averaged ozone-neutral altitude of 12.5 km can be achieved by a fleet-wide 50% reduction in NO_x emissions. However, most aircraft traffic occurs in the Northern Hemisphere, where the sensitivities to column ozone are lower. Under such conditions, a neutral altitude of 11.7 km can be reached with a fleet-wide NO_x emission index of 7.5 $g(NO_2)/kg_{fuel}$. Additionally, at such altitudes, sulfur emissions only contribute to less than 25% of the ozone budget. Significant reductions in fuel sulfur content such as through increased adoption of biofuels would increase.

I estimate that the 13 - 15 km altitude band could be a potential column-ozone neutral for supersonic aviation, under the assumption of ultra-low sulfur fuel or the use of biofuels. I have also assumed a NO_x emission index of 10 g/kg_{fuel} on an NO_2 mass basis for

supersonic aircraft. At such altitudes, fuel sulfur plays a significant role on the column ozone response and I find that desulfurization for supersonic aviation reduces the aviation-attributable ozone depletion at the cost of suppressed sulfur-induced cooling.

This study is the first to identify a column ozone-neutral cruise altitude. These results are obtained using the GEOS-Chem Adjoint, with the UCX chemistry mechanism and the GEOS-5 meteorological dataset. Future work should focus on generating updated sensitivities with more recent meteorological products. Additionally, I do not consider future changes in stratospheric chlorine and sulfur loading, which have been shown to play a role on the ozone response from high-altitude aviation emissions [133].

Following the reduction in the emissions of CFC and other chlorine-bearing compounds, the amount of background inorganic chlorine, Cl_y, is expected to decrease with time. Additionally, previous studies have found that the amount of inorganic chlorine played a critical role in the magnitude of the ozone response due to the sulfur emissions from volcanic eruptions [9, 117]. At low stratospheric chlorine loadings (~0.6 ppbv, typical to pre-industrial era), the ozone response is insensitive to the amount of SO_2 injected in the stratosphere. However, ozone depletion is found to increase with the magnitude of the stratospheric sulfur injection at modern-day stratospheric Cl_y mixing ratios (~2.93 ppbv). For our simulations, the amount of stratospheric inorganic chlorine averaged to 2.76 ppbv.

Chapter 4

Coupled chemistry-climate feedback of commercial aviation emissions

This chapter focuses on the relevance of coupled chemistry-climate interactions when evaluating aviation's environmental response. Section 4.1 presents the motivation for this topic. In Section 4.2, I introduce a newly-coupled model of atmospheric chemistry, coupling a state-of-the-art CTM with a global climate model. Section 4.3 describes the validation approach for this new model, where I compare the results to atmospheric observations and results from other global models. Section 4.4 introduces the results of ensemble runs performed to evaluate aviation's environmental response with this model, as well as quantifying the relevance of the coupled chemistry-climate feedback for this assessment. In Section 4.5, I discuss limitations and future steps.

4.1 Introduction

High-altitude emissions from commercial aircraft activities lead to chemical perturbations that have lasting effects on the atmosphere and the Earth's climate [65, 73, 136, 15, 72]. The air quality and atmospheric ozone responses from aviation emissions have been extensively evaluated using CTMs [65, 32, 7, 64, 28, 15, 100]. All CTMs from the previous studies have found that aviation emissions lead to a net positive surface ozone and $PM_{2.5}$ response. However, when using CTMs, changes in atmospheric composition are not prop-

agated to changes in meteorology. As such, despite the chaotic variability introduced by the climate response, global climate models are necessary to evaluate climate and meteorological feedback (e.g. interaction between emissions and circulation).

A few studies have conducted multi-year simulations of aviation emissions using global climate models (GCMs) and looked at the coupled chemistry-climate pathways through which commercial aircraft activities affect surface ozone and $PM_{2.5}$ [60, 16]. Using a GCM, a study found that there might be significant magnifying effects from atmospheric feedback [60]. Some key findings are that commercial aircraft emissions are found to increase surface temperature by 10 mK, and upper tropospheric temperature by 30 mK on average [60] and account for 5% of the year-2005 total anthropogenic radiative forcing [74]. As a consequence, this leads to enhanced (respectively reduced) atmospheric stability below (respectively above) cruise altitude. This is explained by a larger increase of upper tropospheric temperatures compared to surface temperatures. This leads to a reduction in the downward ozone transport flux from the ozone layer down to the UTLS region, where the subsonic aviation cruise altitude lies. Additionally, aviation emissions are found to lower the globally-averaged cloud cover fraction due to the increased atmospheric stability in the troposphere below cruise altitude, thus also reducing precipitation [60]. Furthermore, the aviation-induced perturbation in aerosol loading at altitude increased the number density of charged cloud particles in convective clouds, and thus the lightning flash rate [60]. Enhanced lightning NO_x emissions are found due to the impact of aviation emissions [60]. All of the four pathways mentioned before cannot be captured by CTMs, and, according to the study, magnify the environmental response to aviation emissions [60]. However, an intercomparative model study of the effects of aircraft emissions on surface air quality found that GCMs have too much variability to resolve any such atmospheric feedback [15]. No other single-model study has found any significant coupled chemistry-climate feedback from aviation emissions.

In this section, I provide a framework and develop numerical models to estimate the relevance of coupled effects in the evaluation of the environmental response of aviation emissions. For this study, I use the state-of-the-art GEOS-Chem CTM, which has previously been used to study the environmental impacts of aviation emissions on surface air quality

and tropospheric and stratospheric atmospheric composition [7, 28]. The Community Earth System Model, CESM2, is a fully-coupled GCM, developed by the National Center for Atmospheric Research (NCAR), that allows the estimation of the past, present, and future climate states of the Earth. For this thesis, I introduce a new model, CESM2-GC, obtained by coupling CESM2 with GEOS-Chem. In this model, CESM2 remains unchanged except for the chemistry modules of the Community Atmosphere Model (CAM). In CAM, all physical processes other than chemistry (such as transport, radiation, ...) are unmodified. CAM thus replaces its existing chemistry module, CAM-Chem, with GEOS-Chem, which then performs its own chemistry using online meteorology.

Such other couplings between the GEOS-Chem CTM and GCMs have been recently introduced such as the WRF-GC model, coupling the regional meteorology model WRF with GEOS-Chem [77, 39], or coupling GEOS-Chem with the NASA GEOS Earth System Model [81].

To evaluate the relevance of a climate feedback on the atmospheric response to aviation emissions, I set up a simulation framework that consists of performing ensemble runs using CESM2-GC. Ensemble runs allow to capture the inner variability of the atmosphere, as a number of parameterizations are extremely sensitive to initial conditions. By introducing small perturbation in the initial conditions, I am able to capture a subset of possible but different states of the atmosphere, and thus different responses to aviation emissions. As the number of ensemble members grows the chaotic variability of the atmosphere should disappear and only the aviation-attributable signal should be statistically significant. However, It is unclear how many ensemble members are needed a priori to capture a statistically significant response from aviation emissions.

In Section 4.2, I present the development steps of CESM2-GC. Section 4.3 focuses on the validation of CESM2-GC against atmospheric measurements, results from CAM-Chem and from the GEOS-Chem CTM. In Section 4.4, I introduce the simulation setup to evaluate the magnitude of the coupled chemistry-climate feedback in the assessment of aviation's environmental response.

4.2 Coupling of CESM2 with GEOS-Chem (CESM2-GC)

In this section, I first describe the implementation and code architecture of the newly-coupled chemistry-climate model, CESM2-GC.

The GEOS-Chem CTM consists of a representation of chemical processes and is, thanks to coding efforts, relatively easy to use. However, like other CTMs and offline models, GEOS-Chem has a number of drawbacks. Offline models use archived meteorology that is used as an input. Thus, future predictions of atmospheric composition with CTMs rely on past meteorology. CTMs are limited by the time span, and sometimes the spatial resolution, of the available meteorological products. As shown in previous studies, the performed interpolation of meteorological data at the current timestep can lead to non-negligible bias in simulations of atmospheric chemistry [137]. Additionally, a critical aspect of this project is to simulate the chemistry-climate interaction, which is not currently feasible with offline CTMs, due to the missing interactions and lack of chemical feedback onto the climate.

GCMs calculate meteorological fields and simulate atmospheric chemistry. In this approach, no temporal interpolation is needed as the calculated fields represent the current state of the atmosphere. GCMs are thus able to capture chemistry-climate feedback (i.e. the meteorological response to changes in aerosol and gas concentrations through interactions with radiation and cloud physics). However, most GCMs have the option to "turn off" this feedback, thus leading to a number of studies quantifying the importance of this coupling [76, 25, 128]. CESM is one example of a widely-used, global, state-of-the-science GCM. It consists of different components (Community Atmosphere Model (CAM), Community Land Model (CLM), Parallel Ocean Program (POP), Community Ice Sheet Model (CISM), ...), representing altogether all of Earth's physical and chemical processes. All of these components are modules that interact with each other through the Common Infrastructure for Modeling the Earth (CIME) coupler. CAM itself consists of different submodules, handling various processes in the Earth's atmosphere. CAM-Chem is the atmospheric chemistry component and is used for simulations of global tropospheric and stratospheric atmospheric composition [71, 120]. CAM-Chem is based on the highly-modulable MOZART chemical mechanism [34] and has taken part in the Coupled Model

Intercomparison Project 6 (CMIP6). Different levels of complexity, represented by different user cases, are available to simulate atmospheric chemistry using MOZART. The Modal Aerosol Model (MAM) is used in CESM to represent the aerosol size distribution and both internal and external mixing between aerosol components. MAM was initially developped for CESM1 [80]. MAM4 is the four-mode version of MAM and has been extensively used and validated in CESM2 [79]. CESM2-GC features a coupling between the bulk aerosol representation in GEOS-Chem and the modal representation of MAM. Aerosols that overlap in both chemical representations (e.g. sulfates) are summed over all bins to estimate the bulk mass and then passed to GEOS-Chem. The mass tendencies for each bin in MAM are then calculated based on the bulk mass tendency from GEOS-Chem and split accordingly between bins based on the bin to bulk mass ratio. For the other aerosols (e.g. nitrates in GEOS-Chem), the aerosol representation is handled by GEOS-Chem.

The software engineering guidelines behind the development of CESM2-GC are presented in Appendix C.

4.3 Validation of CESM2-GC

The evaluation of aviation's environmental impacts on the climate and atmospheric composition requires that CESM2-GC is able to accurately simulate and represent atmospheric chemistry, dry and wet deposition as well as convection and convective scavenging. These processes are critical to simulate the aviation-induced change in atmospheric composition. As such, I here test the accuracy of individual components as well as full-model runs of CESM2-GC against results from CAM-Chem, the GEOS-Chem CTM, and atmospheric observations.

4.3.1 Methods

In this section, all simulations use specified meteorology from MERRA-2. The emission fluxes are fed through HEMCO and are identical (as long as the model represents the emitted species, e.g. iodine chemistry does not exist in CAM-Chem).

The CESM2-GC model is evaluated in three different ways:

- Against the offline GEOS-Chem CTM,
- Against observations, used for benchmarking of the GEOS-Chem CTM,
- Against CESM2 running with CAM-Chem.

Rather than comparing two models between each, I split off the comparisons listed above as follows. First, I evaluate emission fluxes and compare them to recent studies. I then focus on the validation of dry deposition in CESM2-GC. I compare wet deposition fluxes in CESM2-GC with the other models and atmospheric observations. Additionally, I evaluate surface mixing ratios in CESM2-GC against the GEOS-Chem CTM. Finally, I describe a comparison of column totals to satellite observations, and an evaluation of vertical profiles against ozonesondes and upper-atmospheric mixing ratio measurements from aircraft campaigns.

4.3.2 Evaluation of CESM2-GC against atmospheric observations and other atmospheric models

This section conducts a comparison between the offline GEOS-Chem CTM, CAM-Chem (as embedded in CESM2), and CESM2-GC (GEOS-Chem embedded in CESM2). Previous comparison between the offline GEOS-Chem CTM and embedded GEOS-Chem in Earth System Models have been established [81, 77]. The results from the GEOS-Chem CTM are obtained from the high-performance offline GEOS-Chem CTM, GEOS-Chem High Performance (GCHP) [30]. I use the complex SOA simulation in GEOS-Chem in order to match the SOA representation in MAM, which splits organic aerosols into volatility bins.

In this comparison assessment, I select global observation datasets that are previously used to benchmark the offline GEOS-Chem CTM at each major release. These observations include:

- Surface mixing ratio of ozone,
- NO_2 and aerosol species from ground monitors,
- Vertical profile of ozone molecular concentration from ozonesondes,

- Column measurements of ozone from ozonesonde climatology covering multiple decades,

- Vertical profiles of a wide ensemble of species from NASA aircraft campaigns.

The measurements from aircraft campaigns cover different years but they are the only source of vertical distribution information for a large number of species. In the following analysis, I thus plan to ignore interannual variability between different meteorological years for this set of observations.

A comparison to vertical profiles of ozone mixing ratios and ozonesonde climatology [118, 119] is provided, alongside the comparison with CAM-Chem. The inventory covers 16 years of observations and can thus be used to study yearly trends in ozone concentrations.

Ground measurements of ozone and NO_2 are publicly available [101, 122, 35, 62] and have previously been used to validate models of atmospheric chemistry [77] and to predict changes in air quality [20]. I use ground station measurements to validate estimates of surface mass concentrations of selected pollutants by CESM2-GC.

The quasi-biennial oscillation (QBO) of the mean zonal wind is a source of variability in the tropical lower stratosphere [103]. In CESM2, the QBO can either be prescribed or generated internally during the model run. All the simulations performed in this section use a prescribed QBO. Previous validation experiments using CESM2-WACCM, i.e. CESM2 coupled with the Whole Atmosphere Community Climate Model (WACCM), have shown that CESM2 is able to reproduce the periodicity and the amplitude of the QBO [45, 103, 13]. However, CESM2-WACCM has been found to lead to a slow decrease in the QBO amplitude due to poor vertical resolution in the lower stratosphere.

Emission fluxes

In the GEOS-Chem CTM, CESM2-GC, and CAM-Chem, emission fluxes are passed from HEMCO. However, in CESM2-GC, we turn off some emission inventories as CESM provides online estimations of lightning emissions, dust and sea salt emissions, as well as biogenic emissions. We use the online Model of Emissions of Gases and Aerosols from Nature

(MEGAN), as established in CLM, to compute biogenic emissions [50]. Besides the online emission fluxes in CESM, the other emission quantities are identical between the GEOS-Chem CTM and CESM2-GC. A summary of the surface emission totals for CESM2-GC are listed in Appendix C alongside geographical distributions of selected surface emission fluxes. The emission totals presented in Table C.1 of Appendix C are obtained for the year 2016 and match the historical emission totals [34, 71].

Dry deposition

Figure 4-1 shows the annually-averaged ozone dry deposition velocity by the GEOS-Chem CTM and CESM2-GC. In the following, the results of the GEOS-Chem CTM are conservatively gridded to a horizontal resolution of 2° x 2.5°, corresponding to the resolution used in my CESM2-GC simulation. In CESM2-GC, the land types are computed online by CLM, and are passed to the GEOS-Chem dry deposition module through the coupler. These online land types are then mapped to the default land types used in the GEOS-Chem CTM. A similar mapping is derived for leaf area indices. This mapping allows us to have online land types, from CLM, while using the GEOS-Chem dry deposition routine.

Most of the ozone deposition occurs over land, as the ocean dry deposition velocity is of the order of 0.02 cm/s, compared to velocities up to ~1 cm/s over land [123, 52]. On average, ozone dry deposition velocities are 9% larger in CESM2-GC compared to the GEOS-Chem CTM. The largest relative differences occur in polar regions, over the ocean. However, the difference in magnitude in polar regions remains small (less than 0.05 cm/s). In CESM2-GC, lower ozone dry deposition velocities are observed over the Amazon and African rain forests, with differences up to 0.2 cm/s. This discrepancy can be explained by differences in land types over these areas, as well as different values for leaf area indices. The results from CESM2-GC agree qualitatively with the localized measurements of ozone dry deposition velocities over deciduous and coniferous forests [40, 106]. Overall, the ozone dry deposition velocities are in good agreement between both models and previous literature.

Figure 4-2 displays a parity plot between the ozone dry deposition velocities in CESM2-GC and CAM-Chem. Velocities lower than 0.05 cm/s occur over ocean and ice, while the

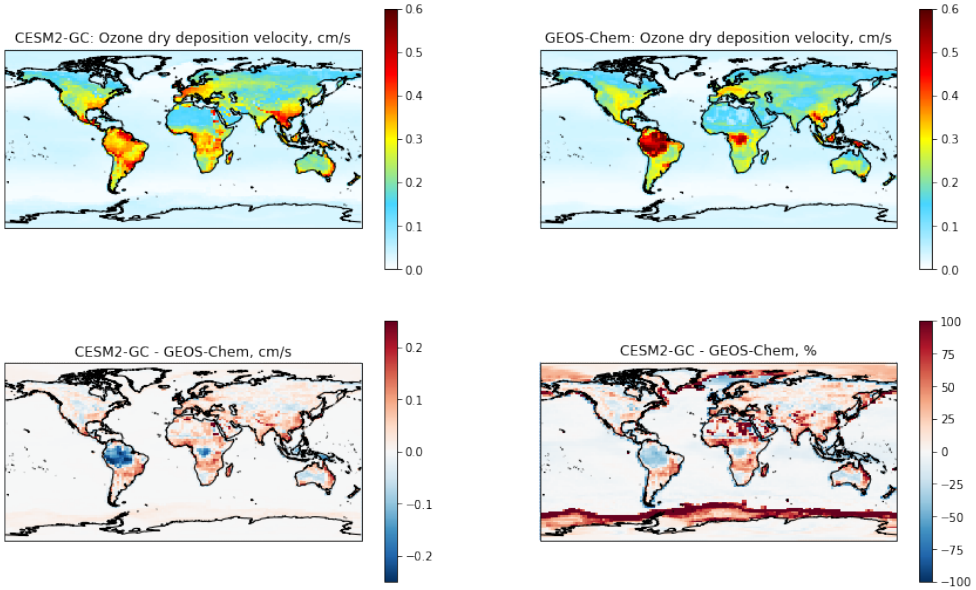

Figure 4-1: Dry deposition velocities of ozone as computed by CESM2-GC and the GEOS-Chem CTM (top left and right respectively), as well as their absolute and relative difference (bottom left and right).

velocities greater than 0.05 cm/s are only found over land. I find that the two models are generally consistent with a correlation coefficient of 0.89. Over the ocean, CAM-Chem computes a dry deposition velocity that is approximately constant at 0.05 cm/s, while they are set to 0 over ice. However, this is not the case in the GEOS-Chem CTM, where dry deposition velocities over ice are equal to ~0.03 cm/s and vary between 0.01 and 0.04 over the oceans. On average, I show that CESM2-GC predicts slightly higher dry deposition velocities over land by 0.05 cm/s.

Wet deposition

I now investigate the model results from CESM2-GC regarding wet deposition. In CESM2-GC, wet deposition tendencies are calculated using the NEU wet deposition scheme, similarly to CAM-Chem [91]. Wet deposition rates have been measured by studying the global precipitation patterns. Recent measurements have provided wet deposition rates in numerous geographical locations for the years 2005 to 2007 [125]. Dry deposition fluxes are also available from the same study but are limited to sulfur and some nitrogen species and are available in fewer locations. Other studies have measured dry deposition velocities,

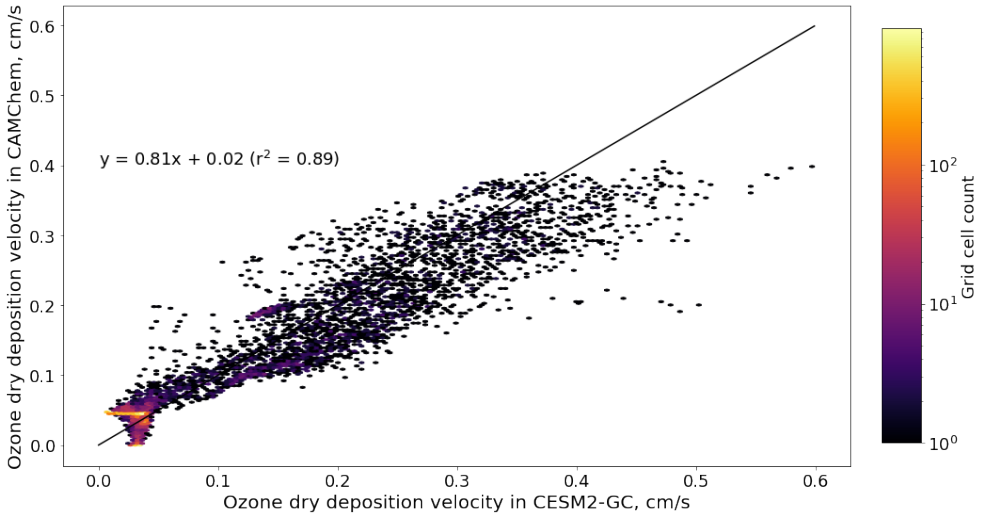

Figure 4-2: Parity plot between the dry deposition velocities of ozone as computed by CESM2-GC and CAM-Chem.

especially for ozone [40, 106], but are, however, limited to localized measurements.

Figure 4-3 displays the surface nitrogen wet deposition flux as evaluated by CESM2-GC, CAM-Chem and the GEOS-Chem CTM. CESM2-GC and CAM-Chem rely on the NEU scheme to evaluate wet deposition fluxes [91]. The total nitrogen flux is calculated by adding all fluxes from each nitrogen compound undergoing wet deposition. Rainwater measurements are also displayed to validate the model results [125]. Overall, the results from CESM2-GC are in good agreement with CAM-Chem and the GEOS-Chem CTM. The models are also consistent with the rainwater observations, as the correlation coefficients reach 0.65, 0.66 and 0.67 for CESM2-GC, CAM-Chem and the GEOS-Chem CTM respectively. On average, the results from CESM2-GC are also closest to the parity line compared to the other models with a slope of 0.6 compared to 0.5 and 0.49 for CAM-Chem and the GEOS-Chem CTM. I find that the simulated results from CESM2-GC are slightly biased towards lower values in North America and in Europe compared to the observations. The wet deposition flux of reduced and oxidized nitrogen compounds have also been compared separately and are consistent with the flux measurements.

Figure 4-4 displays the dry deposition flux of nitrogen compounds at the surface as calculated by CESM2-GC, CAM-Chem and the GEOS-Chem CTM respectively. For CESM2-GC, this calculation uses the land types and leaf area indices computed by CLM.

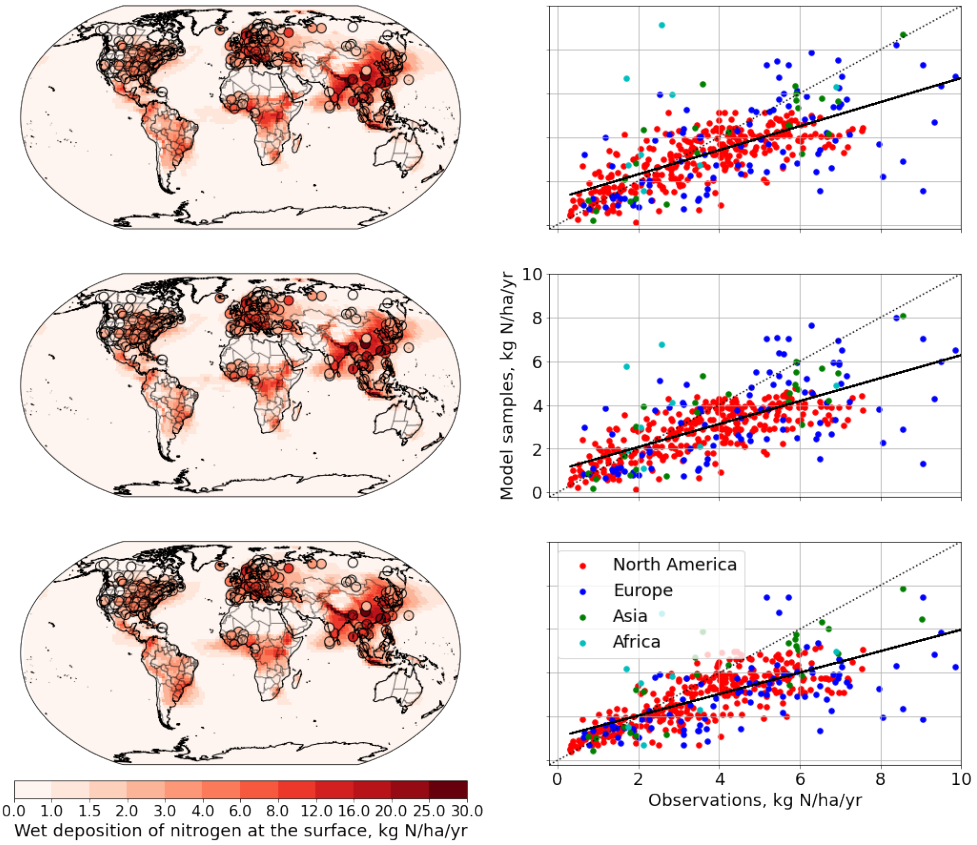

Figure 4-3: Geographical distribution of the wet deposition flux of nitrogen at the surface (left) for CESM2-GC (top), CAM-Chem (middle) and the GEOS-Chem CTM (bottom). A parity plot of the results against rainwater measurements is displayed (right).

The dry deposition velocities are subsequently estimated using the GEOS-Chem dry deposition routines. The in-situ measurements displayed in Figure 4-4 are only available over North America. I find that out of the three models presented here, CESM2-GC yields the lowest bias compared to the observations, even though all three models have a positive bias compared to the measurements from previous literature [125]. This bias could be explained by either larger concentrations of nitrogen compounds or enhanced dry deposition velocities. The discrepancies between the model results and the measurements could also be explained by the fact that measurements are obtained for 2005 to 2007 while the model results used the 2016 meteorological year. Over the decade, nitrogen emissions have increased [34], thus potentially explaining the positive bias.

The SO_2 dry deposition velocity is also qualitatively compared to localized measurements from the literature [40] and lies in the range of observed values.

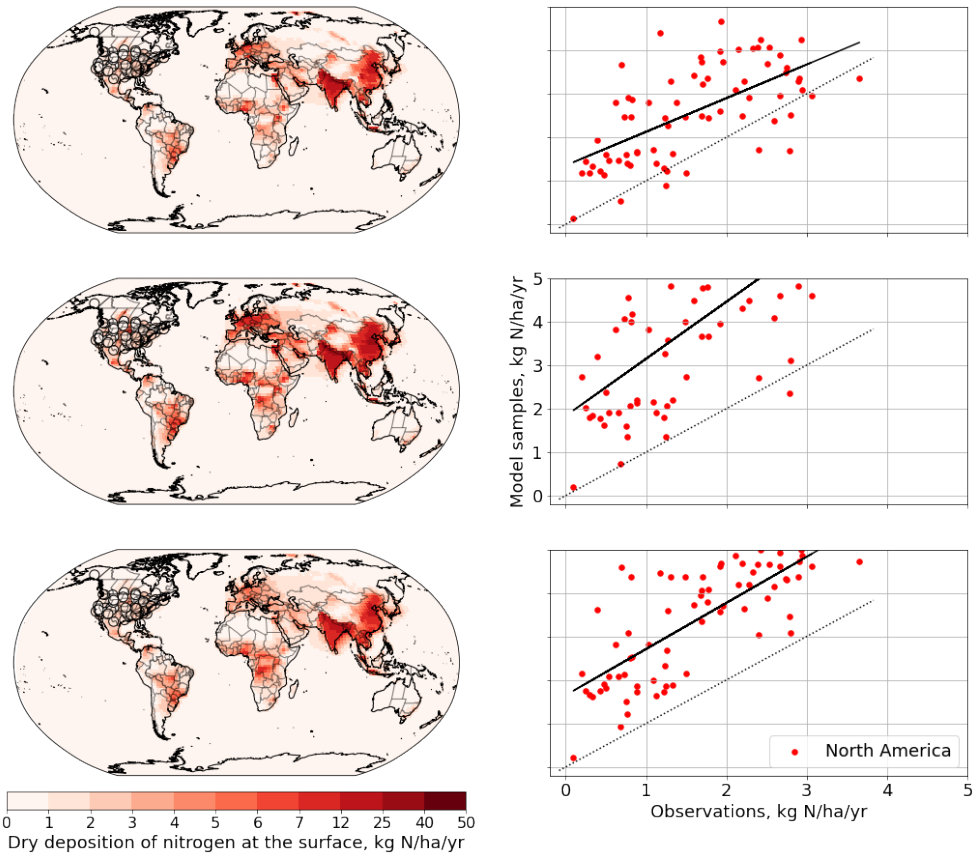

Figure 4-4: Model evaluations of the dry deposition flux of nitrogen at the surface (left) as evaluated by CESM2-GC (top), CAM-Chem (middle), and the GEOS-Chem CTM (bottom). A parity plot of the results against dry deposition measurements is displayed (right). The measurements are only available in the contiguous United States.

Figure 4-5 presents the evaluated wet deposition of non-sea salt sulfur from CESM2-GC, CAM-Chem and the GEOS-Chem CTM alongside rainwater measurements from the literature for 2005 [125]. When comparing across model results, I find that the results are consistent across all models with a global mean of ~1.5 kg S/ha/yr. For instance, I find that the results from CESM2-GC and CAM-Chem are in excellent agreement, with a correlation coefficient greater than 0.9. However, I find a large negative bias between any model results and the rainwater measurements. This bias is location-dependent, as Asia experiences a lower bias compared to North America or Europe. For instance, over North America, the measurements estimate a mean sulfur wet deposition flux of approximately 5 kg S/ha/yr (for the year 2005), while the model results plateau at 1.5 kg S/ha/yr (for the year 2016) for CESM2-GC, CAM-Chem and the GEOS-Chem CTM. This can be explained by the

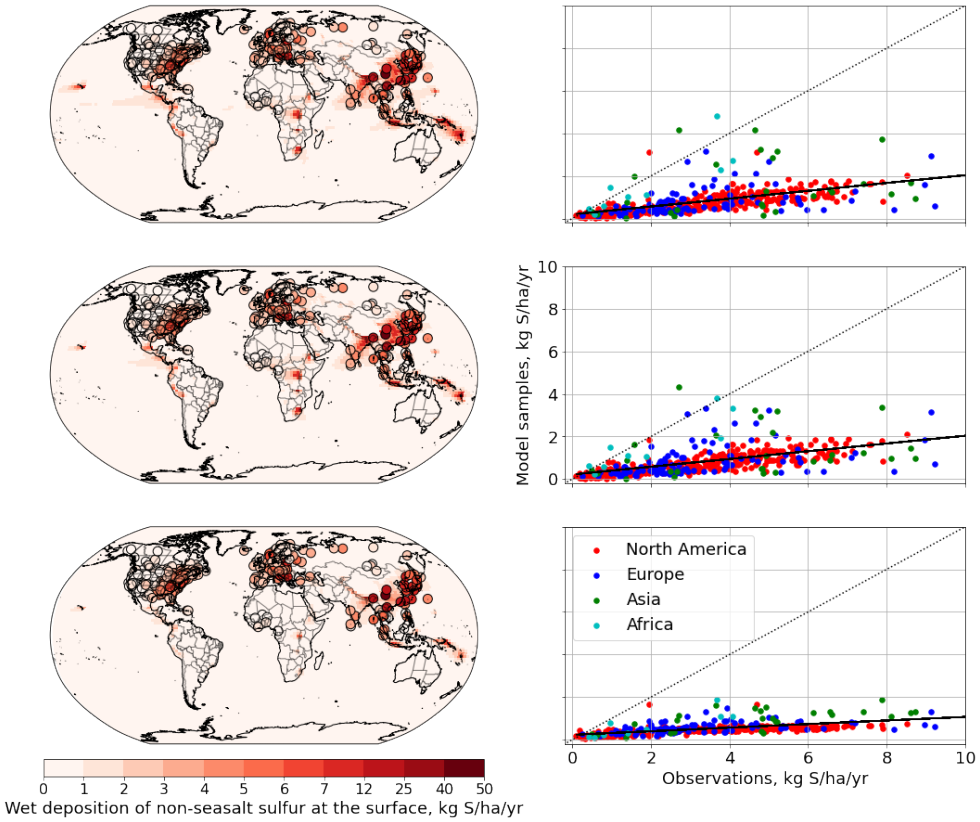

Figure 4-5: Wet deposition flux of non-sea salt sulfur (left) as computed by CESM2-GC (top), CAM-Chem (middle) and the GEOS-Chem CTM (bottom). A parity plot of the simulated results against wet deposition measurements is displayed (right).

reduction in the sulfur wet deposition surface flux over the past decades. Previous literature has found that the deposition rate of sulfur over the Eastern US has been decreasing at a rate of -1 kg S/ha/yr per year (split as ~60% and 40% for dry and wet deposition respectively) since 1990 [139]. Similar findings have been suggested for wet deposition over Europe [115]. A similar, but more recent, decrease over Asia has been observed in the literature [1]. After accounting for a 0.4 kg S/ha/yr reduction per year between 2005 and 2016 over North America and Europe, the simulated results and measurements look more consistent. The simulated results are also in good agreement with the regional results over North America presented in the literature [139].

Surface mixing ratios

In this section, I compare the surface ozone mixing ratio and $PM_{2.5}$ and NO_2 surface mass concentrations to ground station measurements and model results from the GEOS-Chem CTM.

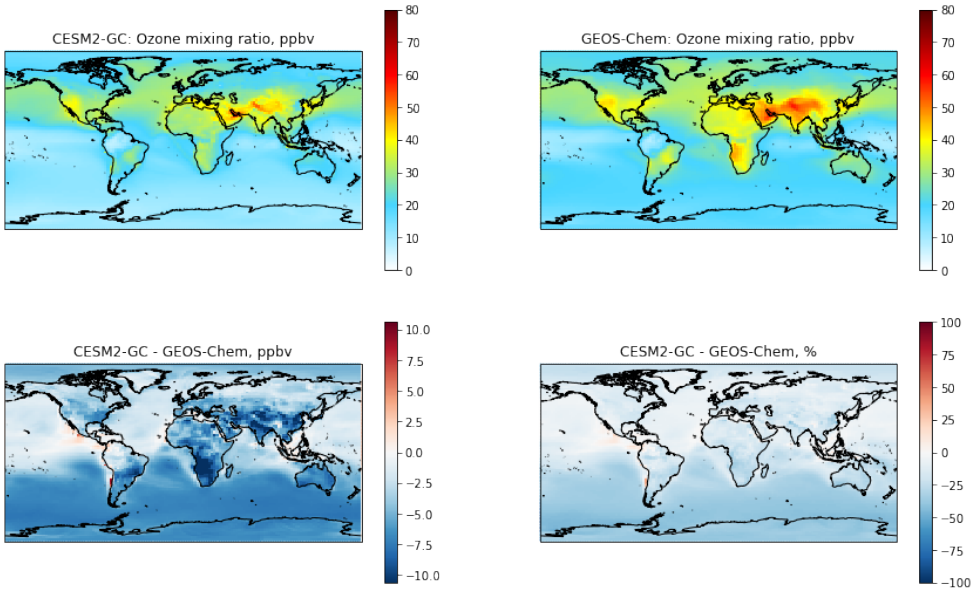

Figure 4-6: Annually-averaged surface ozone mixing ratios estimated by CESM2-GC (top left) and the GEOS-Chem CTM (top right). The absolute and relative differences between both models are shown in bottom left and bottom right panels respectively.

Figure 4-6 compares the simulated annually-averaged surface ozone mixing ratios as estimated by CESM2-GC and the GEOS-Chem CTM. I find that, when globally averaged, CESM2-GC predicts a lower ozone mixing ratio compared to GEOS-Chem. This difference peaks over Southern Africa and over India, reaching an absolute difference of ~10 ppbv. CESM2-GC estimates a lower surface ozone mixing ratio by 6 ppbv and 3 ppbv in the Southern Hemisphere and Northern Hemisphere respectively. This difference in ozone mixing ratio is limited to ~5 ppbv over the oceans. In the Northern Hemisphere, I observe no difference in surface ozone mixing ratio over the oceans, while a decrease of ~4 ppbv can be found over North America, Europe and East Asia. In addition to annual averages, I also consider seasonal variations of surface ozone. Figure 4-7 presents parity plots of monthly-averaged surface ozone mixing ratios for January and July comparing CESM2-GC to the GEOS-Chem CTM. Comparison of the two models for both months shows good

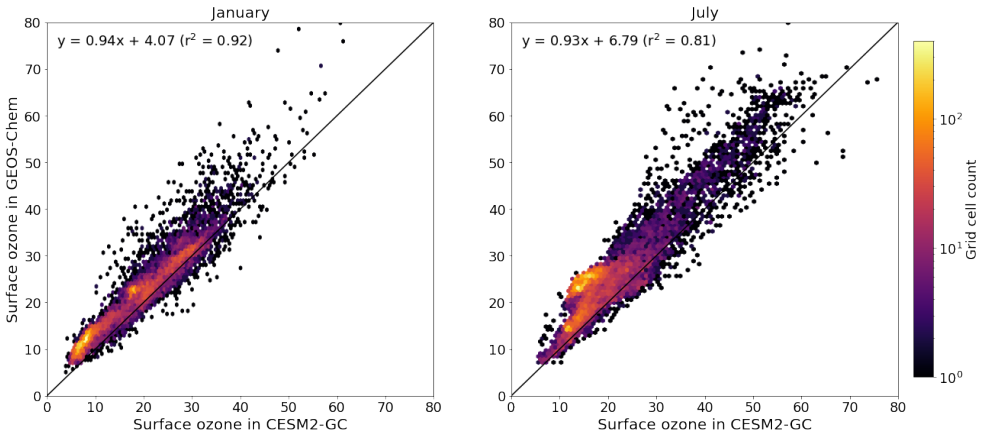

Figure 4-7: Parity plots of surface ozone mixing ratios for January (left) and July (right) comparing CESM2-GC to the GEOS-Chem CTM. Fitting parameters are shown in the top left corner for both months. Both panels share the same color scale.

agreement with correlation coefficients (r^2) above 0.8. In January, both models are in good agreement, as pointed out by a correlation coefficient of 0.92 and a slope of 0.94. In July, this agreement is slightly worsened with a correlation coefficient of 0.81 and a slope of 0.93. For both months, lower ozone surface mixing ratios can be observed in CESM2-GC compared to the GEOS-Chem CTM, as also found in Figure 4-6.

Figure 4-8 shows surface mass concentrations of NO_2 as estimated by CESM2-GC, CAM-Chem, and the GEOS-Chem CTM for 2016 against ground station measurements for North America, Europe, and South-East Asia. The ground station measurements have been annually-averaged. I find that the surface NO_2 concentrations display variable agreement depending on the geographical location. In the U.S., Europe and South-East Asia, the correlation coefficient equals 0.39, 0.21 and 0.42 respectively for CESM2-GC. In all regions with ground monitor measurements, the results from CESM2-GC are slightly better than that of CAM-Chem, for which the correlation coefficients are respectively 0.38, 0.21, and 0.41, but both models provide results that are consistent with each other. The GEOS-Chem CTM provides correlation coefficients equal to 0.36, 0.21, and 0.41 respectively. The relatively low correlation coefficients can be explained by the fact that the ground measurements are point-wise measurements, in regions that can be heavily polluted. Atmospheric models work with coarse grid-cell averages (in this case 2° latitude x 2.5° longitude) and are usually not capable of capturing gradients on small horizontal scales.

In Asia, the correlation coefficient is the highest of the three regions. However, CESM2-GC overestimates surface NO_2 concentrations in regions that are characterized with ground measurements between 6 and 15 $\mu g/m^3$. Even though the model's horizontal resolution is coarse, the surface NO_2 concentrations over Japan follow the ground measurements with good agreement. The regression slope for observations over Japan is 1.02 and the correlation coefficient is 0.35.

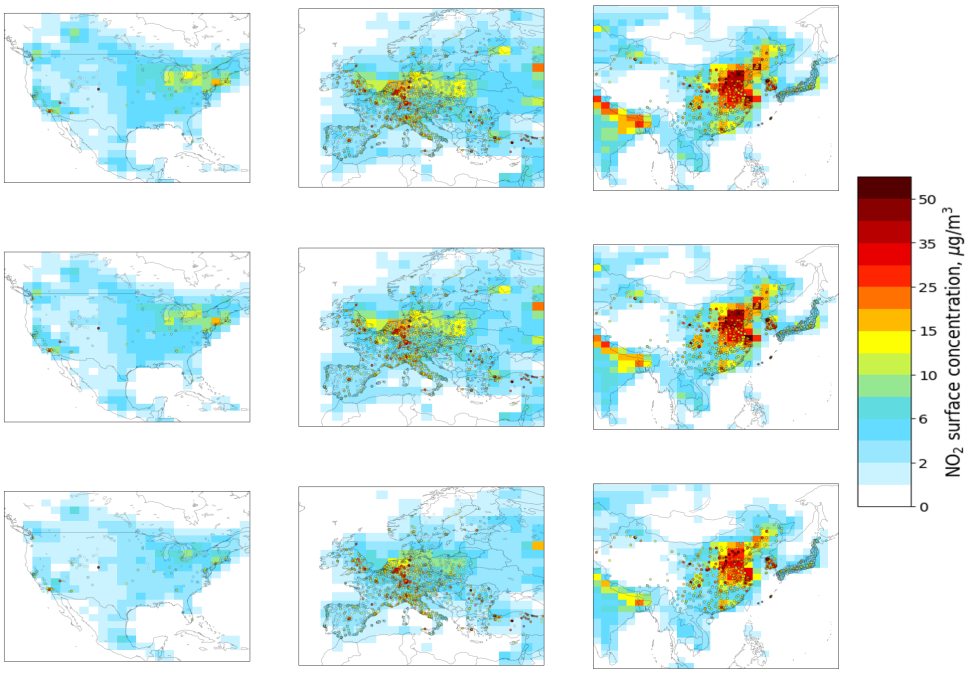

Figure 4-8: Surface NO_2 mass concentrations simulated by CESM2-GC (top), CAM-Chem (middle), and the GEOS-Chem CTM (bottom) for 2016 for North America (left), Europe (middle), and South-East Asia (right) alongside ground station measurements [101, 35, 62].

Figure 4-9 displays annually-averaged surface ozone mass concentrations over North America, Europe and South-East Asia as estimated by CESM2-GC, CAM-Chem, and the GEOS-Chem CTM. The model results are compared to ground station measurements [101, 35, 62]. The models provide consistent results with the ground measurements for North America and Europe. The correlation coefficient between the model simulation results over the U.S. and Europe and the surface measurements for surface ozone is 0.37 and 0.44 respectively. While CAM-Chem and the GEOS-Chem CTM predict correlation coefficients of 0.24 and 0.44, and 0.28 and 0.43 respectively. The geographical pattern is also consistent, with high surface ozone concentrations over the Mediterranean sea and lower

concentrations over Northern Europe. However, the model results from CESM2-GC appear to be slightly biased toward smaller ozone surface concentrations. Over South-East Asia, all models appear to underestimate the high ozone mass surface concentrations. CESM2-GC predicts relatively low surface ozone concentrations compared to the other two models. More work is needed to understand the large biases in surface ozone over China.

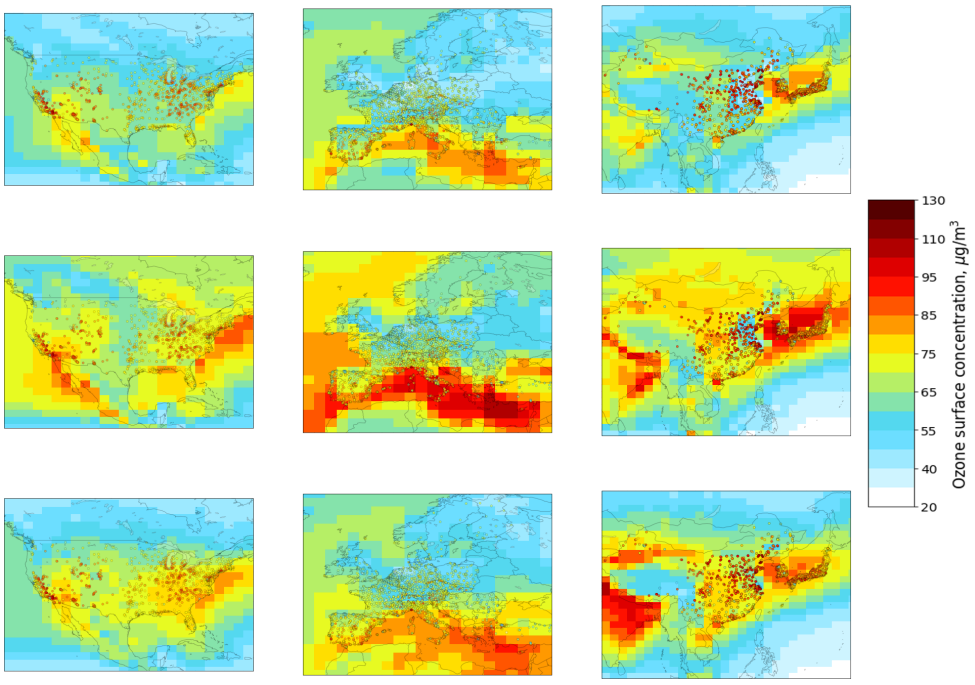

Figure 4-9: Surface ozone mass concentrations simulated by CESM2-GC (top), CAM-Chem (middle), and the GEOS-Chem CTM (bottom) for 2016 for North America (left), Europe (middle), and South-East Asia (right) alongside ground station measurements [101, 35, 62].

Finally, I compare mass concentrations of particulate matter with diameter lower than 2.5 micrometers ($PM_{2.5}$) between CESM2-GC and the GEOS-Chem CTM. I define the $PM_{2.5}$ surface concentration as:

$$
\begin{aligned}
PM_{2.5} = {} & 1.33 \times (NH_4 + NIT + SO_4) \\
& + BC_{\text{hydrophilic}} + BC_{\text{hydrophobic}} \\
& + 2.10 \times (OC_{\text{hydrophilic}} + 1.16 OC_{\text{hydrophobic}}) \\
& + 1.16 \times (\text{2ndary organic aerosols}) \\
& + 1.86 \times (\text{fine sea salt aerosol}).
\end{aligned}
$$

I excluded dust from the definition of $PM_{2.5}$ as most of the dust is mapped to DST4 in GEOS-Chem, which is excluded from the definition of $PM_{2.5}$.

Figure 4-10 compares annually-averaged surface mass concentrations of $PM_{2.5}$ from both model simulations. The two models are in good agreement as the correlation coefficient reaches 0.86. At low $PM_{2.5}$ concentrations, CESM2-GC reproduces the results from the GEOS-Chem CTM with good accuracy ($r^2 > 0.95$ at concentrations lower than 30 $\mu g/m^3$), while CESM2-GC slightly underpredicts $PM_{2.5}$ concentrations in regions with large $PM_{2.5}$ mass concentrations. Finally, the surface $PM_{2.5}$ seasonal variations in the GEOS-Chem CTM are reproduced in CESM2-GC.

Comparison to column totals, ozonesondes and remote measurements from aircraft campaigns

We first focus on the evaluation of the vertical profile of ozone mixing ratios by comparing CESM2-GC, CAM-Chem, and the GEOS-Chem CTM to ozonesonde climatology [119]. Over the past decades, observations from ozonesondes in different locations provide a valuable dataset of the evolution of ozone mixing ratios in the troposphere and stratosphere. Figure 4-11 provides a Taylor-like diagram comparison between the CESM2-GC, CAM-Chem, and the GEOS-Chem CTM simulations to the climatology, representative of the 1995-2010 time period. The pressure levels are chosen to be 900, 500, 250 and 50 hPa and are split by latitude ranges (tropics, mid latitudes, high latitudes). In Figure 4-11, the normalized mean difference between simulations and observations for each region is shown on the radius, and the correlation of the seasonal cycle is shown as the angle from

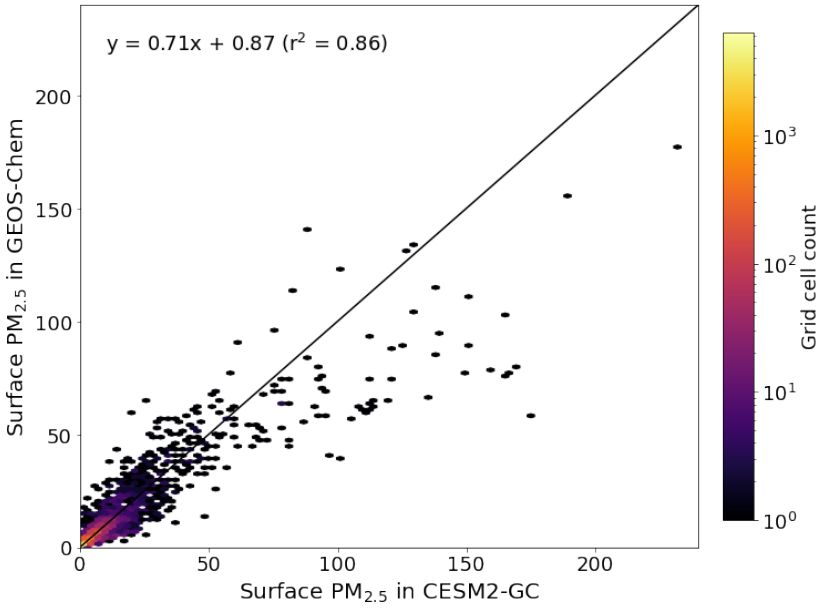

Figure 4-10: Parity plot of annually-averaged surface $PM_{2.5}$ mass concentrations for CESM2-GC and the GEOS-Chem CTM. Fitting parameters are shown in the top left corner.

the y-axis. Model results are interpolated to the locations of the observations (top: 900 hPa; middle: 500 hPa; bottom: 250 hPa). The numbers correspond to specific regions [119]: Left panels (tropics): 1, NH subtropics; 2, W Pacific/E Indian Ocean; 3, Equatorial Americas; 4, Atlantic/Africa. Middle panels (mid latitudes): 1, Western Europe; 2, Eastern United States; 3, Japan; 4, SH mid latitudes. Right panels (high latitudes): 1, NH Polar West; 2. NH Polar East; 3, Canada; 4, SH polar.

In the tropics, both CESM2-GC and CAM-Chem estimate similar ozone mixing ratios, where both models are slightly biased towards lower mixing ratios than the ozonesonde climatology in the troposphere. Model results from the GEOS-Chem CTM display better correlation, but similar bias with respect to the ozonesonde climatology. In the mid latitudes and in the troposphere, CESM2-GC and the GEOS-Chem CTM provide lower ozone mixing ratios than CAM-Chem at any pressure. CAM-Chem has lower biases at 900 and 500 hPa, while CESM2-GC and the GEOS-Chem CTM perform better than CAM-Chem at 250 and 50 hPa in the mid latitude band. At high latitudes, CESM2-GC and GEOS-Chem underpredict the ozone mixing ratios throughout the troposphere, where CAM-Chem performs better. However, the differences in behavior between CESM2-GC and CAM-Chem

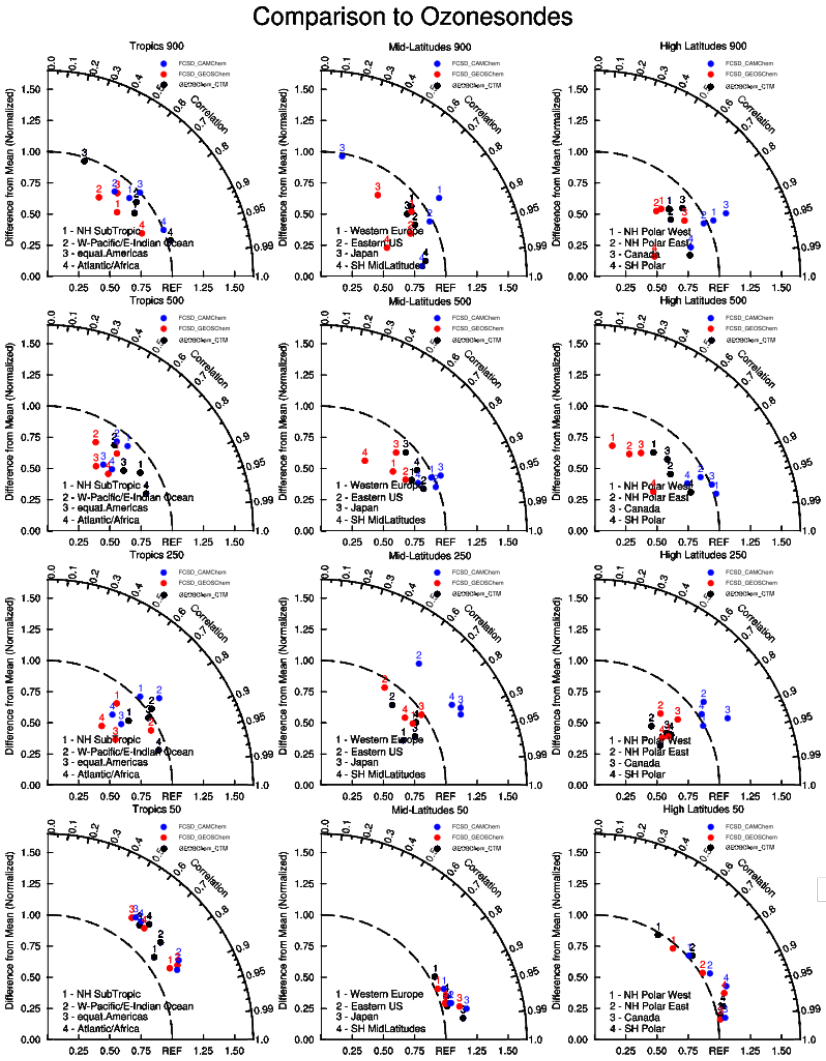

Figure 4-11: Taylor diagrams of the comparison of CESM2-GC, CAM-Chem, and the GEOS-Chem CTM simulations to a present-day (1995-2010) ozonesonde climatology (blue: CAM-Chem, red: CESM2-GC, black: GEOS-Chem CTM).

vanish in the stratosphere at high latitudes.

Figure 4-12 shows annually-averaged ozone columns, expressed in Dobson Units, as measured by the Aura Ozone Monitoring Instrument (OMI) and Microwave Limb Sounder (MLS). The results from the satellite observations are compared to results from CESM2-GC, CAM-Chem, and the GEOS-Chem CTM. I find that on average the results from CESM2-GC are approximately 8 DU lower than the observations, mostly driven by an overestimation of stratospheric ozone depletion during the Antarctic spring by up to ~16 DU. CAM-Chem predicts a total ozone column that is ~7 DU larger than the global mean

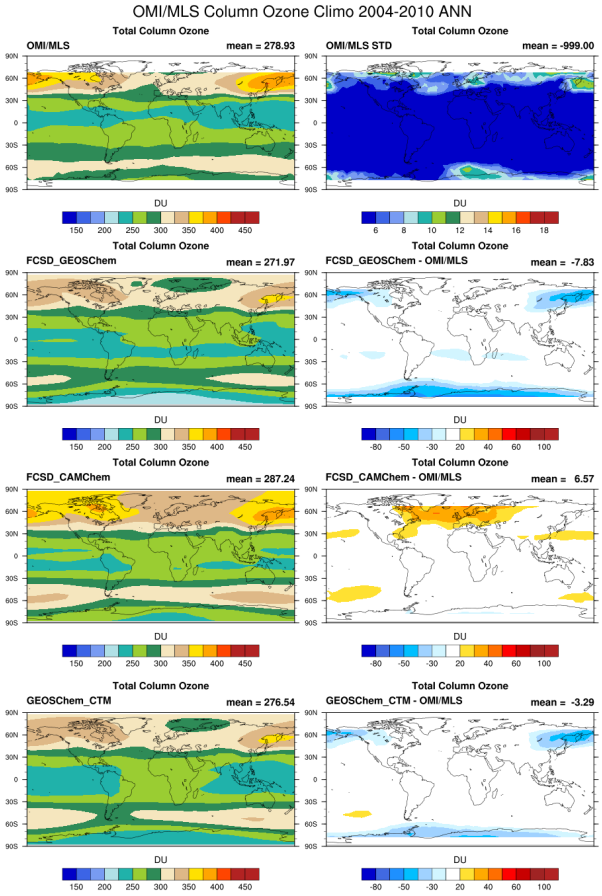

Figure 4-12: Total ozone column as observed by the Aura Ozone Monitoring Instrument (OMI) and Microwave Limb Sounder (MLS) for the 2004-2010 time period (1st row), compared to the results from CESM2-GC (2nd row), CAM-Chem (3rd row), and the GEOS-Chem CTM (4th row) for the year 2016. The measurements and model results are presented on the left, while the standard deviation from the observation and the model biases are shown on the right.

ozone column. When broken down by tropospheric and stratospheric ozone column, I find that the annually-averaged bias in the stratospheric and tropospheric ozone columns for CESM2-GC is -2 and -6 DU respectively, compared to +9.5 and -2.5 DU for CAM-Chem. Additionally, I find that the bias in seasonal variations of total column ozone as predicted by CESM2-GC range between -16 and -6 DU, while the variations range from -3 to +7 DU for CAM-Chem. The model results from the GEOS-Chem CTM predict similar geographical biases in total ozone column as CESM2-GC, with smaller overall magnitude.

Figure 4-13 compares atmospheric column concentrations of carbon monoxide, expressed in mole/cm^2, to CO observations retrieved from the Measurements of Pollution

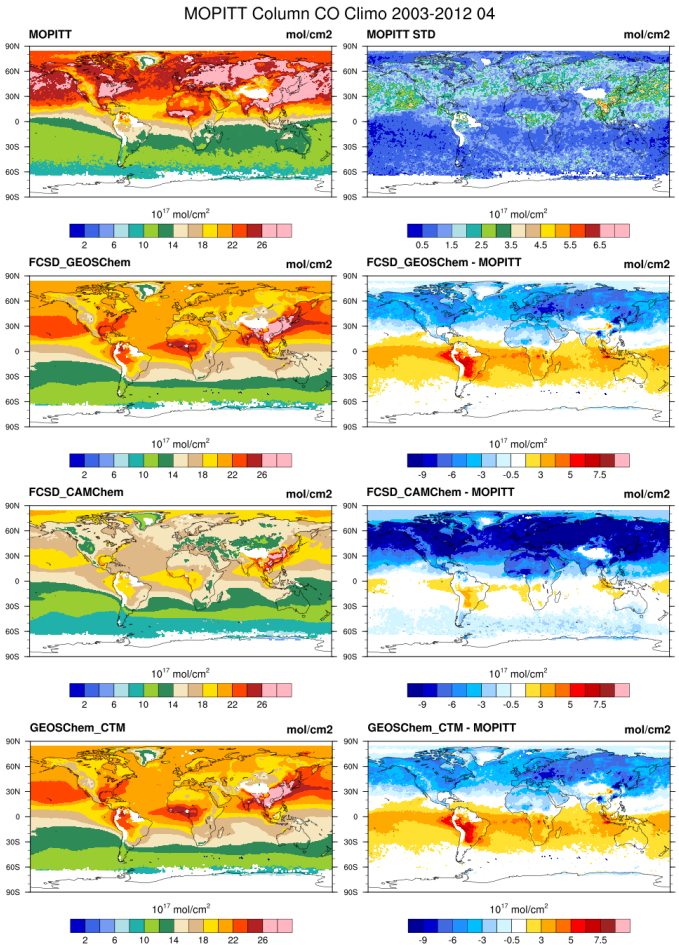

Figure 4-13: Carbon monoxide column totals, expressed in mole/cm^2. The first row displays the satellite observations from MOPITT (left) as well as the standard deviations from the measurements (right). The simulation results and biases are presented for CESM2-GC (2nd row), CAM-Chem (3rd row), and the GEOS-Chem CTM (4th row). The model evaluations are shown for April 2016.

in The Troposphere (MOPITT) for the year 2003-2012. The model results as well as the model biases are shown in Figure 4-13 for April 2016. The CO model estimates using CAM-Chem are characterized by a strong negative bias in the Northern Hemisphere (compared to other latitudes) that has been observed in previous model evaluations [34]. In CESM2-GC, a negative bias still exists in the Northern Hemisphere, but only reaches -5 mole/cm^2, compared to -9 mole/cm^2 for CAM-Chem. A stronger positive bias exists in the Southern Hemisphere when using CESM2-GC, but does not exceed +5 mole/cm^2. On average, CESM2-GC leads to a smaller globally-averaged bias than CAM-Chem, with negative biases in the Northern Hemisphere counterbalancing a positive bias in the Southern

Hemisphere. The results from the GEOS-Chem CTM are in agreement with CESM2-GC.

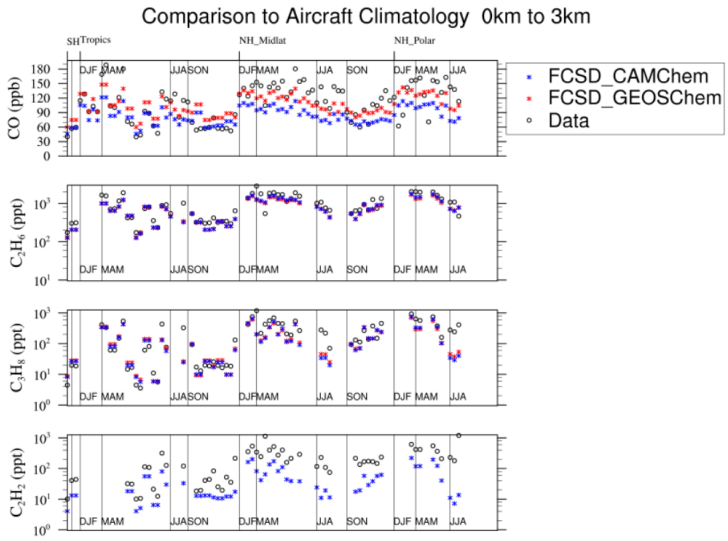

Figure 4-14: Airborne observations from aircraft campaigns and model results for CESM2-GC (red) and CAM-Chem (blue) for CO, C_2H_6, C_3H_8, C_2H_2. The observations and model results here focus on the 0 to 3 km altitude band. Each observation point represents an average over the altitude band and aircraft campaigns, while the model results are averaged over the same location and altitude range for the corresponding observation month.

Figures 4-14 and 4-15 compare carbonated species to observations from airborne field experiments that have been collected over a wide range of locations and seasons [33, 120]. Results from both CAM-Chem and CESM2-GC are compared to these aircraft observations for CO, C_2H_6, C_3H_8, C_2H_2. Figure 4-14 shows the observations alongside the model results in the 0 to 3 km altitude band, while Figure 4-15 focuses on the 2 to 7 km band. Each observation point represents an average over the altitude band and aircraft campaigns, while the model results are averaged over the same location and altitude range for the corresponding observation month. The results are also broken down by latitude band (Southern Hemisphere, tropics, Northern Hemisphere mid latitudes, and Northern Hemisphere high latitudes).

The model simulations are consistent with the airborne observations. Similarly to Figure 4-13, I find that CAM-Chem underpredicts CO mixing ratios in the Northern Hemisphere.

Additional comparisons with airborne measurements from aircraft campaigns in numerous locations and seasons are presented in Appendix C.

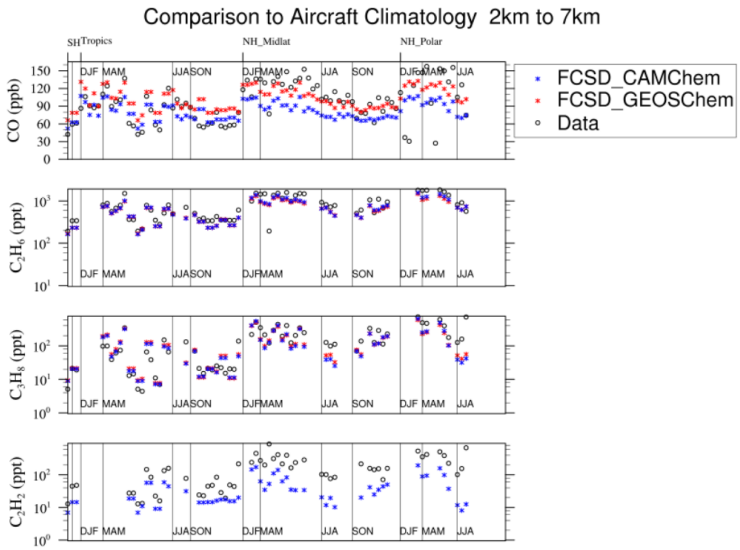

Figure 4-15: Same as Figure 4-14, but observations and model results are only sampled in the 2 to 7 km altitude band.

4.4 Evaluation of the coupled chemistry-climate feedback of commercial aviation emissions

This section aims to describe the simulation framework to evaluate the climate feedback of aviation emissions onto atmospheric composition using the newly-developed chemistry-climate model, CESM2-GC.

4.4.1 Methods

Four full-model large ensemble sets of simulations are performed, each performed over a decade to capture the short and long-term atmospheric feedback. The goal of running an ensemble of simulations is to capture the underlying uncertainties in the climate system. In this section, five ensemble members per simulation set are performed, thus accounting for the sensitivity of parameterizations in CAM and CLM to small perturbations.

The baseline set of simulations is Set 1, described by:

- Set 1: Run with aviation emissions and online meteorology

Other simulations differ from Set 1 as following:

- Set 2: Run without aviation emissions and online meteorology
- Set 3: Run with aviation emissions and with nudged meteorology from Set 1
- Set 4: Run without aviation emissions and with nudged meteorology from Set 1

Set 1 represents the baseline case with standard emissions. I thus decide to archive high-frequency meteorological fields for each ensemble member of Set 1 that are used in Sets 3 and 4 to nudge the meteorology. In Set 1, three dimensional fields of temperature, zonal and meridional winds are archived at an eight hour frequency.

The climate feedback on atmospheric composition from commercial aviation emissions is obtained by taking the difference between Set 2 and Set 1. In these simulations, the chemistry-climate feedback is accounted for.

The difference between Set 3 and Set 4 captures the change in atmospheric composition from aviation emissions owing to atmospheric chemistry only. No climate feedback on atmospheric composition are captured from these simulations, as they use nudged meteorology as an input.

For Sets 1 and 3, I used the aviation emission inventory for the year 2019, derived from the Aviation Emissions Inventory Code (AEIC) [109]. Flights are simulated based on schedule data from the 2019 OAG schedule [93]. The emissions are gridded at a horizontal resolution of 0.5° latitude by 0.625° longitude with a daily temporal resolution. The emission inventory adds up to a total of 258 Tg of fuel burn and 4.51 Tg of NO_x (on a NO_2 mass basis), with 91% of the fuel burn released in the Northern Hemisphere. 73% of the total fuel consumption occurs above 8 km.

Sets 3 and 4 are using nudged meteorology archived from Set 1. Nudging allows to constrain the evolution of the meteorology of Sets 3 and 4 such that it remains close to the evolution of Set 1 [57]. Nudging has been commonly used in global climate models [132, 113]. The nudged variables used for this study are three-dimensional fields of temperature, meridional and zonal winds, which are saved every eight hours. Only a few variables are typically nudged as the rest of the meteorological fields are allowed to change following atmospheric processes [113].

4.4.2 Results

In this section, I first present the results from the fully-coupled sets of simulation using online meteorology. The results are obtained by taking the difference between Sets 2 and 1 and averaged across all ensemble members. I then quantify the aviation emissions' response from the nudged simulations by taking the difference between Sets 4 and 3.

Fully-coupled simulations with online meteorology

Figure 4-16 presents the change in ensemble-averaged surface ozone mixing ratio from commercial aviation emissions. The results are consistent with previous estimates of commercial aircraft activities using GEOS-Chem [7, 28]. In the Northern Hemisphere, ozone mixing ratios are increased between 0.1 and ~3 ppbv, while in the Southern Hemisphere, the changes are limited to 0.4 ppbv. This is explained by the fact that most aviation fuel burn is released in the Northern Hemisphere and by the slow inter-hemispheric transport. The ozone response is larger in tropical areas compared to higher latitudes, in agreement with previous studies [7]. Aviation emissions result in an increase of 0.44 ppbv in the area-averaged surface ozone response, while the population-weighted average reaches 0.56 ppbv, consistent with previous studies [15, 28]. I also find that the ensemble mean leads to a global increase in surface ozone, even though individual ensemble members can display regions of negative ozone response from aviation emissions.

To quantify this chaotic variability within ensemble members, the hatched areas in Figure 4-16 represent regions that are not statistically significant at the 0.05 level using a two-sided Student's t-test. In these regions, more ensemble members would be needed to conclude that aviation emissions lead to a change in surface ozone mixing ratios. I find that most of the Southern Hemisphere is characterized by changes in surface ozone mixing ratios that are not statistically significant. With five ensemble members, I find that most of the Northern Hemisphere has a statistically significant ozone response from aviation emissions, conflicting with previous results using a fully-coupled CESM simulation with CAM5, which found that only very localized regions show a statistically significant signal using a single ensemble run [15]. I anticipate that longer simulations could yield

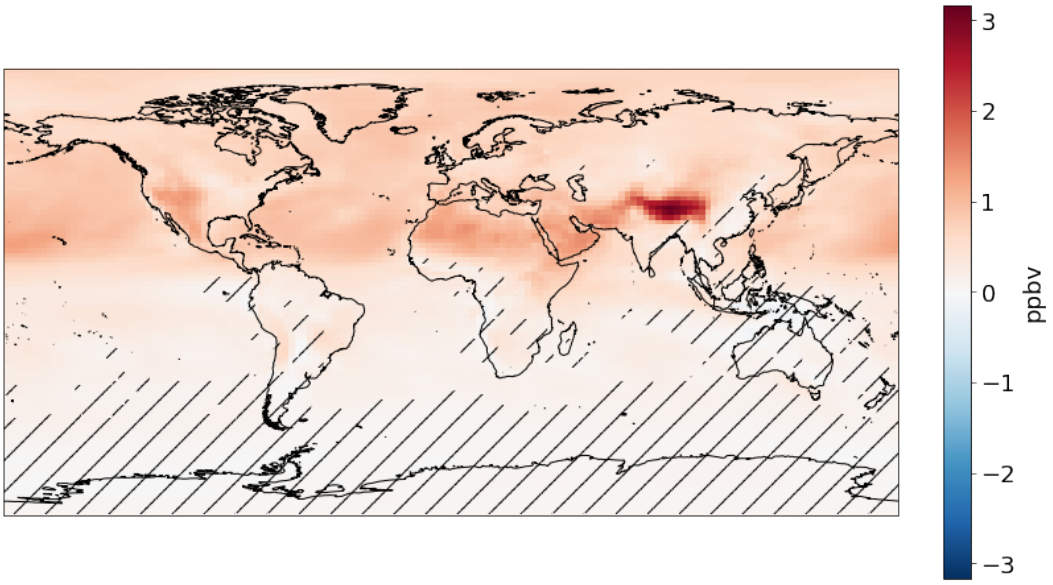

Figure 4-16: Ensemble average of the change in surface ozone mixing ratio owing to commercial aviation emissions. The hatched area represents regions that are not statistically significant at the 0.05 level using a two-sided Student's t-test.

more geographical locations where statistical confidence surpasses 95%. However, more work would be needed to quantify the length of these simulations. Figure 4-17 shows the standard deviation of surface ozone across all ensemble members. Regions of low standard deviation means that most ensemble members have a similar estimate of aviation's impact on surface ozone. South-East Asia and South America have the largest standard deviations. A comparison of the aviation response to the results from the nudged simulations is presented in the following paragraph.

Zonally-averaged ozone mixing ratios are shown in Figure 4-18, with hatched areas representing statistically significant regions. The ensemble members predict a statistically significant signal in the mid to upper-troposphere in the North Hemisphere, reaching responses up to ~10 ppbv, locally. The largest increase in upper-tropospheric ozone occurs where most aviation fuel is burnt. The aviation-induced ozone perturbation decreases with altitude. The model also predicts both negative values in the Southern Hemisphere and large positive values in the Southern Hemisphere, but these are not considered statistically significant at the 0.05 level, as more ensemble members would be needed. The increase in mid and upper-tropospheric mixing ratios is consistent with the scientific literature, after

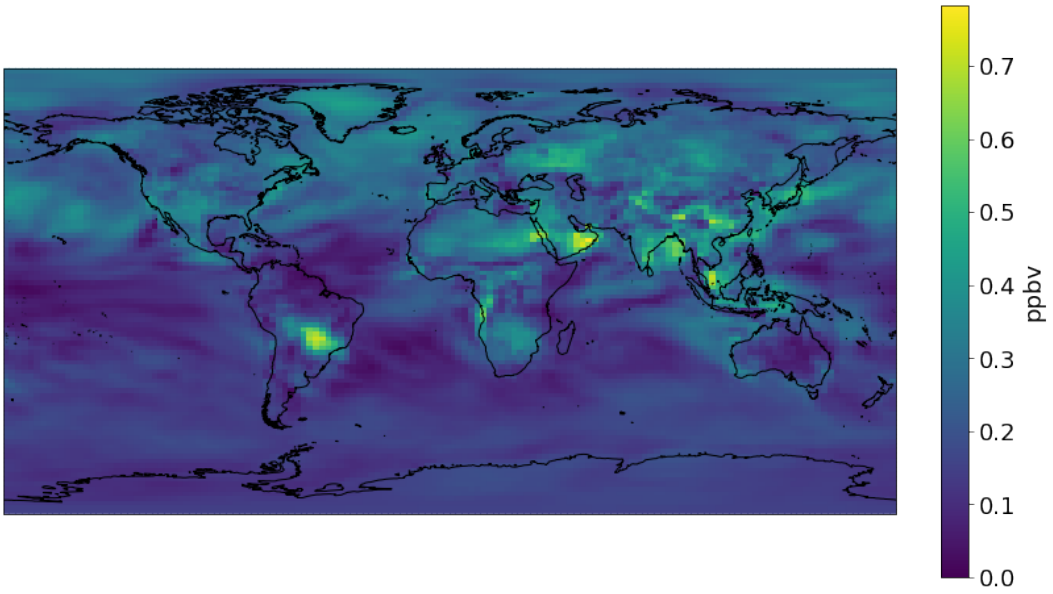

Figure 4-17: Standard deviation of the change in surface ozone mixing ratio owing to commercial aviation emissions.

considering the higher fuel burn values used in this study, based on the more recent aircraft emission inventory [64, 28].

The ensemble mean temporal evolution of the aviation emissions' response on surface ozone mixing ratios is shown in Figure 4-19 for the 2015 to 2025 period. I show that aviation's signal on surface ozone is stronger during boreal winter time and weaker during summer time in agreement with previous studies using the GEOS-Chem chemistry model [15, 28, 75, 114, 7]. During winter time, ozone reaches peaks of ~2-3 ppbv (except during the 2018-2019 winter period, which is characterized with a peak up to 4 ppbv). The increase in the ozone response during winter time is due to its increased lifetime in the mid-troposphere, despite the slower transport and mixing rates compared to the summer season. This seasonal variation in ozone mixing ratios due to aircraft activities has been observed previously [15, 28]. I also study the variations of globally-averaged surface ozone response across all ensemble members. I find that the range of possible values lies within ± 5 ppbv of the ensemble mean throughout the integration period. Additionally, I find that the boreal winter surface ozone signal is statistically-significant at the 0.05 level in the Northern Hemisphere. However, given the smaller magnitude of the surface ozone response in the Southern Hemisphere and during boreal summer, more ensemble members or longer runs

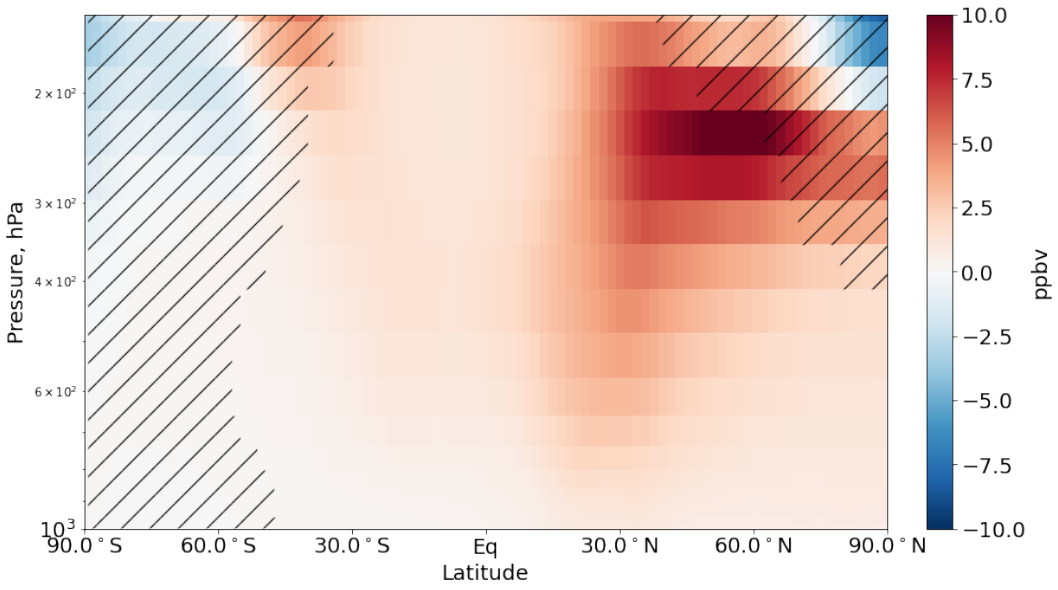

Figure 4-18: Change in zonally-averaged ozone mixing ratio from commercial aviation emissions. The hatched area represents regions that are not statistically significant at the 0.05 level using a two-sided Student's t-test.

would be needed to reach statistical significance at the 0.05 level.

Figure 4-20 displays the change in atmospheric NO_x mixing ratios from aviation emissions in the Northern Hemisphere. Most of the NO_x atmospheric response from commercial aircraft activities occur in the Northern Hemisphere. At cruise altitudes (~220 hPa), the response is characterized by a strong positive signal reaching 0.1 ppbv. During winter time, the aviation contribution to upper-tropospheric NO_x can reach 85%. At lower altitudes, I find that aviation emissions lead to a reduction in near-surface NO_x mixing ratios by 25 pptv, when averaged globally. These findings are consistent with previous studies [7, 64, 31, 28]. The NO_x upper-tropospheric response to aviation emissions is statistically significant at the 0.05 level. However, I would need more ensemble members or longer simulations to further estimate the magnitude of the NO_x near-surface depletion.

Emissions of NO_x, water vapor, and unburned hydrocarbons (such as HCHO or CH_3CHO) from commercial aviation leads to increased OH mixing ratios at cruise altitudes. This increase extends up to 100 hPa and is limited to tropical regions and the North Hemisphere. The peak value change of 0.05 pptv is reached at 30°N at cruise altitude.

Additionally, I find that black carbon aircraft emissions over the Arctic contribute up

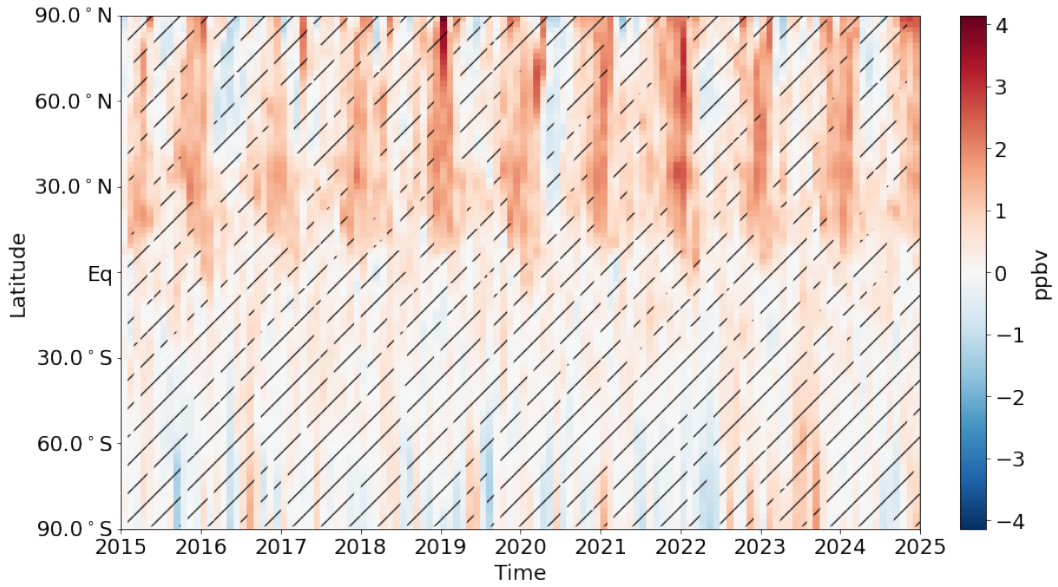

Figure 4-19: Temporal evolution of longitudinally-averaged surface ozone mixing ratios across all ensemble members. The hatched areas designate regions that are not statistically significant at the 0.05 level.

to 20% to the total column black carbon emissions from all sources. Previous studies have found a relative contribution of 10% for the year 2006 [60]. Commercial aviation represents the dominant black emission source over Arctic sea ice alongside local shipping. I find that above 45°N and at cruise altitudes, aviation black carbon emissions contribute to approximately 10% of the upper-tropospheric black carbon mass concentrations, compared to less than 1% at the surface at mid Northern latitudes. Given the relatively lower precipitation in the Arctic compared to mid latitudes, black carbon emitted at cruise altitude over the Arctic has a longer lifetime compared to other latitudes, but also compared to surface emissions. This longer lifetime at higher latitudes leads to an increase in the number of aerosol particles above 250 hPa and above 45°N. The aviation-induced contributions to aerosol particles are concentrated in the accumulation and coarse modes with respective changes of 2×10^6 and 5×10^4 particles/kg respectively at 200 hPa at high Northern latitudes, corresponding to approximately 4% of the background aerosol number. I find no statistically-significant aviation-induced changes in cloud condensation nuclei at the 0.05 level.

Finally, I find that the ensemble runs predict a positive aviation-attributable surface $PM_{2.5}$ change over Europe, Northern India and North-Eastern China of the order of 0.4

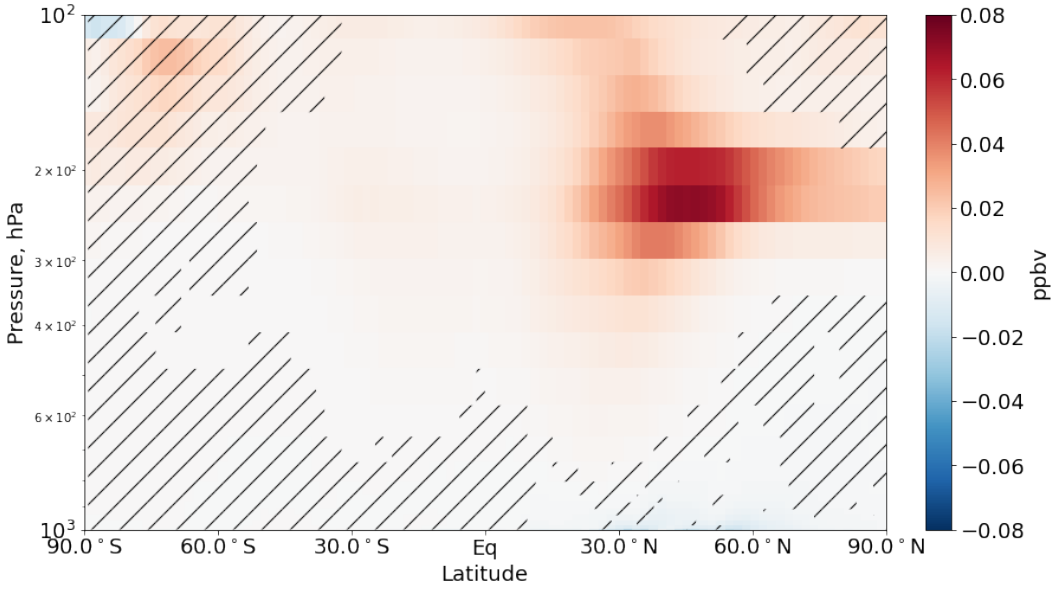

Figure 4-20: Change in zonally-averaged NO_x mixing ratio from commercial aviation emissions. The hatched areas designate regions that are not statistically significant at the 0.05 level.

$\mu g/m^3$, consistent with previous studies [7, 28, 14]. However, the results are subject to large inner variability making the results not statistically significant at the 0.05 level using only five ensemble runs.

I find that the increase in surface $PM_{2.5}$ mass concentrations is almost entirely due to changes in secondary sulfate-ammonium-nitrate aerosol, consistent with previous studies [7]. However, ammonium and nitrate aerosols are currently not accounted for in the radiative balance in the atmospheric component of CESM2, CAM. This aviation-attributable change in tropospheric aerosol concentrations can induce changes in cloudiness through the aerosol indirect effect, thus affecting precipitation, photolysis, air mixing, and temperature. Additionally, changes in near-surface aerosol concentrations can induce changes in near-surface meteorology, such as wind speeds. In turn, these small changes affect dust, sea salt and biogenic emission fluxes. Previous studies have found that these aerosol-induced feedbacks are the leading factors influencing surface chemistry and $PM_{2.5}$ production [129, 82]. More work is needed to include secondary aerosols in the radiation calculations and to quantify the magnitude of these phenomena.

No statistically significant change in surface or upper-tropospheric circulation has been

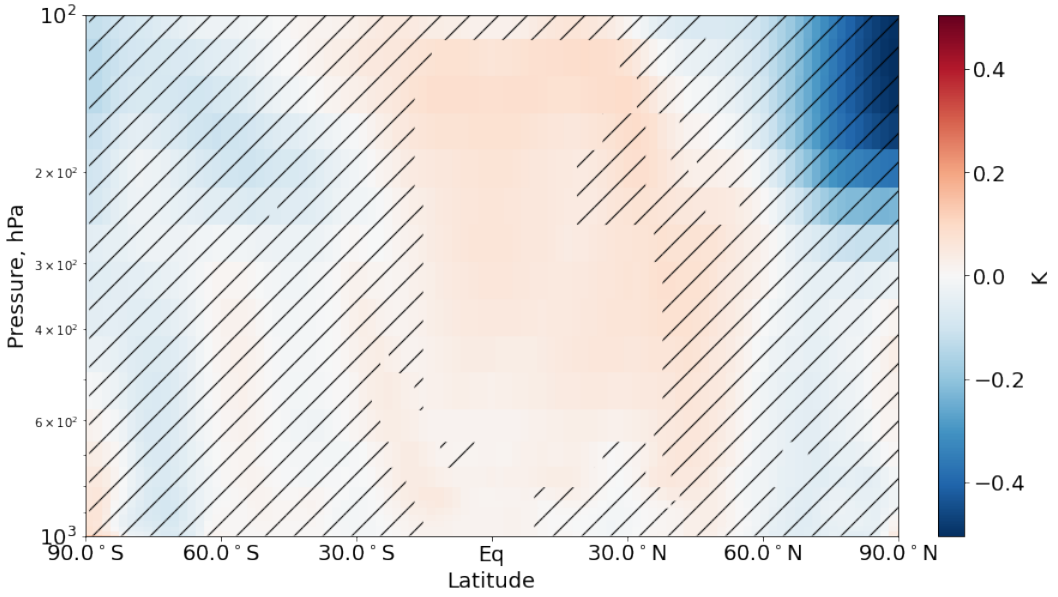

Figure 4-21: Change in zonally-averaged temperature from commercial aviation emissions. The hatched areas indicate regions that are not statistically significant at 0.05 level using a two-sided Student's t-test.

observed based on the results of Sets 1 and 2. However, I find that the simulations lead to a statistically significant increase in tropospheric temperatures in the tropics by ~70 mK as displayed in Figure 4-21. This statistically significant region extends up to 100 hPa. This increase in tropospheric temperatures also extends up to 50°N, but becomes less statistically significant at the 0.05 level at mid latitudes. This positive change in tropospheric temperatures can be explained by the aviation-induced change in upper-atmospheric ozone in the Northern Hemisphere, where the aviation-attributable ozone response is maximal. Ozone acts as a greenhouse gas and is included in the radiative calculations in CESM2.

For the other meteorological variables, I find that the climate variability introduced in each ensemble member dampens the aviation-attributable signal and is within the cross-ensemble standard deviation, such that no statistical significance can be pointed out. Additionally, I find no statistically-significant changes in lightning NO_x emissions from the effect of commercial aviation emissions. CAM computes lightning NO_x emissions based on the lightning flash frequency, which is estimated following the model cloud height, with different parameterizations over ocean and land. The NO lightning production rate in CAM is assumed proportional to the lightning discharge energy with 10^{17} atoms of ni-

trogen released per Joule [99]. The lightning NO_x emissions are then distributed over the complete column of grid boxes. This differs from previous studies, where lightning NO_x emissions are calculated based on the number of liquid and ice cloud nuclei [60]. Zonal changes in circulation patterns, cloud properties, vertical atmospheric stability and lightning NO_x emissions owing to commercial aircraft activities are displayed in Appendix C. In CESM2-GC, black carbon from commercial aviation emissions influence clouds in two major ways: (1) through both indirect effects (increase in cloud reflectivity and lifetime effect), and (2) through the semi-direct effect (change in cloudiness from the absorption of aerosol particles, thus affecting the near-cloud relative humidity). I find that the ensemble mean global change in cloud fraction increases by 0.039% (when the average is performed below 100 hPa). These changes are driven by large contributions from the poles, with local increases up to 1% in the Arctic below cruise altitudes and 2% in the Antarctic at 500 hPa. However, most of these changes are not statistically-significant at the 0.05 level. Longer simulations or more ensemble members would be needed to reach statistical significant in aviation-induced cloudiness at the 0.05 level.

Comparison to the nudged simulations

In this section, I compare how the results obtained from Section 4.4.2 are modified when nudging the meteorology towards that of Set 1.

Figure 4-22 compares the results of the fully-coupled simulations to the nudged simulations for surface ozone mixing ratios and surface $PM_{2.5}$ mass concentrations. The average is performed over the last nine years of the 10-year simulations, allowing for one year of spin up. I find that the ozone response is consistent between both simulation sets with a population-weighted surface exposure of 0.56 ppbv. However, stronger cross-ensemble variability is observed in the fully-coupled simulations, allowing for climate feedback. In these simulations, the aviation response is not statistically significant over South-East Asia, Oceania and at high southern latitudes, while the results are statistically significant at any location in the nudged simulations.

The surface $PM_{2.5}$ response to aviation emissions have more discrepancy between the two approaches. I find that both approaches still predict a statistically significant surface

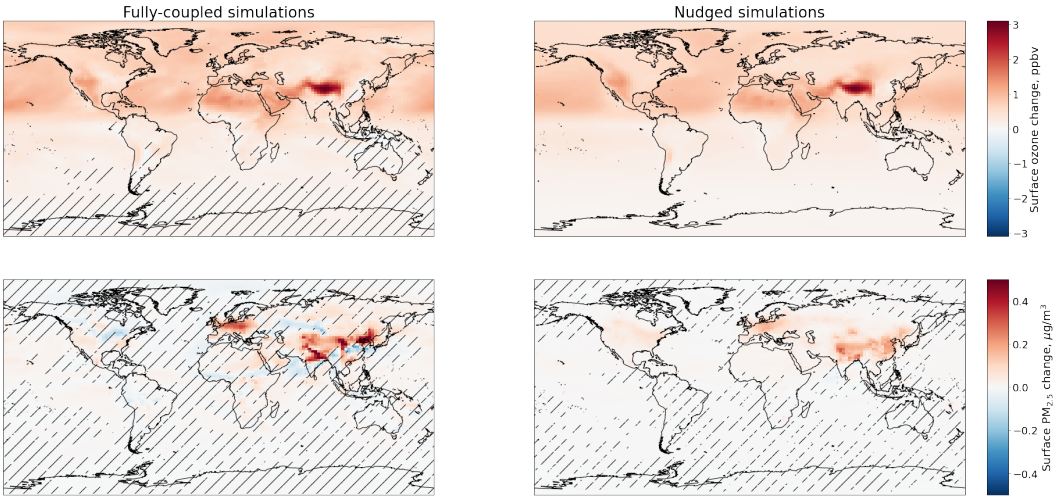

Figure 4-22: Surface changes in surface ozone mixing ratios (top) and surface $PM_{2.5}$ mass concentrations (bottom) for the fully-coupled (left) and nudged (right) ensemble runs using CESM2-GC. The results are averaged over the last nine years of the 10-year simulations. Hatched areas display regions that are not statistically significant at the 0.90 level.

$PM_{2.5}$ response over the West coast of the United States, Europe, Northern India and North-Eastern China. Because of their lower inner variability, the nudged simulations predict a statistically significant response over North America, Europe, Northern Africa and most of Asia. In the fully-coupled simulations, the population-weighted change in $PM_{2.5}$ exposure reaches 0.08 µg/m^3, mainly driven by large increases over North India and Eastern China, while I find that the nudged simulations predict a change equal to 0.07 µg/m^3.

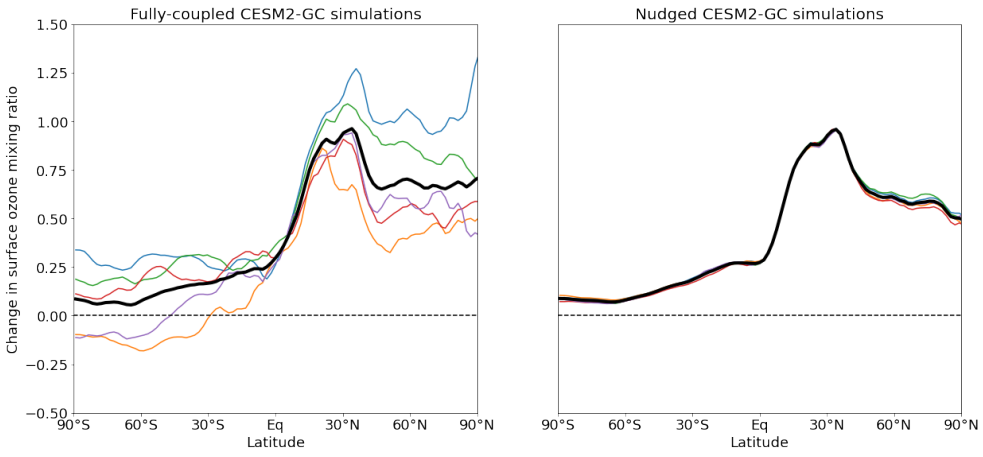

Figure 4-23: Comparison of the change in zonally and annually-averaged surface ozone mixing ratios across all ensemble members in the fully-coupled (left) and nudged (right) simulations. The dashed line represents the ensemble mean.

Figure 4-23 shows the change in zonal surface ozone due to commercial aircraft activities for each individual ensemble member. First, the results from the nudged simulations show that the mean surface ozone response to aviation emissions is 0.44 ppbv (0.56 ppbv when population weighted), consistent with the fully-coupled simulations. However, the fully-coupled simulations display much higher latitudinal variability relative to the nudged simulations. In the latter, statistical significance in the surface ozone signal is reached at any location. I also show that the Southern Hemisphere and Arctic regions are characterized by larger variability across ensemble members compared to the tropical and mid-latitudes in the Northern Hemisphere. The annual mean, as displayed in Figure 4-23, is consistent in both approaches with a maximum difference of 0.15 ppbv in the Arctic.

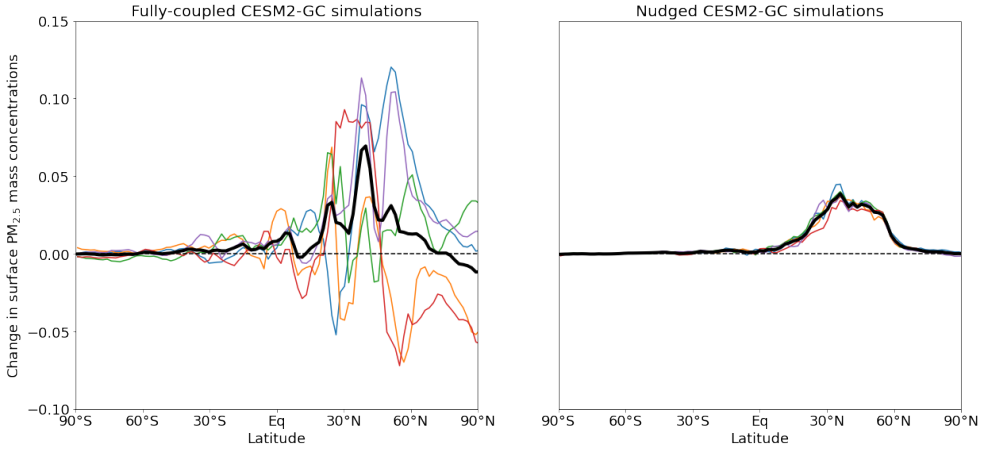

Figure 4-24: Same as Figure 4-23, but here considering the surface $PM_{2.5}$ mass concentrations across all ensemble members. The average is performed over the last nine years of the 10-year simulations.

Figure 4-24 displays zonally and annually-averaged $PM_{2.5}$ surface concentrations owing to aviation emissions. Similarly to Figure 4-23, I find that the fully-coupled simulations using CESM2-GC are characterized with much stronger inner-variability across ensemble members. As a comparison, the mean standard deviation at the surface is 0.13 $\mu g/m^3$ and 0.03 $\mu g/m^3$ for the fully-coupled and nudged simulations respectively. The magnitude of the response from both simulation sets is consistent with previous studies using CTMs [28, 7, 15]. For instance, the annually-averaged population-weighted change in surface $PM_{2.5}$ response is 0.08 $\mu g/m^3$ for the fully-coupled simulations (while it is 0.07 $\mu g/m^3$ for the nudged simulations). A recent study found an aviation-induced increase in sur-

face $PM_{2.5}$ equal to 0.053 μg/m^3 from aviation emissions [28]. The area-weighted $PM_{2.5}$ change is 0.007 μg/m^3 for both sets, in good agreement with previous values from the scientific literature ranging between 0.003 and 0.008 μg/m^3 [15]. The geographical distributions, displayed in Figure 4-22, are also in good agreement with previous studies, with regions over Europe, India and East Asia experiencing local increases up to 0.5 μg/m^3 in surface $PM_{2.5}$ due to aviation emissions. However, I find that the number of ensemble runs is still too low to conclude that the results from the fully-coupled simulations are statistically significant regarding surface $PM_{2.5}$. Longer runs would also make the aviation signal statistically significant as atmospheric variability decreases with time averaging.

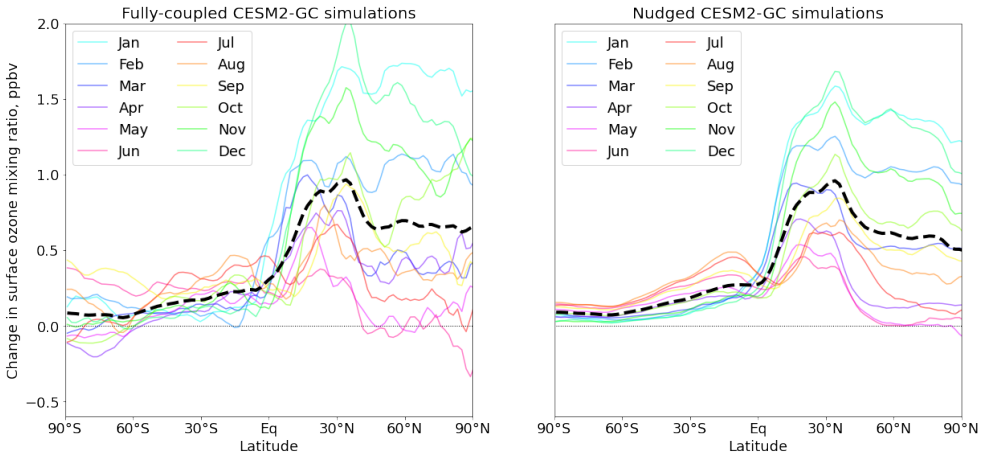

Figure 4-25: Comparison of the ensemble means of the change in monthly-averaged surface ozone mixing ratio for the fully-coupled (left) and nudged (right) simulations. The black dashed line represents the annual mean.

Figure 4-25 describes the change in zonally-averaged surface ozone due to aviation emissions, averaged over each simulated month. Similarly to Figure 4-23, I find that the fully-coupled simulations display larger variability and stronger variations with latitude when compared to the nudged simulations. The seasonal pattern is identical in the fully-coupled and nudged simulations, with winter months characterized with a stronger ozone response.

The results presented in Figure 4-25 can be compared against previous literature results [15]. In this previous study, CESM2 was run with CAM5 and using CAM-Chem assuming an aviation emission inventory representation of 2006. The results were averaged over six

years. Here I use CESM2-GC, thus relying on the GEOS-Chem chemistry representation, with CAM6 and using an aviation emission inventory for 2019. This 2019 emission inventory has approximately twice the amount of aviation fuel burn compared to the 2006 emission scenario. Additionally, I have used five ensemble members for each set of simulation and averaging the results over a decade. These are possible causes that explain the differences between these results and the intercomparative previous study using CESM2 [15]. More work would be needed to identify which cause leads to these differences, by reproducing the simulation set, with aviation emissions for 2006 and using CAM-Chem.

4.5 Discussion and limitations

In this chapter, I evaluated the environmental response of aviation emissions using fully-coupled climate simulations, allowing for meteorological feedback. This analysis was driven by a previous study suggesting that the effects of aviation emissions on upper-tropospheric and surface mixing ratios were magnified by climate feedback [60]. To test this hypothesis, I develop a newly-coupled model, CESM2-GC, unifying a GCM, CESM2, with the GEOS-Chem chemistry model, which has previously been used extensively to estimate the role of aviation emissions.

I present a validation of CESM2-GC against results from the native chemistry option in CESM2, CAM-Chem, as well as the GEOS-Chem CTM. I provide additional comparisons to ground station, aircraft and satellite measurements. With all emission fluxes identical and specified dynamics for all runs, I find that CESM2-GC generates results that are consistent with observations and other models. I show that CESM2-GC surface ozone mixing ratios agree with results from the GEOS-Chem CTM, while they are slightly lower than estimates from CAM-Chem. Furthermore, Column ozone totals in CESM2-GC are underestimated compared to satellite measurements, with a negative bias of 8 DU. CESM2-GC also underestimates local column ozone in polar events, such as the Antarctic spring, where I find a negative bias up to 16 DU. Comparisons of carbon monoxide to satellite measurements show that CESM2-GC provides a smaller globally-averaged bias, balancing out a negative bias in the Northern Hemisphere with a positive bias in the Southern Hemisphere.

Finally, I also show results from CAM-Chem and CESM2-GC against measurements from aircraft campaigns. The model results are consistent with the observations and between each other, with a small negative bias in ozone observed for CESM2-GC.

In the second part of this chapter, I use CESM2-GC to perform ensemble runs to evaluate the role of climate feedback on the environmental assessment of aviation emissions. Using fully-coupled simulations, I find that aviation emissions lead to a population-weighted surface increase in ozone mixing ratios of 0.56 ppbv, in agreement with previous studies [15]. The increase in surface ozone is statistically significant in most of the Northern Hemisphere. I also show that the simulations also lead to an increase in surface $PM_{2.5}$ over Europe, Northern India and East China, however, more ensemble members or longer simulations would be needed to make the results statistically-significant. Furthermore, I perform additional ensemble member simulations using nudging the meteorology. The nudged simulations generally agree with the fully-coupled simulations and provide a population-weighted surface ozone response to aviation emissions also equal to 0.56 ppbv. However, I find that the results from the nudged simulations display much lower inner-variability compared to the fully-coupled simulations. I show that the fully-coupled simulations reproduce a statistically-significant change in surface $PM_{2.5}$ over Europe, Northern India and Eastern China, in agreement with the nudged simulations and previous studies [7]. I find that the model estimates an increase in population-weighted $PM_{2.5}$ exposure by 0.08 and 0.07 $\mu g/m^3$ for the fully-coupled and nudged simulations respectively. The $PM_{2.5}$ response is also characterized by less variations across ensemble members in the nudged simulations. Despite their larger chaotic behavior, the fully-coupled simulations are able to reproduce the seasonal pattern in aviation-attributable surface ozone and $PM_{2.5}$, observed in previous studies [15, 28].

Finally, I evaluate the role of climate feedback from high-altitude aviation emissions. I find that the fully-coupled simulations introduce no statistically significant changes in circulation patterns, cloud fractions or surface temperatures when using five ensemble members and decadal simulations. However, I show that the ensemble members capture a change in the 10-year averaged tropospheric temperatures in tropical regions and Northern mid latitudes, up to 70 mK. This can be explained by the increase in aviation-attributable

ozone, which is maximized in the Northern Hemisphere. Future work should focus on whether longer simulations or additional ensemble members would change the statistical significance of the magnitude of climate feedback due to aviation emissions.

The fully-coupled simulations used in this chapter do not account for the radiation feedback of aviation-induced aerosols, such as nitrates and ammonium. For instance, the aerosol indirect effect translates changes in aerosol concentrations into cloud coverage, thus affecting photolysis, temperatures, air mixing, and precipitation, all of which affect lower-tropospheric and surface chemistry [129]. Further work to include nitrates and ammonium as components of the radiative scheme in CAM and quantify the magnitude of this aerosol-driven feedback is necessary.

Chapter 5

Conclusion

The work presented in this thesis aims to improve the scientific understanding of the environmental impacts of commercial aircraft activities from the non-linear plume-scale processes up to global climate and atmospheric responses. Given the complexity of the different atmospheric pathways involved and the different temporal and spatial scales associated with aircraft emissions, the work of this thesis is divided into chapters each aiming to resolve a different question.

5.1 Key findings

Commercial aircraft emissions degrade surface air quality, have lasting effects on the ozone layer, and are a growing contributor to climate change. The three chapters of this thesis tackle each individual aspect of the environmental impact of aviation emissions.

In Section 2, I use an aircraft plume model to estimate the role of plume-scale processes in the evaluation of the impact of aviation emissions. I find that a processing of aircraft emissions to include non-linear plume effects leads to a reduction in the aviation-induced ozone perturbation by approximately 5% globally, despite large spatial and seasonal heterogeneities. The largest absolute change in aviation-attributable ozone occurs at subsonic aircraft altitude, at ~11 km, while surface conditions experience both increases or decreases in aviation-attributable ozone exposure, with urban areas having increases in ozone from plume-scale effects.

In Section 3, I evaluate a column-ozone neutral altitude at which aviation emissions would lead to no net change in column ozone, and thus surface UV flux and the incidence rate of human skin cancer. I extend an adjoint model of atmospheric chemistry to include stratospheric chemistry and I use decadal adjoint-derived sensitivities to show that emissions between 12 and 15 km altitude are approximately column ozone-neutral. This ozone-neutral altitude varies as a function of latitude and composition of aircraft emissions. Furthermore, I find that nitrogen oxides and sulfur emissions are the two emission components driving changes in the ozone-neutral altitude. Water vapor emissions contribute to the aviation-attributable ozone response by less than 5% below 15 km. In the stratosphere, I show that seasonality of emissions can influence the ozone response. For instance, I find that, at altitudes above 15 km, the net, simulation-averaged ozone depletion resulting from a single flight varies by a factor of two depending on the season of emissions. Ultimately, under the assumption of ultra-low sulfur fuel, I find that a flight at 14 km would be ozone neutral.

Finally, in Section 4, I evaluate the role of climate feedback in the assessment of aviation's environmental response. I develop a newly-coupled global climate model, CESM2-GC, unifying CESM2 with GEOS-Chem. I validate the results from CESM2-GC against atmospheric measurements, the native chemistry option in CESM2, CAM-Chem, and the GEOS-Chem CTM. I find that the results of CESM2-GC are consistent with other models and observations. CESM2-GC predicts lower ozone mixing ratios in the troposphere compared to CAM-Chem, but has a lower absolute bias in total carbon monoxide column compared to satellite measurements. I then perform ensemble runs using CESM2-GC to estimate the magnitude of the coupled chemistry-climate feedback on aviation emissions' response. I show that the fully-coupled simulations predict a statistically significant population-weighted surface ozone and $PM_{2.5}$ change from aviation emissions equal to 0.56 ppbv and 0.08 $\mu g/m^3$ respectively, consistent with previous studies. Nudged simulations find similar results, but with a much lower variability. Additionally, I find that the full-model runs predict an increase in tropospheric temperatures in the tropics and at mid-latitudes of 70 mK. This change is explained by the radiative contribution of aviation-induced ozone in the troposphere.

5.2 Future work

In Section 2, I quantify the role of plume-scale processes on the long-term atmospheric response to aviation emissions. The plume-scale results used in this evaluation do not include variations in mixing rates. Difference in in-plume mixing rates can influence ozone production by diluting emitted NO_x in a larger plume area, as suggested in previous studies. More work would be necessary to evaluate the role of mixing rates on the plume-scale perturbations from individual aircraft and to quantify how these individual perturbations would propagate to the global-scale response to aviation emissions.

In Section 3, I calculate the column ozone-neutral altitude and its sensitivity to fleet-wide emission characteristics assuming current atmospheric conditions. However, future changes in atmospheric composition, such as the slow decay in stratospheric chlorine loading, could change the magnitude of stratospheric ozone depletion from high-altitude emissions. Reduction in stratospheric chlorine would reduce the magnitude of the adjoint sensitivities of column ozone in the stratosphere. However, a more thorough analysis should be conducted to evaluate how this would impact the ozone-neutral altitude for current and future subsonic aviation scenarios, accounting for market growth, and also for the possible reborn supersonic high-altitude aircraft fleet.

In Section 4, The assessment of the magnitude of the role of climate feedback when evaluating the environmental response of aviation emissions is presented in this thesis. More work would be needed to quantify the dependence of the results presented to the number of ensemble members and simulation length. However, the results presented do not account for the feedback of aviation-induced aerosol change on the meteorology. This could be important as the aerosol indirect effect has been mentioned in the literature as the dominant process influencing near-surface chemistry and $PM_{2.5}$ production. Further work is needed to quantify the magnitude of this effect on the response to aviation emissions.

Appendix A

Appendix to Chapter 2

A.1 Plume-scale results

Figure A-1 displays histograms of the remaining fraction of in-plume NO_x as stored in the look-up table. The values are extracted from the look-up table for a flight-level pressure of 220 hPa and latitude of 60°N and are plotted as a function of temperature. Each histogram represents a different season. Figure A-1 shows a strong dependence of the NO_x remaining fraction on the season of emissions with values greater than ~90% during winter, but reaching ~40% during the summer months. This agrees with previous studies on aircraft plume modeling [127, 42]. Additionally, higher temperatures lead to greater conversion of emitted nitrogen oxides to reservoir species. The temperature dependence is weaker during the winter months.

A.2 Aviation emissions

The commercial aviation emission inventory is derived for the year 2015 from the Aviation Emissions Inventory Code (AEIC) [109, 112]. AEIC identifies routings and model flight time, fuel burn and engine emissions using look-up tables of aircraft performance. Aviation fuel burn and emissions are derived from the Official Airline Guide (OAG) schedule for 2015. The global aircraft emission inventory consists of ~220 Tg fuel burn. This compares to ~190 Tg of fuel burn in 2006 [28] and ~240 Tg in 2015 [42] according to the global

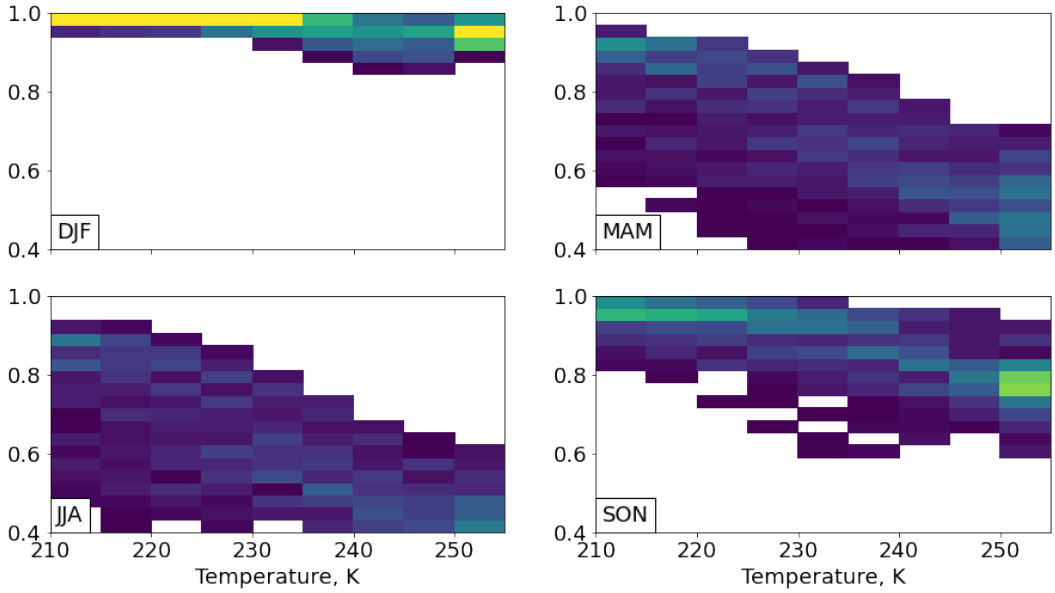

Figure A-1: Two-dimensional histograms of in-plume remaining NO_x fractions as a function of flight-level temperature for a cruise pressure of 220 hPa and latitude of 60°N. Each subplot displays the look-up table values for each season (DJF, MAM, JJA, SON). All histograms use the same color scale.

emission dataset from the Federal Aviation Administration (FAA) Aviation Environmental Design Tool (AEDT). In our emission scenario, aviation NO_x emissions reach a total of 3.93 Tg (on a NO_2 mass basis). Fuel burn density of the emission inventory used for this study is displayed in Figure A-2.

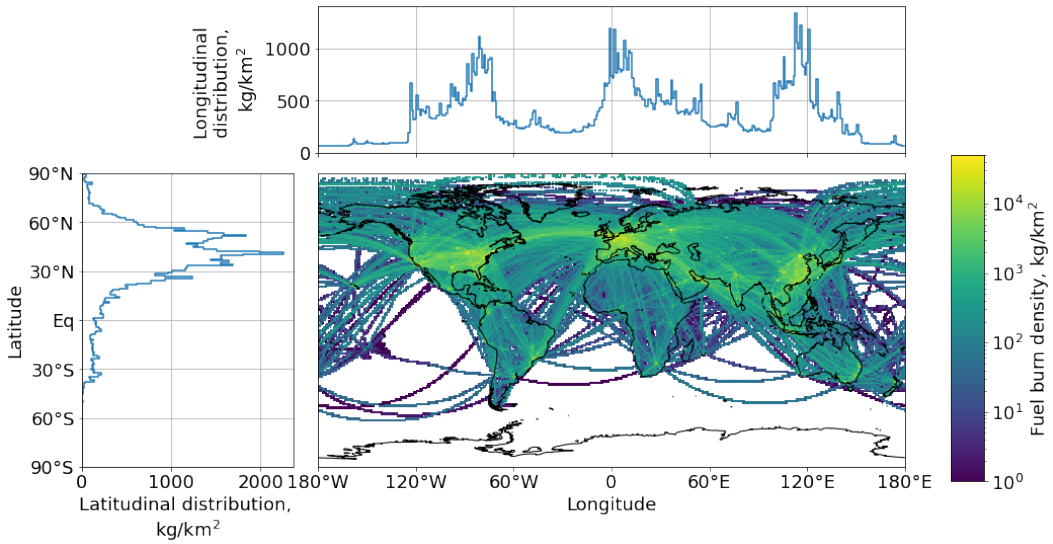

Figure A-2: Commercial aviation fuel burn density for the year 2015, as estimated by AEIC (bottom right) and its latitudinal and longitudinal dependence (left and top respectively) [109]. All aviation emissions are released below 13 km. Aviation fuel burn adds up to ~220 Tg.

Appendix B

Appendix to Chapter 3

B.1 Validation of the sensitivities of column ozone to stratospheric sulfur emissions

Stratospheric sulfur, through sulfuric acid aerosol particles, plays an important role on the Earth's radiative balance by reflecting incoming radiation. Additionally, sulfate aerosols act as a surface for heterogeneous chemical reactions. The role of sulfur on stratospheric ozone has been extensively studied over the past few decades in the context of sulfate geoengineering as one of the possible policies for solar radiation management [98, 92, 135]. The five year integration period, used to obtain adjoint sensitivities, are necessary to capture the long-term feedback from sulfur injection as stratospheric sulfur lifetimes have been estimated to be ~1.9 years [134].

To estimate the sensitivities of total ozone column to changes in SO_2 and H_2SO_4 concentrations, I compare the obtained adjoint sensitivities against forward model sensitivities obtained by scaling a supersonic aviation emission inventory, with a ceiling altitude at 66,000 ft (~20 km).

The top pane in Figure B-1 displays the sulfur-attributable forward model response to the supersonic aviation scenario considered. Sulfur emissions lead to immediate ozone depletion that stabilizes after ~2 years, leading to a time-averaged ozone response of -245 mDU for ~15 Gg S/year of injected sulfur (on an elemental sulfur mass basis). The

forward-derived sensitivity of -16.3 mDU/(Gg S/year) is approximately an order of magnitude greater than the sensitivity to NO_x emissions, at the corresponding altitude. Given conventional emission indices and fuel sulfur content, NO_x emissions are ~10 times greater than sulfur emissions, making the component-wise attributions of the same order of magnitude. The share of sulfur in the total ozone column response from supersonic aviation depends critically on the cruising altitude. The middle panes of Figure B-1 show the zonally and temporally averaged sensitivities to changes in SO_2 and H_2SO_4 concentrations. The dashed contour lines represent subsonic and supersonic levels of aviation fuel burn. Sensitivities to sulfur compounds are negligible in the troposphere and reach a local minimum at 20 km. In the 18-22 km band, the equatorial sensitivities are smaller in magnitude compared to extratropical and polar sensitivities.

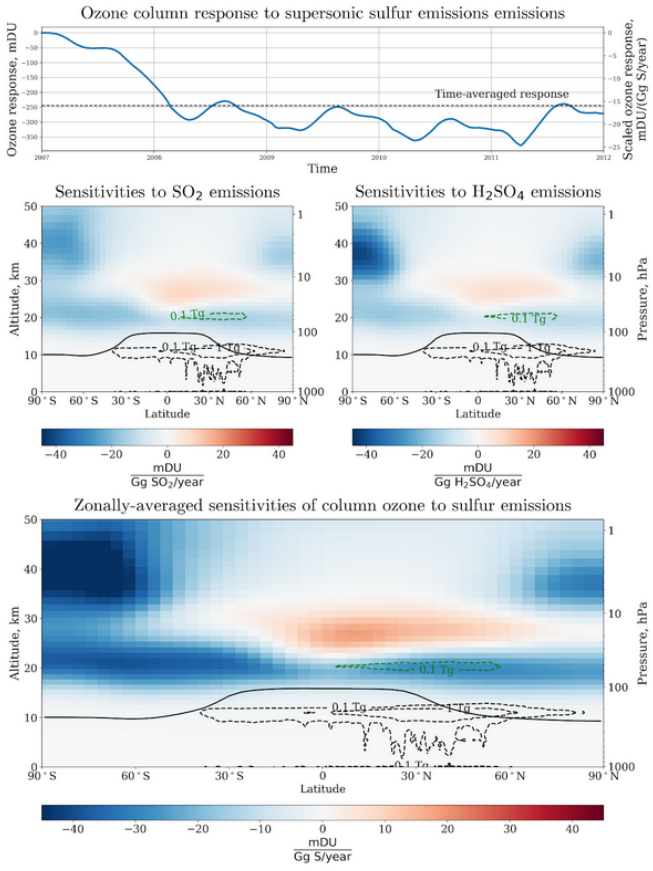

Figure B-1: Five-year forward model-derived response to supersonic sulfur emissions, assuming a fuel sulfur content of 600 ppm (top); zonally-averaged sensitivities of total ozone column to sulfur emissions when emitted as SO_2 (middle left) and H_2SO_4 (middle right); adjoint sensitivities weighted by sulfur conversion (bottom).

Sulfate geoengineering scenarios consist of injecting sulfur compounds in the rising air current of the Brewer-Dobson circulation above the tropical tropopause. The impact of solar geoengineering scenarios on stratospheric ozone has been quantified in previous studies [30]. By using adjoint-derived sensitivities, I am able to rapidly evaluate changes in total ozone column from such scenarios. However, the adjoint sensitivities do not account for meteorological feedback, such as tropospheric cooling, stratospheric warming and changes in precipitation.

By averaging the obtained sensitivities between 20 and 25 km, from 30°S to 30°N, I find that emissions of sulfur would lead to a normalized 5-year average ozone column response of -2.19 DU / (Tg SO_2/year) and -1.59 DU / (Tg H_2SO_4/year) whether sulfur is released as SO_2 or H_2SO_4. The values cited previously are for a stratospheric chlorine loading of 2.76 ppbv.

The bottom pane of Figure B-1 displays the sensitivity of total column ozone to element sulfur from aviation emissions, as a weighted combination of sensitivities to sulfur compounds, expressed as

$$\frac{\partial J}{\partial S} = (1-\alpha)\frac{\partial J}{\partial SO_2}\frac{MW_{SO_2}}{MW_S} + \alpha\frac{\partial J}{\partial H_2SO_4}\frac{MW_{H_2SO_4}}{MW_S} \tag{B.1}$$

where α represents the fraction of sulfur converted to H_2SO_4 on a molecular basis. For this study, I use a value of α equal to 2%. Using the supersonic emission scenario for validation purposes, I obtain an adjoint-derived 5-year total ozone column change of -290 mDU, corresponding to a normalized response of approximately -19 DU / (Tg S/year), off from the GEOS-Chem forward-derived response by 16%.

B.2 Sensitivity of aerosol optical depth to emissions

I now present the sensitivities of area-averaged AOD to changes in concentrations. I focus here on the role of sulfur and compare the adjoint-derived sensitivities to results from the existing literature on the impact of sulfur geoengineering following an injection in the tropical lower stratosphere. Figure B-2 displays adjoint sensitivities of area-weighted AOD

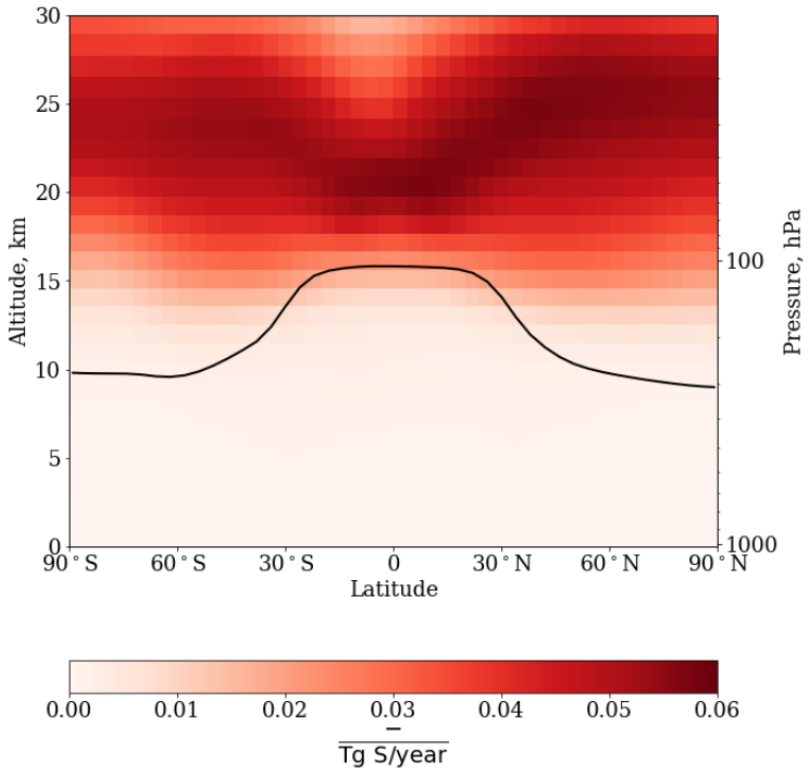

Figure B-2: Zonally-averaged adjoint sensitivities of total aerosol optical depth with respect to sulfur emissions. The sensitivities are expressed per Tg of elemental sulfur per year.

to sulfur emissions, expressed on an elemental sulfur basis. The sensitivities are approximately uniform in the troposphere, with an average value of 0.0035 / (Tg S/year) in the 10-12 km band. In the 15-30 km layer, changes in sulfur concentrations in the stratosphere have a more profound impact on the total AOD, due to the lack of removal processes in the stratosphere, reaching up to 0.05 / (Tg S/year). Indeed, the typical age of air at 20 km ranges between 2 years and approximately 4 years in the tropics and extratropical regions respectively [18], meaning that injected sulfur above 15 km will typically have a longer lifetime compared to injection in the troposphere.

Injection of sulfur at a rate of 1 Tg S/year in the equatorial region (between 30°S and 30°N) and in the 20-25 km altitude band leads to a change in area-weighted AOD of 0.05. Sensitivities are higher in the extratropical and polar regions. For a similar injection pattern, a previous study quotes a forward model-derived sensitivity of mean stratospheric AOD of 0.079 [30]. In this study, I expect smaller sensitivities as the averaging is performed

throughout the entire atmosphere. Injection in the 20-25 km altitude band will lead to a greater aerosol loading in the stratosphere compared to the troposphere, such that the stratospheric average is expected to be larger than a full column AOD average.

Appendix C

Appendix to Chapter 4

C.1 Engineering of coupling GEOS-Chem with CESM2

One of the drawbacks of atmospheric chemistry models embedded in GCMs is that it appears challenging to maintain the representation of atmospheric processes up-to-date, when compared to offline models. In online models, the feedback and interactions between different physical and chemical modules are oftentimes hardwired. This means that software development requires significant effort to maintain or update such modules. For this reason, user modifications can be difficult to propagate back to the main branch.

In order to tackle the previous concern, I have developed CESM2-GC with the following intents:

- The interfacing between GEOS-Chem and CESM is, as much as possible, dissociated from the parent models.
- The parent models are not modified (i.e. CESM and GEOS-Chem interact only through a coupler which does not modify either CESM nor GEOS-Chem)
- The computational resources used by the interface is minimal and does not affect any of the parent models
- The interface between both models is documented, freely accessible, version controlled, and it does not hinder the installation of any of the parent models.

The first two points are introduced to make any future updates to the parent models easy to implement in the interface routines.

The next generation of the CESM atmosphere model will seek to provide a unified framework for atmospheric simulations on a very wide range of scales. The System for Integrated Modeling of the Atmosphere (SIMA) will be developed using the NUOPC-based Common Physics Framework (CPF) [47] to allow selection of various components within the atmosphere model [97]. The objective of SIMA is to have individual components for physical parameterizations and chemical modules linked to the dynamical core through the CPF with a common coupling structure. The MOZART chemistry mechanism, used by CAM-Chem, will be incorporated into the new Model Independent Chemistry Module (MICM) to be implemented in SIMA. MICM is currently under development and will provide a single entry point for the specification of the MOZART chemical mechanism and parameterizations.

The intermediate step is to implement the GEOS-Chem chemical module as an alternative to MICM. This facilitates the software engineering development of this project. Integrating the GEOS-Chem module into SIMA in parallel with the development of MICM will allow a more complete consideration of the needs in coupling and modularizing the chemistry components. The end step of this project is to break up the GEOS-Chem chemical module into components in order to exploit the generic modular framework enabled by CPF. This allows users to freely choose GEOS-Chem and non-GEOS-Chem components for their atmospheric chemistry simulations. At this step, emissions, chemistry, wet deposition, and dry deposition will be implemented in separate components. Breaking up GEOS-Chem into its internal process-based components will allow testing and intercomparison of different representations of processes at a granular level. The integrity of GEOS-Chem within SIMA and its referenceability to the standard GEOS-Chem model will still be maintained as a specific SIMA configuration of components and settings. Again, I will ensure that GEOS-Chem modularization as done for SIMA is also implemented in the standard GEOS-Chem model so that the two continue to use exactly the same scientific code base.

Evaluation of the GEOS-Chem simulation within SIMA is a valuable part of the work.

Species	Emission totals
NO	44.1 Tg N
CO	366 Tg C
C_2H_6	5.19 Tg C
C_3 alkenes (PRPE*)	8.93 Tg C
C_3H_8	4.55 Tg C
CH_2O	4.46 Tg C
CH_3CHO (ALD2*)	23.7 Tg C
C_4 alkanes (ALK4*)	15.33 Tg C
C_2H_5OH (EOH*)	7.58 Tg C
CH_3OH (MOH*)	44.53 Tg C
Toluene (TOLU*)	1.16 Tg C
Xylene (XYLE*)	0.89 Tg C
NH_3	66.84 Tg N

Table C.1: Emission totals for selected species in CESM2-GC.
* Emitted species in GEOS-Chem.

Swapping GEOS-Chem and MICM components for emissions, chemistry, and deposition will further expand the range of model evaluation and is likely to result in significant improvement in the ability to model chemistry within CESM.

C.2 Surface emission fluxes

Table C.1 lists surface emission fluxes of selected species in CESM2-GC. The emission fluxes are passed through HEMCO and the emission totals are in agreement with the scientific literature [34].

Additionally, this section intends to provide a geographical comparison of emission fluxes in CESM2-GC and the GEOS-Chem CTM. In this thesis, CESM2-GC, CAM-Chem and the GEOS-Chem CTM use HEMCO to handle emission inputs into the model. This means that all three models have identical emissions with slight modifications due to dependencies of emission extensions (such as sea flux emissions) on the meteorology. However, these differences should be relatively small. For CESM2-GC and CAM-Chem, lightning NOx, dust, sea salt, and biogenic emissions are computed within the model and are not read or estimated from HEMCO.

Figures C-1, C-2 and C-3 display surface emission fluxes of CO, NO, and NH3 for

CESM2-GC and the GEOS-Chem CTM. The emission fluxes between CESM2-GC and the GEOS-Chem CTM are almost identical and only differ by small amounts.

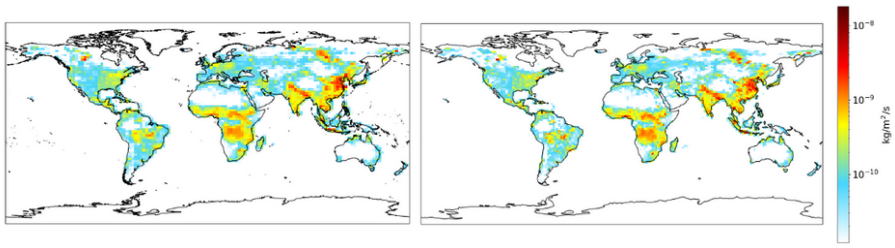

Figure C-1: Surface CO emission flux for CESM2-GC (left) and the GEOS-Chem CTM (right)

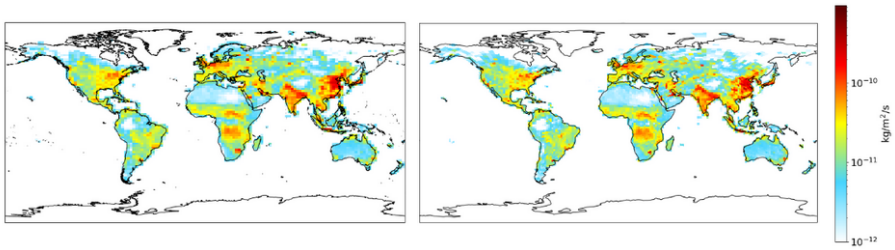

Figure C-2: Surface NO emission flux for CESM2-GC (left) and the GEOS-Chem CTM (right)

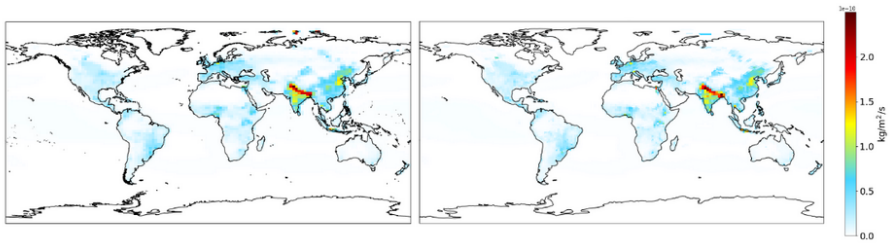

Figure C-3: Surface NH3 emission flux for CESM2-GC (left) and the GEOS-Chem CTM (right)

C.3 Additional aircraft campaign observations and comparison to model evaluations

This section compares results from the CESM2-GC and CAM-Chem simulations to measurements from aircraft campaigns. The results are only compared to observations in the

0 to 3 km altitude band. I find that CESM2-GC displays a larger ozone bias than CAM-Chem, when compared to the observations. This bias has already been observed in Section 4.3. Other species displayed in Figure C-4 show good agreement between CESM2-GC and CAM-Chem and with the remote measurements.

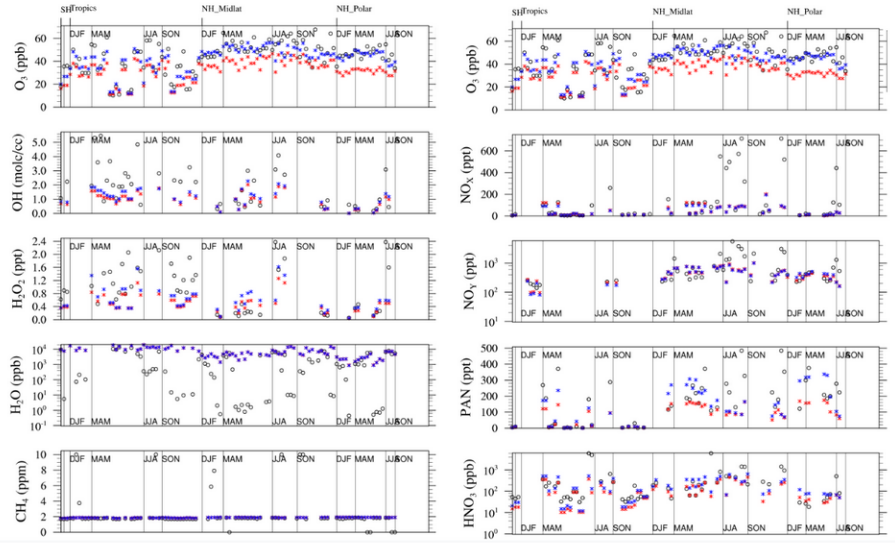

Figure C-4: Comparison of the results from CESM2-GC and CAM-Chem to aircraft observations in the 0 to 3 km altitude range. The results from CESM2-GC and CAM-Chem are displayed in red and blue respectively. The measurements are shown as black circles.

C.4 Aviation-induced feedback on atmospheric circulation, vertical stability, cloud fraction, and lightning NO_x emissions

This section presents the impact of commercial aviation emissions on annually-averaged atmospheric circulation, atmospheric stability, cloud coverage, and lightning NO_x emissions.

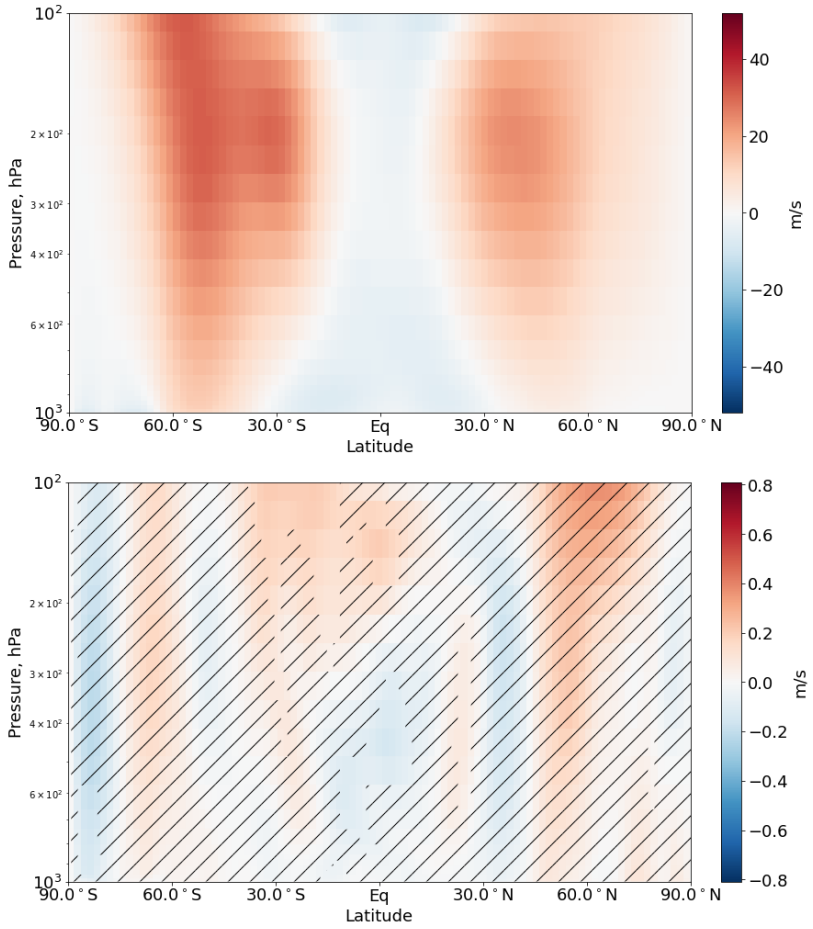

Figure C-5: Estimated zonal wind in CESM2-GC (top) and aviation-induced change in zonally-averaged zonal wind from commercial aviation emissions (bottom). The hatched areas indicate regions that are not statistically significant at 0.05 level using a two-sided Student's t-test.

Figures C-5 and C-6 show aviation-induced changes to zonal and meridional winds respectively, averaged over the ten years of the fully-coupled simulations described in Section 4. No statistically-significant changes at the 0.05 level are observed in the Northern Hemisphere, where most of aviation fuel is burnt. Only statistically-significant changes are observed in tropical regions for zonal wind and austral regions for meridional wind. However, these statistically-significant regions are highly sensitive to the averaging period and to the number of ensemble members considered. Larger ensemble sets or longer simulations would be needed to confirm that these changes are the results of climate feedback

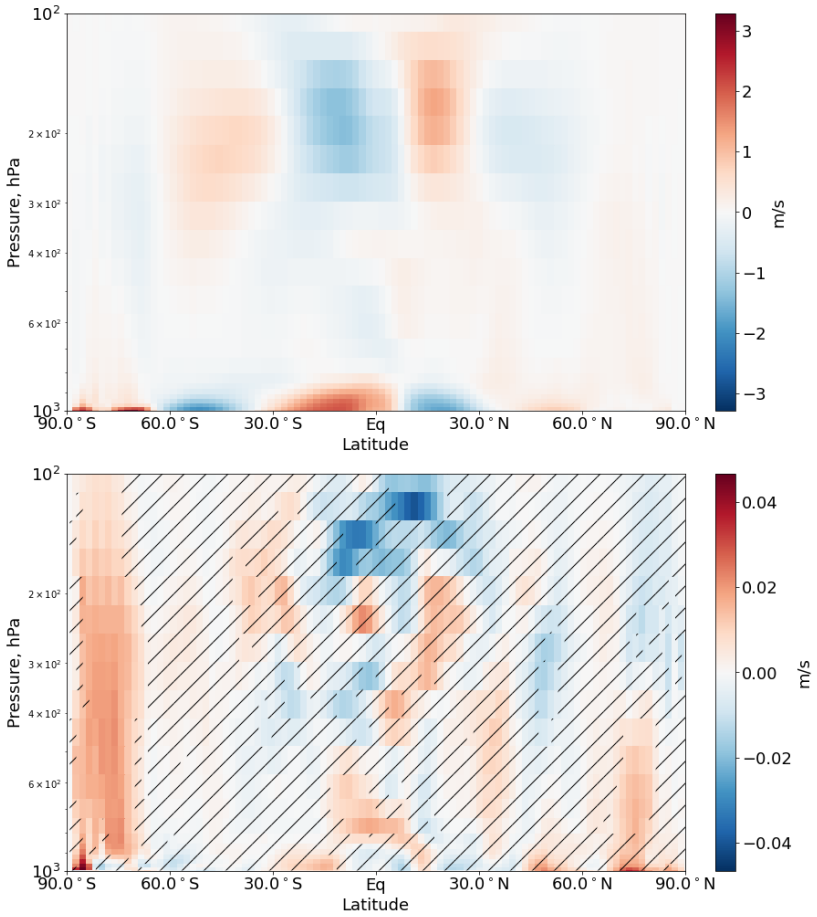

Figure C-6: Estimated meridional wind in CESM2-GC (top) and aviation-induced change in zonally-averaged meridional wind from commercial aviation emissions (bottom). The hatched areas indicate regions that are not statistically significant at 0.05 level using a two-sided Student's t-test.

from commercial aviation emissions.

Figure C-7 shows changes in cloud fractions estimated by CESM2-GC from commercial aviation emissions. I find that only a decrease in upper-tropospheric tropical cloud fractions and an increase in mid-tropospheric cloud fractions in austral regions are statistically significant. Similarly to the circulation patterns, these changes are highly sensitive to the number of ensemble members and averaging period used.

Figure C-8 displays the change in zonally-averaged vertical pressure velocity owing to commercial aviation emissions. The aviation-induced change in vertical pressure velocity from commercial aircraft activities is less than 1% of the reference values, except around the South Pole, where the results indicate a contribution up to ~10%. Only the mid and

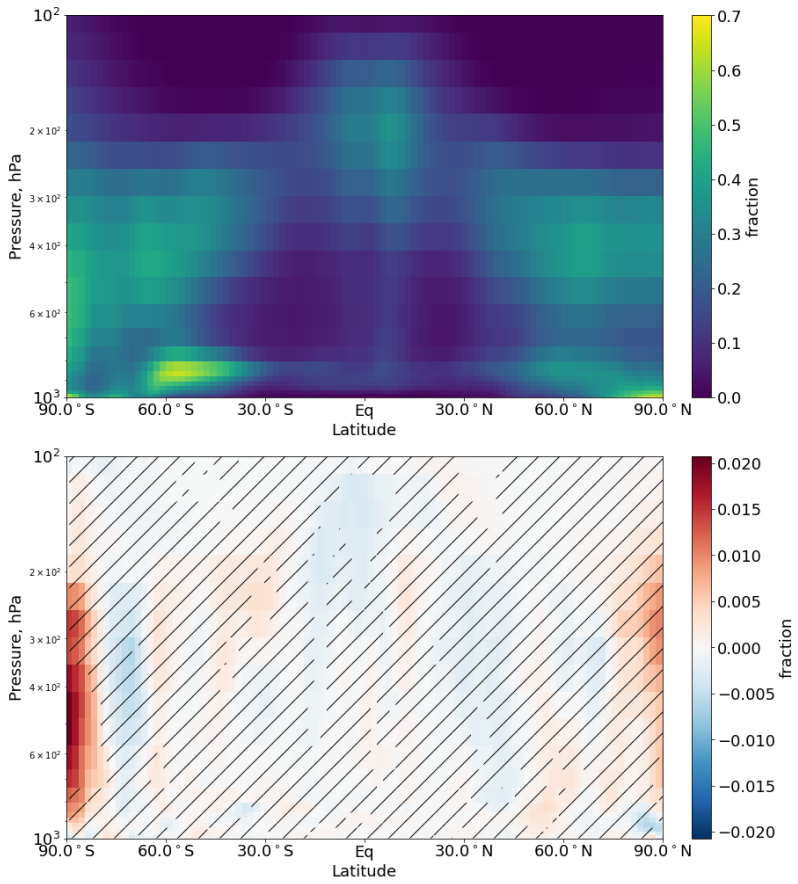

Figure C-7: Estimated cloud fraction in CESM2-GC (top) and aviation-induced change in zonally-averaged cloud fraction from commercial aviation emissions (bottom). The hatched areas indicate regions that are not statistically significant at 0.05 level using a two-sided Student's t-test.

lower tropospheric austral region is statistically-significant at the 0.05 level. However, this may be explained by the high sensitivity in polar regions and chaotic behaviors of individual ensemble members. More ensemble members would be needed to confirm that this statistically-significant change is indeed caused by aviation emissions.

Finally, Figure C-9 shows the rate of NO_x production from lightning. I find no statistically-significant change in lightning NO_x emissions at the 0.05 level from commercial aviation emissions. The aviation-induced change in NO_x emission rates from lightning is limited to 1% in tropical regions and 2% in North-hemispheric mid-latitude regions.

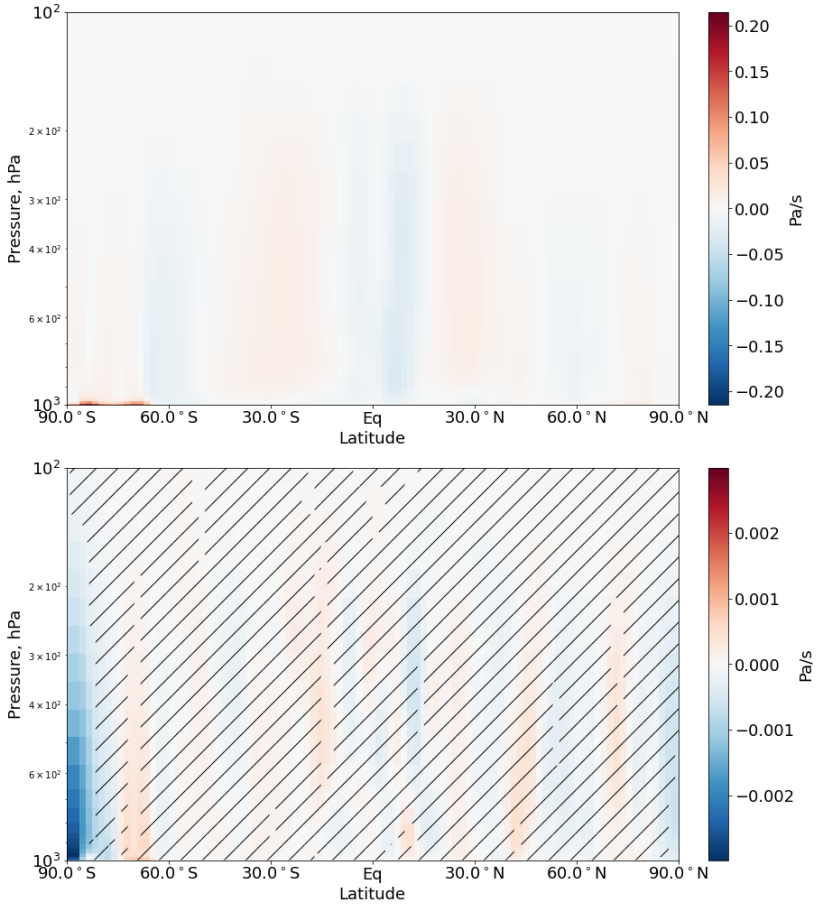

Figure C-8: Estimated vertical pressure velocity in CESM2-GC (top) and aviation-induced change in zonally-averaged vertical pressure velocity from commercial aviation emissions (bottom). The hatched areas indicate regions that are not statistically significant at 0.05 level using a two-sided Student's t-test.

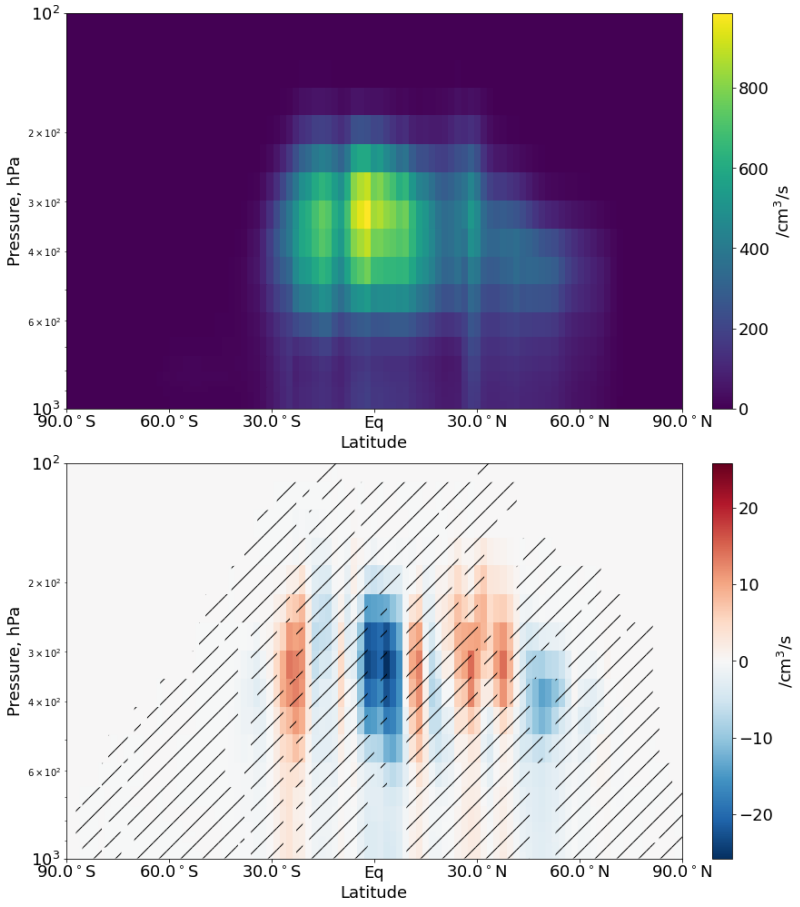

Figure C-9: Estimated lightning NO_x emissions in CESM2-GC (top) and aviation-induced change in zonally-averaged lightning NO_x emissions from commercial aviation emissions (bottom). The hatched areas indicate regions that are not statistically significant at 0.05 level using a two-sided Student's t-test.

Bibliography

[1] Wenche Aas, Augustin Mortier, Van Bowersox, Ribu Cherian, Greg Faluvegi, Hilde Fagerli, Jenny Hand, Zbigniew Klimont, Corinne Galy-Lacaux, Christopher M B Lehmann, Cathrine Lund Myhre, Gunnar Myhre, Dirk Olivié, Keiichi Sato, Johannes Quaas, P S P Rao, Michael Schulz, Drew Shindell, Ragnhild B Skeie, Ariel Stein, Toshihiko Takemura, Svetlana Tsyro, Robert Vet, and Xiaobin Xu. Global and regional trends of atmospheric sulfur. *Sci. Rep.*, 9(1):953, January 2019.

[2] Aerion. Aerion. `https://aerionsupersonic.com/as2/`, 2020. Accessed: 2021-2-17.

[3] Elizabeth A Ainsworth. Understanding and improving global crop response to ozone pollution. *Plant J.*, 90(5):886–897, June 2017.

[4] Arno M Arellano, Jordi Vilà-Guerau de Talmon and Peter J H Builtjes. A chemically reactive plume model for the $NO/NO_2/O_3$ system, 1990.

[5] M R Ashmore. Assessing the future global impacts of ozone on vegetation, 2005.

[6] Akshay Ashok, Irene C Dedoussi, Steve H L Yim, Hamsa Balakrishnan, and Steven R H Barrett. Quantifying the air quality-CO2 tradeoff potential for airports, 2014.

[7] Steven R H Barrett, Rex E Britter, and Ian A Waitz. Global mortality attributable to aircraft cruise emissions. *Environ. Sci. Technol.*, 44(19):7736–7742, October 2010.

[8] Boom. Boom. `https://boomsupersonic.com/`, 2020. Accessed: 2020-5-5.

[9] G Brasseur and C Granier. Mount pinatubo aerosols, chlorofluorocarbons, and ozone depletion. *Science*, 257(5074):1239–1242, August 1992.

[10] G P Brasseur, R A Cox, D Hauglustaine, I Isaksen, J Lelieveld, D H Lister, R Sausen, U Schumann, A Wahner, and P Wiesen. European scientific assessment of the atmospheric effects of aircraft emissions, 1998.

[11] Elza Brunelle-Yeung, Tudor Masek, Julien J Rojo, Jonathan I Levy, Saravanan Arunachalam, Sondra M Miller, Steven R H Barrett, Stephen R Kuhn, and Ian A Waitz. Assessing the impact of aviation environmental policies on public health. *Transp. Policy*, 34:21–28, July 2014.

[12] Richard Burnett, Hong Chen, Mieczysław Szyszkowicz, Neal Fann, Bryan Hubbell, C Arden Pope, 3rd, Joshua S Apte, Michael Brauer, Aaron Cohen, Scott Weichenthal, Jay Coggins, Qian Di, Bert Brunekreef, Joseph Frostad, Stephen S Lim, Haidong Kan, Katherine D Walker, George D Thurston, Richard B Hayes, Chris C Lim, Michelle C Turner, Michael Jerrett, Daniel Krewski, Susan M Gapstur, W Ryan Diver, Bart Ostro, Debbie Goldberg, Daniel L Crouse, Randall V Martin, Paul Peters, Lauren Pinault, Michael Tjepkema, Aaron van Donkelaar, Paul J Villeneuve, Anthony B Miller, Peng Yin, Maigeng Zhou, Lijun Wang, Nicole A H Janssen, Marten Marra, Richard W Atkinson, Hilda Tsang, Thuan Quoc Thach, John B Cannon, Ryan T Allen, Jaime E Hart, Francine Laden, Giulia Cesaroni, Francesco Forastiere, Gudrun Weinmayr, Andrea Jaensch, Gabriele Nagel, Hans Concin, and Joseph V Spadaro. Global estimates of mortality associated with long-term exposure to outdoor fine particulate matter. *Proc. Natl. Acad. Sci. U. S. A.*, 115(38):9592–9597, September 2018.

[13] Neal Butchart, James A Anstey, Yoshio Kawatani, Scott M Osprey, Jadwiga H Richter, and Tongwen Wu. Qbo changes in cmip6 climate projections. *Geophysical Research Letters*, 47(7):e2019GL086903, 2020.

[14] Fabio Caiazzo, Akshat Agarwal, Raymond L Speth, and Steven R H Barrett. Impact of biofuels on contrail warming, 2017.

[15] M A Cameron, M Z Jacobson, Steven R H Barrett, Haitao Bian, C C Chen, Sebastian D Eastham, A Gettelman, A Khodayari, Q Liang, H B Selkirk, and Others. An intercomparative study of the effects of aircraft emissions on surface air quality. *J. Geophys. Res. D: Atmos.*, 122(15):8325–8344, 2017.

[16] Mary A Cameron, Mark Z Jacobson, Alexander D Naiman, and Sanjiva K Lele. Effects of plume-scale versus grid-scale treatment of aircraft exhaust photochemistry, 2013.

[17] D Cariolle, D Caro, R Paoli, D A Hauglustaine, B Cuénot, A Cozic, and R Paugam. Parameterization of plume chemistry into large-scale atmospheric models: Application to aircraft NO_x emissions, 2009.

[18] Simon Chabrillat, Corinne Vigouroux, Yves Christophe, Andreas Engel, Quentin Errera, Daniele Minganti, Beatriz M Monge-Sanz, Arjo Segers, and Emmanuel Mahieu. Comparison of mean age of air in five reanalyses using the BASCOE transport model, 2018.

[19] Tianfeng Chai, Gregory R Carmichael, Youhua Tang, Adrian Sandu, Andreas Heckel, Andreas Richter, and John P Burrows. Regional NO_x emission inversion through a four-dimensional variational approach using SCIAMACHY tropospheric NO_2 column observations, 2009.

[20] Guillaume P Chossière, Haofeng Xu, Yash Dixit, Stewart Isaacs, Sebastian D Eastham, Florian Allroggen, Raymond L Speth, and Steven R H Barrett. Air pol-

lution impacts of COVID-19–related containment measures. *Science Advances*, 7(21):eabe1178, May 2021.

[21] Derek M Cunnold, Fred N Alyea, and Ronald G Prinn. Relative effects on atmospheric ozone of latitude and altitude of supersonic flight, 1977.

[22] F R de Gruijl and J C Van der Leun. Estimate of the wavelength dependency of ultraviolet carcinogenesis in humans and its relevance to the risk assessment of a stratospheric ozone depletion. *Health Phys.*, 67(4):319–325, October 1994.

[23] Irene Constantina Dedoussi. *Adjoint sensitivity analysis of the atmospheric impacts of combustion emissions*. PhD thesis, Massachusetts Institute of Technology, 2018.

[24] Mark A Delucchi, James J Murphy, and Donald R McCubbin. The health and visibility cost of air pollution: a comparison of estimation methods, 2002.

[25] A J Ding, C B Fu, X Q Yang, J N Sun, T Petäjä, V-M Kerminen, T Wang, Y Xie, E Herrmann, L F Zheng, W Nie, Q Liu, X L Wei, and M Kulmala. Intense atmospheric pollution modifies weather: a case of mixed biomass burning with fossil fuel combustion pollution in eastern china, 2013.

[26] T Duncan Fairlie, Daniel J Jacob, and Rokjin J Park. The impact of transpacific transport of mineral dust in the united states. *Atmos. Environ.*, 41(6):1251–1266, February 2007.

[27] M Dutta, K O Patten, and D J Wuebbles. Parametric analyses of potential effects on upper Tropospheric/Lower stratospheric ozone chemistry by a future fleet of high speed civil transport (HSCT). 2005.

[28] Sebastian D Eastham and Steven R H Barrett. Aviation-attributable ozone as a driver for changes in mortality related to air quality and skin cancer. *Atmos. Environ.*, 144:17–23, November 2016.

[29] Sebastian D Eastham, Debra K Weisenstein, and Steven R H Barrett. Development and evaluation of the unified tropospheric–stratospheric chemistry extension (UCX) for the global chemistry-transport model GEOS-Chem. *Atmos. Environ.*, 89:52–63, June 2014.

[30] Sebastian D Eastham, Debra K Weisenstein, David W Keith, and Steven R H Barrett. Quantifying the impact of sulfate geoengineering on mortality from air quality and UV-B exposure, 2018.

[31] L K Emmons, P G Hess, J-F Lamarque, and G G Pfister. Tagged ozone mechanism for MOZART-4, CAM-chem and other chemical transport models. *Geosci. Model Dev.*, 5(6):1531–1542, December 2012.

[32] L K Emmons, S Walters, P G Hess, J-F Lamarque, G G Pfister, D Fillmore, C Granier, A Guenther, D Kinnison, T Laepple, J Orlando, X Tie, G Tyndall, C Wiedinmyer, S L Baughcum, and S Kloster. Description and evaluation of the model for ozone and related chemical tracers, version 4 (MOZART-4), 2010.

[33] Louisa K Emmons, Didier A Hauglustaine, Jean-François Müller, Mary Anne Carroll, Guy P Brasseur, Dominik Brunner, Johannes Staehelin, Valerie Thouret, and Alain Marenco. Data composites of airborne observations of tropospheric ozone and its precursors. *J. Geophys. Res.*, 105(D16):20497–20538, August 2000.

[34] Louisa K Emmons, Rebecca H Schwantes, John J Orlando, Geoff Tyndall, Douglas Kinnison, Jean-françois Lamarque, Daniel Marsh, Michael J Mills, Simone Tilmes, Charles Bardeen, Rebecca R Buchholz, Andrew Conley, Andrew Gettelman, Rolando Garcia, Isobel Simpson, Donald R Blake, Simone Meinardi, and Gabrielle Pétron. The chemistry mechanism in the community earth system model version 2 (CESM2), 2020.

[35] European Environment Agency. European air quality portal. `https://discomap.eea.europa.eu/map/fme/AirQualityExport.htm`, 2021. Accessed: 2021-6-7.

[36] Simon J Evans, Ralf Toumi, John E Harries, Martyn R Chipperfield, and James M Russell. Trends in stratospheric humidity and the sensitivity of ozone to these trends, 1998.

[37] V Eyring, D S Stevenson, A Lauer, F J Dentener, T Butler, W J Collins, K Ellingsen, M Gauss, D A Hauglustaine, I S A Isaksen, M G Lawrence, A Richter, J M Rodriguez, M Sanderson, S E Strahan, K Sudo, S Szopa, T P C van Noije, and O Wild. Multi-model simulations of the impact of international shipping on atmospheric chemistry and climate in 2000 and 2030, 2007.

[38] Majid Ezzati, Alan D Lopez, Anthony A Rodgers, and Christopher J L Murray. *Comparative quantification of health risks: global and regional burden of disease attributable to selected major risk factors*. World Health Organization, 2004.

[39] Xu Feng, Haipeng Lin, Tzung-May Fu, Melissa P Sulprizio, Jiawei Zhuang, Daniel J Jacob, Heng Tian, Yaping Ma, Lijuan Zhang, Xiaolin Wang, et al. Wrf-gc (v2. 0): online two-way coupling of wrf (v3. 9.1. 1) and geos-chem (v12. 7.2) for modeling regional atmospheric chemistry–meteorology interactions. *Geoscientific Model Development*, 14(6):3741–3768, 2021.

[40] Peter L Finkelstein, Thomas G Ellestad, John F Clarke, Tilden P Meyers, Donna B Schwede, Eric O Hebert, and Julie A Neal. Ozone and sulfur dioxide dry deposition to forests: Observations and model evaluation, 2000.

[41] Johnny Freiberg. The iron catalyzed oxidation of SO2 to acid sulphate mist in dispersing plumes, 1976.

[42] Thibaud M Fritz, Sebastian D Eastham, Raymond L Speth, and Steven R H Barrett. The role of plume-scale processes in long-term impacts of aircraft emissions. *Atmos. Chem. Phys.*, 20(9):5697–5727, May 2020.

[43] S Fueglistaler, A E Dessler, T J Dunkerton, I Folkins, Q Fu, and P W Mote. Tropical tropopause layer, 2009.

[44] Ronald Gelaro, Will McCarty, Max J Suárez, Ricardo Todling, Andrea Molod, Lawrence Takacs, Cynthia Randles, Anton Darmenov, Michael G Bosilovich, Rolf Reichle, Krzysztof Wargan, Lawrence Coy, Richard Cullather, Clara Draper, Santha Akella, Virginie Buchard, Austin Conaty, Arlindo da Silva, Wei Gu, Gi-Kong Kim, Randal Koster, Robert Lucchesi, Dagmar Merkova, Jon Eric Nielsen, Gary Partyka, Steven Pawson, William Putman, Michele Rienecker, Siegfried D Schubert, Meta Sienkiewicz, and Bin Zhao. The Modern-Era retrospective analysis for research and applications, version 2 (MERRA-2). *J. Clim.*, 30(Iss 13):5419–5454, June 2017.

[45] A Gettelman, MJ Mills, DE Kinnison, RR Garcia, AK Smith, DR Marsh, S Tilmes, F Vitt, CG Bardeen, J McInerny, et al. The whole atmosphere community climate model version 6 (waccm6). *Journal of Geophysical Research: Atmospheres*, 124(23):12380–12403, 2019.

[46] Christopher K Gilmore, Steven R H Barrett, Jamin Koo, and Qiqi Wang. Temporal and spatial variability in the aviation NO x -related O 3 impact, 2013.

[47] S Goldhaber. The new physics coupling framework (CPF), workshop on the integration of GEOS-Chem into NCAR models. `https://www2.acom.ucar.edu/workshop/integration-geos-chem-ncar-models-agenda`, 2018. Accessed: 2020-11-15.

[48] V Grewe, A Stenke, M Ponater, R Sausen, G Pitari, D Iachetti, H Rogers, O Dessens, J Pyle, I S A Isaksen, L Gulstad, O A Søvde, C Marizy, and E Pascuillo. Climate impact of supersonic air traffic: an approach to optimize a potential future supersonic fleet – results from the EU-project SCENIC, 2007.

[49] Carla Grobler, Philip J Wolfe, Kingshuk Dasadhikari, Irene C Dedoussi, Florian Allroggen, Raymond L Speth, Sebastian D Eastham, Akshat Agarwal, Mark D Staples, Jayant Sabnis, and Steven R H Barrett. Marginal climate and air quality costs of aviation emissions, 2019.

[50] A B Guenther, X Jiang, C L Heald, T Sakulyanontvittaya, T Duhl, L K Emmons, and X Wang. The model of emissions of gases and aerosols from nature version 2.1 (MEGAN2.1): an extended and updated framework for modeling biogenic emissions. *Geosci. Model Dev.*, 5(6):1471–1492, November 2012.

[51] Amir Hakami, Daven K Henze, John H Seinfeld, Kumaresh Singh, Adrian Sandu, Soontae Kim, Daewon Byun, and Qinbin Li. The adjoint of CMAQ. *Environ. Sci. Technol.*, 41(22):7807–7817, November 2007.

[52] C L Heald, D A Ridley, J H Kroll, S R H Barrett, K E Cady-Pereira, M J Alvarado, and C D Holmes. Contrasting the direct radiative effect and direct radiative forcing of aerosols. *Atmos. Chem. Phys.*, 14(11):5513–5527, 2014.

[53] D K Henze, A Hakami, and J H Seinfeld. Development of the adjoint of GEOS-Chem, 2007.

[54] D K Henze, J H Seinfeld, and D T Shindell. Inverse modeling and mapping US air quality influences of inorganic $PM_{2.5}$ precursor emissions using the adjoint of GEOS-Chem, 2009.

[55] James I Hileman, Russell W Stratton, and Pearl E Donohoo. Energy content and alternative jet fuel viability. *J. Propul. Power*, 26(6):1184–1196, November 2010.

[56] Gerard Hoek, Ranjini M Krishnan, Rob Beelen, Annette Peters, Bart Ostro, Bert Brunekreef, and Joel D Kaufman. Long-term air pollution exposure and cardio-respiratory mortality: a review. *Environ. Health*, 12(1):43, May 2013.

[57] James E Hoke and Richard A Anthes. The initialization of numerical models by a Dynamic-Initialization technique. *Mon. Weather Rev.*, 104(12):1551–1556, December 1976.

[58] C D Holmes, M J Prather, and G C M Vinken. The climate impact of ship NO_x emissions: an improved estimate accounting for plume chemistry, 2014.

[59] P Huszar, H Teyssèdre, M Michou, A Voldoire, D J L Olivié, D Saint-Martin, D Cariolle, S Senesi, D Salas Y Melia, A Alias, F Karcher, P Ricaud, and T Halenka. Modeling the present and future impact of aviation on climate: an AOGCM approach with online coupled chemistry, 2013.

[60] M Z Jacobson, J T Wilkerson, A D Naiman, and S K Lele. The effects of aircraft on climate and pollution. part II: 20-year impacts of exhaust from all commercial aircraft worldwide treated individually at the subgrid scale. *Faraday Discuss.*, 165:369–382, 2013.

[61] Lyatt Jaegle, Daniel J Jacob, Yuhua Wang, Andrew J Weinheimer, Brian A Ridley, Teresa L Campos, Glen W Sachse, and Donald E Hagen. Sources and chemistry of NO_x in the upper troposphere over the united states. *Geophys. Res. Lett.*, 25(10):1705–1708, 1998.

[62] Japan National Institute for Environmental Studies. Environmental numerical database. `http://www.nies.go.jp/igreen/index.html`, 2021. Accessed: 2021-6-7.

[63] Michael Jerrett, Richard T Burnett, C Arden Pope, 3rd, Kazuhiko Ito, George Thurston, Daniel Krewski, Yuanli Shi, Eugenia Calle, and Michael Thun. Long-term ozone exposure and mortality. *N. Engl. J. Med.*, 360(11):1085–1095, March 2009.

[64] M O Köhler, G Rädel, K P Shine, H L Rogers, and J A Pyle. Latitudinal variation of the effect of aviation NO_x emissions on atmospheric ozone and methane and related climate metrics, 2013.

[65] Marcus O Köhler, Gaby Rädel, Olivier Dessens, Keith P Shine, Helen L Rogers, Oliver Wild, and John A Pyle. Impact of perturbations to nitrogen oxide emissions from global aviation. *J. Geophys. Res.*, 113(D11), June 2008.

[66] Paul Konopka. *Analytical Gaussian solutions for anisotropic diffusion in a linear shear flow*. 1994.

[67] Jamin Koo, Qiqi Wang, Daven K Henze, Ian A Waitz, and Steven R H Barrett. Spatial sensitivities of human health risk to intercontinental and high-altitude pollution, 2013.

[68] M Kopacz, D J Jacob, J A Fisher, J A Logan, L Zhang, I A Megretskaia, R M Yantosca, K Singh, D K Henze, J P Burrows, M Buchwitz, I Khlystova, W W McMillan, J C Gille, D P Edwards, A Eldering, V Thouret, and P Nedelec. Global estimates of CO sources with high resolution by adjoint inversion of multiple satellite datasets (MOPITT, AIRS, SCIAMACHY, TES), 2010.

[69] Anne Gunn Kraabøl. Impacts of no_x emissions from subsonic aircraft in a global three-dimensional chemistry transport model including plume processes, 2002.

[70] Anne Gunn Kraabøl, Paul Konopka, Frode Stordal, and Hans Schlager. Modelling chemistry in aircraft plumes 1: comparison with observations and evaluation of a layered approach, 2000.

[71] J-F Lamarque, L K Emmons, P G Hess, D E Kinnison, S Tilmes, F Vitt, C L Heald, E A Holland, P H Lauritzen, J Neu, J J Orlando, P J Rasch, and G K Tyndall. CAM-chem: description and evaluation of interactive atmospheric chemistry in the community earth system model, 2012.

[72] D S Lee, D W Fahey, A Skowron, M R Allen, U Burkhardt, Q Chen, S J Doherty, S Freeman, P M Forster, J Fuglestvedt, A Gettelman, R R De León, L L Lim, M T Lund, R J Millar, B Owen, J E Penner, G Pitari, M J Prather, R Sausen, and L J Wilcox. The contribution of global aviation to anthropogenic climate forcing for 2000 to 2018. *Atmos. Environ.*, page 117834, September 2020.

[73] D S Lee, David W Fahey, Piers M Forster, Peter J Newton, Ron C N Wit, Ling L Lim, Bethan Owen, and Robert Sausen. Aviation and global climate change in the 21st century, 2009.

[74] D S Lee, G Pitari, V Grewe, K Gierens, J E Penner, A Petzold, M J Prather, U Schumann, A Bais, T Berntsen, D Iachetti, L L Lim, and R Sausen. Transport impacts on atmosphere and climate: Aviation. *Atmos. Environ.*, 44(37):4678–4734, December 2010.

[75] H Lee, S C Olsen, D J Wuebbles, and D Youn. Impacts of aircraft emissions on the air quality near the ground. *Atmos. Chem. Phys.*, 13(11):5505–5522, June 2013.

[76] Zhanqing Li, Feng Niu, Jiwen Fan, Yangang Liu, Daniel Rosenfeld, and Yanni Ding. Long-term impacts of aerosols on the vertical development of clouds and precipitation, 2011.

[77] Haipeng Lin, Xu Feng, Tzung-May Fu, Heng Tian, Yaping Ma, Lijuan Zhang, Daniel J Jacob, Robert M Yantosca, Melissa P Sulprizio, Elizabeth W Lundgren, Jiawei Zhuang, Qiang Zhang, Xiao Lu, Lin Zhang, Lu Shen, Jianping Guo, Sebastian D Eastham, and Christoph A Keller. WRF-GC (v1.0): online coupling of WRF (v3.9.1.1) and GEOS-Chem (v12.2.1) for regional atmospheric chemistry modeling – part 1: Description of the one-way model, 2020.

[78] Haipeng Lin, Daniel J Jacob, Elizabeth W Lundgren, Melissa P Sulprizio, Christoph A Keller, Thibaud M Fritz, Sebastian D Eastham, Louisa K Emmons, Patrick C Campbell, Barry Baker, Rick D Saylor, and Raffaele Montuoro. Harmonized emissions component (HEMCO) 3.0 as a versatile emissions component for atmospheric models: application in the GEOS-Chem, NASA GEOS, WRF-GC, CESM2, NOAA GEFS-Aerosol, and NOAA UFS models. *Geoscientific Model Development*, 2021.

[79] X Liu, P-L Ma, H Wang, S Tilmes, B Singh, RC Easter, SJ Ghan, and PJ Rasch. Description and evaluation of a new four-mode version of the modal aerosol module (mam4) within version 5.3 of the community atmosphere model. *Geoscientific Model Development*, 9(2):505–522, 2016.

[80] Xiaohong Liu, Richard C Easter, Steven J Ghan, R Zaveri, P Rasch, Xiangjun Shi, J-F Lamarque, A Gettelman, H Morrison, Francis Vitt, et al. Toward a minimal representation of aerosols in climate models: Description and evaluation in the community atmosphere model cam5. *Geoscientific Model Development*, 5(3):709–739, 2012.

[81] M S Long, R Yantosca, J E Nielsen, C A Keller, A da Silva, M P Sulprizio, S Pawson, and D J Jacob. Development of a grid-independent GEOS-Chem chemical transport model (v9-02) as an atmospheric chemistry module for earth system models, 2015.

[82] P A Makar, W Gong, C Hogrefe, Y Zhang, G Curci, R Žabkar, J Milbrandt, U Im, A Balzarini, R Baró, R Bianconi, P Cheung, R Forkel, S Gravel, M Hirtl, L Honzak, A Hou, P Jiménez-Guerrero, M Langer, M D Moran, B Pabla, J L Pérez, G Pirovano, R San José, P Tuccella, J Werhahn, J Zhang, and S Galmarini. Feedbacks between air pollution and weather, part 2: Effects on chemistry, 2015.

[83] Hermann Mannstein, Richard Meyer, and Peter Wendling. Operational detection of contrails from NOAA-AVHRR-data, 1999.

[84] Mauro Masiol and Roy M Harrison. Aircraft engine exhaust emissions and other airport-related contributions to ambient air pollution: A review. *Atmos. Environ.*, 95:409–455, October 2014.

[85] E W Meijer, P F J van Velthoven, A M Thompson, L Pfister, H Schlager, P Schulte, and H Kelder. Model calculations of the impact of NO_x from air traffic, lightning, and surface emissions, compared with measurements, 2000.

[86] E W Meijer, P F J van Velthoven, W M F Wauben, J P Beck, and G J M Velders. The effects of the conversion of nitrogen oxides in aircraft exhaust plumes in global models, 1997.

[87] O T Melo, M A Lusis, and R D S Stevens. Mathematical modelling of dispersion and chemical reactions in a plume — oxidation of no to NO2 in the plume of a power plant, 1978.

[88] L Menut, R Vautard, M Beekmann, and C Honoré. Sensitivity of photochemical pollution using the adjoint of a simplified chemistry-transport model, 2000.

[89] Laurent Menut. Adjoint modeling for atmospheric pollution process sensitivity at regional scale, 2003.

[90] Lee T Murray, Daniel J Jacob, Jennifer A Logan, Rynda C Hudman, and William J Koshak. Optimized regional and interannual variability of lightning in a global chemical transport model constrained by LIS/OTD satellite data: IAV OF LIGHTNING CONSTRAINED BY LIS/OTD. *J. Geophys. Res.*, 117(D20), October 2012.

[91] J L Neu and M J Prather. Toward a more physical representation of precipitation scavenging in global chemistry models: cloud overlap and ice physics and their impact on tropospheric ozone, 2012.

[92] Peer Johannes Nowack, Nathan Luke Abraham, Peter Braesicke, and John Adrian Pyle. Stratospheric ozone changes under solar geoengineering: implications for UV exposure and air quality, 2016.

[93] OAG. OAG, flight database & statistics. `http://www.oag.com`, 2021. Accessed: 2021-6-3.

[94] Seth C Olsen, Guy P Brasseur, Donald J Wuebbles, Steven R H Barrett, Hongyan Dang, Sebastian D Eastham, Mark Z Jacobson, Arezoo Khodayari, Henry Selkirk, Andrei Sokolov, and Nadine Unger. Comparison of model estimates of the effects of aviation emissions on atmospheric ozone and methane, 2013.

[95] R Paoli, D Cariolle, and R Sausen. Review of effective emissions modeling and computation, 2011.

[96] H Petry, J Hendricks, M Möllhoff, E Lippert, A Meier, A Ebel, and R Sausen. Chemical conversion of subsonic aircraft emissions in the dispersing plume: Calculation of effective emission indices, 1998.

[97] Gabriele Pfister, Andrew Conley, Mary Barth, Louisa Emmons, Forrest Lacey, and Rebecca Schwantes. MUSICA - modeling for chemistry, weather and climate, 2020.

[98] Giovanni Pitari, Valentina Aquila, Ben Kravitz, Alan Robock, Shingo Watanabe, Irene Cionni, Natalia De Luca, Glauco Di Genova, Eva Mancini, and Simone Tilmes. Stratospheric ozone response to sulfate geoengineering: Results from the geoengineering model intercomparison project (GeoMIP), 2014.

[99] Colin Price, Joyce Penner, and Michael Prather. No_x from lightning: 1. global distribution based on lightning physics. *Journal of Geophysical Research: Atmospheres*, 102(D5):5929–5941, 1997.

[100] Flávio D A Quadros, Mirjam Snellen, and Irene C Dedoussi. Regional sensitivities of air quality and human health impacts to aviation emissions. *Environ. Res. Lett.*, 15(10):105013, October 2020.

[101] China Air Quality. China air quality historical data. `https://quotsoft.net/air/`, 2021. Accessed: 2021-6-7.

[102] S Randolph Kawa. *Assessment of the Effects of High-speed Aircraft in the Stratosphere*. 1999.

[103] Jadwiga H Richter, James A Anstey, Neal Butchart, Yoshio Kawatani, Gerald A Meehl, Scott Osprey, and Isla R Simpson. Progress in simulating the quasi-biennial oscillation in cmip models. *Journal of Geophysical Research: Atmospheres*, 125(8):e2019JD032362, 2020.

[104] Michele M Rienecker, Max J Suarez, Ronald Gelaro, Ricardo Todling, Julio Bacmeister, Emily Liu, Michael G Bosilovich, Siegfried D Schubert, Lawrence Takacs, Gi-Kong Kim, Stephen Bloom, Junye Chen, Douglas Collins, Austin Conaty, Arlindo da Silva, Wei Gu, Joanna Joiner, Randal D Koster, Robert Lucchesi, Andrea Molod, Tommy Owens, Steven Pawson, Philip Pegion, Christopher R Redder, Rolf Reichle, Franklin R Robertson, Albert G Ruddick, Meta Sienkiewicz, and Jack Woollen. MERRA: NASA's Modern-Era retrospective analysis for research and applications, 2011.

[105] C Rojo, X Vancassel, P Mirabel, J-L Ponche, and F Garnier. Impact of alternative jet fuels on aircraft-induced aerosols, 2015.

[106] A Rondón, C Johansson, and L Granat. Dry deposition of nitrogen dioxide and ozone to coniferous forests, 1993.

[107] Adrian Sandu, Dacian N Daescu, Gregory R Carmichael, and Tianfeng Chai. Adjoint sensitivity analysis of regional air quality models, 2005.

[108] Hauke Schmidt. Adjoint sensitivity of episodic ozone in the paris area to emissions on the continental scale, 2003.

[109] Nicholas W Simone, Marc E J Stettler, and Steven R H Barrett. Rapid estimation of global civil aviation emissions with uncertainty quantification. *Transp. Res. Part D: Trans. Environ.*, 25:33–41, December 2013.

[110] C H Song. Dispersion and chemical evolution of ship plumes in the marine boundary layer: Investigation of $O_3/NO_y/HO_x$ chemistry, 2003.

[111] Raymond L Speth, Sebastian D Eastham, Thibaud M Fritz, Inés Sanz-Morére, Akshat Agarwal, Florian Allroggen, Prakash Prashanth, and Steven R H Barrett. Global environmental impact of supersonic cruise aircraft in the stratosphere. Technical Report 20205009400, NASA Technical Reports Server, February 2021.

[112] Marc E J Stettler, Adam M Boies, Andreas Petzold, and Steven R H Barrett. Global civil aviation black carbon emissions. *Environ. Sci. Technol.*, 47(18):10397–10404, September 2013.

[113] Jian Sun, Kai Zhang, Hui Wan, Po-lun Ma, Qi Tang, and Shixuan Zhang. Impact of nudging strategy on the climate representativeness and hindcast skill of constrained EAMv1 simulations. *J. Adv. Model. Earth Syst.*, 11(12):3911–3933, December 2019.

[114] L Tarrasón, J E Jonson, T K Berntsen, and others. Study on air quality impacts of non-LTO emissions from aviation. *Norwegian*, 2004.

[115] Mark R Theobald, Marta G Vivanco, Wenche Aas, Camilla Andersson, Giancarlo Ciarelli, Florian Couvidat, Kees Cuvelier, Astrid Manders, Mihaela Mircea, Maria-Teresa Pay, and Others. An evaluation of european nitrogen and sulfur wet deposition and their trends estimated by six chemistry transport models for the period 1990–2010. *Atmos. Chem. Phys.*, 19(1):379–405, 2019.

[116] Xue Xi Tie, Guy Brasseur, Xing Lin, Pierre Friedlingstein, Claire Granier, and Philip Rasch. The impact of high altitude aircraft on the ozone layer in the stratosphere, 1994.

[117] Xuexi Tie and Guy Brasseur. The response of stratospheric ozone to volcanic eruptions: Sensitivity to atmospheric chlorine loading, 1995.

[118] S Tilmes, J-F Lamarque, L K Emmons, A Conley, M G Schultz, M Saunois, V Thouret, A M Thompson, S J Oltmans, B Johnson, and D Tarasick. Ozonesonde climatology between 1995 and 2009: description, evaluation and applications, 2011.

[119] S Tilmes, J-F Lamarque, L K Emmons, A Conley, M G Schultz, M Saunois, V Thouret, A M Thompson, S J Oltmans, B Johnson, and D Tarasick. Technical note: Ozonesonde climatology between 1995 and 2011: description, evaluation and applications, 2012.

[120] S Tilmes, J-F Lamarque, L K Emmons, D E Kinnison, P-L Ma, X Liu, S Ghan, C Bardeen, S Arnold, M Deeter, F Vitt, T Ryerson, J W Elkins, F Moore, J R Spackman, and M Val Martin. Description and evaluation of tropospheric chemistry and aerosols in the community earth system model (CESM1.2), 2015.

[121] Michelle C Turner, Michael Jerrett, C Arden Pope, Daniel Krewski, Susan M Gapstur, W Ryan Diver, Bernardo S Beckerman, Julian D Marshall, Jason Su, Daniel L Crouse, and Richard T Burnett. Long-Term ozone exposure and mortality in a large prospective study, 2016.

[122] US EPA AirNow Program. AirNow API. https://docs.airnowapi.org/, 2021. Accessed: 2021-6-7.

[123] M Val Martin, C L Heald, and S R Arnold. Coupling dry deposition to vegetation phenology in the community earth system model: Implications for the simulation of surface O_3, 2014.

[124] Arjan van Dijk, Harry Slaper, Peter N den Outer, Olaf Morgenstern, Peter Braesicke, John A Pyle, Hella Garny, Andrea Stenke, Martin Dameris, Andreas Kazantzidis, Kleareti Tourpali, and Alkiviadis F Bais. Skin cancer risks avoided by the montreal protocol–worldwide modeling integrating coupled climate-chemistry models with a risk model for UV. *Photochem. Photobiol.*, 89(1):234–246, January 2013.

[125] Robert Vet, Richard S Artz, and Silvina Carou. A global assessment of precipitation chemistry and deposition of sulfur, nitrogen, sea salt, base cations, organic acids, acidity and ph, and phosphorus, 2014.

[126] G C M Vinken, K F Boersma, D J Jacob, and E W Meijer. Accounting for non-linear chemistry of ship plumes in the GEOS-Chem global chemistry transport model. *Atmos. Chem. Phys.*, 11(22):11707–11722, November 2011.

[127] P F Vohralik, L K Randeniya, I C Plumb, and S L Baughcum. Effect of plume processes on aircraft impact. *J. Geophys. Res.*, 113(D5), March 2008.

[128] Jiandong Wang, Shuxiao Wang, Jingkun Jiang, Aijun Ding, Mei Zheng, Bin Zhao, David C Wong, Wei Zhou, Guangjie Zheng, Long Wang, Jonathan E Pleim, and Jiming Hao. Impact of aerosol–meteorology interactions on fine particle pollution during china's severe haze episode in january 2013, 2014.

[129] Kai Wang, Yang Zhang, Khairunnisa Yahya, Shiang-Yuh Wu, and Georg Grell. Implementation and initial application of new chemistry-aerosol options in WRF/Chem for simulating secondary organic aerosols and aerosol indirect effects for regional air quality. *Atmos. Environ.*, 115:716–732, August 2015.

[130] Nan Wang, Xiaopu Lyu, Xuejiao Deng, Xin Huang, Fei Jiang, and Aijun Ding. Aggravating O_3 pollution due to NO_x emission control in eastern china. *Sci. Total Environ.*, 677:732–744, August 2019.

[131] Yuhang Wang, Daniel J Jacob, and Jennifer A Logan. Global simulation of tropospheric O_3-NO_x-hydrocarbon chemistry: 3. origin of tropospheric ozone and effects of nonmethane hydrocarbons, 1998.

[132] Kathrin Wehrli, Benoît P Guillod, Mathias Hauser, Matthieu Leclair, and Sonia I Seneviratne. Improved dynamics due to introducing a nudging approach in the community earth system model (CESM) and thermodynamic origin of the remaining errors. page 12237, April 2018.

[133] Debra K Weisenstein, Malcolm K W Ko, Igor G Dyominov, Giovanni Pitari, Lucrezia Ricciardulli, Guido Visconti, and Slimane Bekki. The effects of sulfur emissions from HSCT aircraft: A 2-D model intercomparison, 1998.

[134] Debra K Weisenstein, Glenn K Yue, Malcolm K W Ko, Nien-Dak Sze, Jose M Rodriguez, and Courtney J Scott. A two-dimensional model of sulfur species and aerosols, 1997.

[135] Lili Xia, Peer J Nowack, Simone Tilmes, and Alan Robock. Impacts of stratospheric sulfate geoengineering on tropospheric ozone, 2017.

[136] Steve H L Yim, Gideon L Lee, In Hwan Lee, Florian Allroggen, Akshay Ashok, Fabio Caiazzo, Sebastian D Eastham, Robert Malina, and Steven R H Barrett. Global, regional and local health impacts of civil aviation emissions. *Environ. Res. Lett.*, 10(3):034001, February 2015.

[137] Karen Yu, Christoph A Keller, Daniel J Jacob, Andrea M Molod, Sebastian D Eastham, and Michael S Long. Errors and improvements in the use of archived meteorological data for chemical transport modeling: an analysis using GEOS-Chem v11-01 driven by GEOS-5 meteorology, 2018.

[138] Jun Zhang, Donald Wuebbles, Douglas Kinnison, and Steven L Baughcum. Potential impacts of supersonic aircraft emissions on ozone and resulting forcing on climate: An update on historical analysis. *J. Geophys. Res.*, 126(6), March 2021.

[139] Yuqiang Zhang, Rohit Mathur, Jesse O Bash, Christian Hogrefe, Jia Xing, and Shawn J Roselle. Long-term trends in total inorganic nitrogen and sulfur deposition in the U.S. from 1990 to 2010. *Atmos. Chem. Phys.*, 18(12):9091–9106, June 2018.

[140] L Zhu, D K Henze, K E Cady-Pereira, M W Shephard, M Luo, R W Pinder, J O Bash, and G -R. Jeong. Constraining U.S. ammonia emissions using TES remote sensing observations and the GEOS-Chem adjoint model, 2013.